Project No. 09-828

Data Collection Methods for Validation of Advanced Multi-Resolution Fast Reactor Simulations

Fuel Cycle

Dr. Akira Tokuhiro
University of Idaho

In collaboration with:
Argonne National Laboratory
University of Tennessee, Knoxville

Rob Versluis, Federal POC
Dave Pointer, Technical POC

NEUP Nuclear Energy University Programs
U.S. Department of Energy

Nuclear Energy University Programs (NEUP)

Final Report on

Data Collection Methods for Validation of Advanced Multi-Resolution Fast Reactor Simulations

Project Number: 09-321(828)
Technical Work Scope Identification**:**
AFCI Regulatory and Safety, Models, codes and data
to address fast reactor safety, AFG-2

Report Prepared by: Akira Tokuhiro[a] Olumuyiwa Omotowa[a]

PIs: Akira Tokuhiro[a],
Art Ruggles[b], W. David Pointer[c,d]

Student Investigators: Nathan Seaver (M.E.) [a], Matthew Cromwell (M.E.)[a],
Caitlin Flynn-Harker (M.E.)[a], Olumuyiwa Omotowa (Ph.D.)[a],
Lee Tschaepe (Ph.D.)[b], Spero Peters[b]

[a] Department of Mechanical Engineering, University of Idaho
[b] University of Tennessee - Knoxville
[c,d]Argonne National Laboratory (currently at ORNL)

Acknowledgments

The lead author wishes to express special thanks to Professor Art Ruggles and his UTK students for the collaboration. He also thanks Argonne National Laboratory's Nuclear Engineering Division and its distinguished staff who contributed in some way to this project; Drs. David Pointer, Stephen Lomperski, Mitchell Farmer.

Gratitude also goes out to the U.S. Department of Energy's Nuclear Energy University Program for generous support under *NEUP 09-321, Data Collection Methods for Validation of Advanced Multi-Resolution Fast Reactor Simulations.*

Special thanks also go to University of Idaho students and interns as follows who contributed to the project: Matthew Cromwell, Caitlin Flynn-Harker, Nathan Seaver, Olumuyiwa Omotowa, John Downing and David Kim.

Finally, in memory of the late Gerard Gogniat, founder and owner of Met-Flow SA, who commercially realized the ultrasonic Doppler velocimeter.

Abstract

In pool-type Sodium Fast Reactors (SFR) the regions most susceptible to thermal striping are the upper instrumentation structure (UIS) and the intermediate heat exchanger (IHX). This project experimentally and computationally (CFD) investigated the thermal mixing in the region exiting the reactor core to the UIS. The thermal mixing phenomenon was simulated using two vertical jets at different velocities and temperatures as prototypic of two adjacent channels out of the core. Thermal jet mixing of anticipated flows at different temperatures and velocities were investigated. Velocity profiles are measured throughout the flow region using Ultrasonic Doppler Velocimetry (UDV), and temperatures along the geometric centerline between the jets were recorded using a thermocouple array. CFD simulations, using COMSOL, were used to initially understand the flow, then to design the experimental apparatus and finally to compare simulation results and measurements characterizing the flows.

The experimental results and CFD simulations show that the flow field is characterized into three regions with respective transitions, namely, convective mixing, (flow direction) transitional, and post-mixing. Both experiments and CFD simulations support this observation. For the anticipated SFR conditions the flow is momentum dominated and thus thermal mixing is limited due to the short flow length associated from the exit of the core to the bottom of the UIS. This means that there will be thermal striping at any surface where poorly mixed streams impinge; rather unless lateral mixing is 'actively promoted out of the core, thermal striping will prevail. Furthermore we note that CFD can be considered a 'separate effects (computational) test' and is recommended as part of any integral analysis[1]. To this effect, poorly mixed streams then have potential impact on the rest of the SFR design and scaling, especially placement of internal components, such as the IHX that may see poorly mixed streams.

Finally, due to lack or infrastructural support for carrying out sodium experiments, only water experiments and CFD studies were realized in, an otherwise sodium approved facility. It is hoped that the NEUP Office takes this into consideration.

[1] This result was generated per leveraged NEUP project on the water RCCS design with the University of Wisconsin and Texas A&M University. The Ph.D. thesis by O. Omotowa contains describes this work.

Table of Contents

List of Figures

List of Tables

Chapter 1. Introduction

Increasing global energy demand, limited oil and gas reserves, climate change concerns, and insufficient throughput from alternative energy sources, e.g., wind and solar led the United States Department of Energy (DOE) in 2002 to start the Generation IV (Gen-IV) International Forum. The purpose was to ensure that nuclear power remained a key component of the US energy mix and reassure the public of the safety of nuclear technology. The international forum was supported by ten countries (Argentina, Brazil, Canada, France, Japan, South Korea, South Africa, Switzerland, USA, and UK), and was tasked with developing reactor systems with advanced safety features. Specifically, these advanced reactor system designs were to have significant improvements over current reactor systems in terms of safety, reliability, economics, waste minimization, sustainability, and proliferation resistance (US DOE Nuclear Energy Research Advisory Committee and the Generation IV Int. Forum, 2002).

Six different reactor concepts emerged from the forum to have technological viability and commercial potential based on the Gen-IV criteria. They are the Very High Temperature Reactor (VHTR), Super-Critical Water-cooled Reactor (SCWR), Molten Salt Reactor (MSR), Gas-Cooled Fast Reactor (GCFR), Lead Fast Reactor (LFR), and the Sodium Fast Reactor (SFR). The VHTR and SCWR use a thermal neutron spectrum whereas the GCFR, LFR, and SFR employ a fast neutron spectrum to achieve a high utilization of nuclear materials through recycling. The MSR uses a circulating liquid fuel mixture, which also allows for high nuclear material utilization through recycling. The concept of interest for this work is the SFR.

The SFR has a compact high power density core when compared to the current Light Water Reactor (LWR). This gives the SFR the capability of producing more power than the LWR. Additionally, the sodium coolant remains in liquid state during operating conditions without needing any pressurization; hence the design pressure for components is nearly atmospheric, leading to lower wall thicknesses for structures. To further make the concept more economically viable several components including the Intermediate Heat Exchanger (IHX), the Upper Instrumentation Structure (UIS), and Pump are located within the reactor vessel.

With renewed interest in the SFR and a closed fuel cycle, the majority of the R&D issues that remain are technology performance and demonstration related. Under the NEUP 09-321 research grant, "Data Collection Methods for Validation of Advanced Multi-Resolution Fast Reactor Simulations," it was undertaken to address some of the principal technology issues related to sodium-cooled fast reactors.

The international sodium fast reactor R&D effort, as summarized in the R&D Program Plan for the Sodium Fast Reactor, rested on well-established technologies and a reactor engineering knowledge and experience base (Ichimiya, et al., 2006). Thus, there was a need to re-address SFR viability in terms of design concept economics, in-service inspection and repair (ISI&R), verification of inherent safety and updated analyses (i.e. advanced simulations). Additionally, a panel of experts assembled by the US DOE developed Phenomena, Identification and Ranking Table (PIRT), Table 1, as part of a safety review for

each of the six Gen-IV concepts. The table was developed by ranking various phenomena expected to occur during normal and off normal conditions based on safety response importance and level of knowledge within the scientific community. The thermal striping phenomenon, or thermal mixing problem, was identified to be of high importance with lower knowledge.

New methods are needed for the collection, reduction, characterization and the comparison of experimental validation data to support the development, deployment and application of advanced multi-scale or multi-resolution thermofluid simulation tools. The proposed project scope will include the design and construction of two new separate effects facilities relevant to advanced fast reactor design and safety, qualification of new instrumentation methods, development of high-performance computing solutions for data management and analysis, and development of best practices for validation of the advanced multi-resolution thermofluids simulation tools. These efforts will seek to leverage recent developments in instrumentation for fluid dynamics and heat transfer measurements, availability of massively parallel computing resources and participants' collective experience in the design of validation experiments for liquid metal cooled systems and advanced reactors.

In legacy experiments for validation of nuclear simulation tools, data collection has largely focused on measuring integral behavior over large control volumes. This approach allows the use of sparse instrumentation largely based on thermocouple, dynamic pressure, or single point bulk velocity measurements. Experiments of this type are scaled based on the familiar dimensionless scaling parameters such as the Reynolds, Prandtl, or Grashof numbers. While these dimensionless parameters describe the characteristic spatio-temporal turbulence effects in the system, they do not provide any information about the localized phenomena that may be key to the spatio-temporal result.

The inclusion of high-resolution computational fluid dynamics codes as part of the thermofluid simulation suite clearly requires that data be collected at high spatial densities and high frame rates. However, simply applying high-resolution measurement methods to experiments scaled (or as separate effects) for validation of correlation based system design tools may not be sufficient if experiments are not designed to provide characteristic turbulence length scales and shear stresses, then subsequent data fidelity to establish spatio-temporal average field values.

In legacy validation experience, the limited thermal-hydraulic (TH) state space considered in the experimental program restricted the applicability of the legacy codes to a very limited subset of the design state space. Of significance, separate effect experiments nor CFD modeling and simulations studies have (unfortunately) not been scaled. The broader applicability of the computational fluid dynamics tools will allow the multi-resolution thermofluids simulation tools to be applied to a much broader design state space (different than the TH space), extending opportunities for significant improvements in efficiency, safety, and economic performance.

The proposed effort will provide additional 'modern' data to support the development of the advanced tools, develop methods for the reduction and characterization of the very large data

sets generated using the high-resolution measurement methods, develop methods for time correlation of fluid dynamic and heat transfer data from high-resolution measurements, identify new technologies and surrogate materials to facilitate high-resolution measurements at Peclet numbers for fast reactor systems, and develop initial best practices to guide the development of rigorous validation, verification and benchmarking requirements for the advanced codes. Here we recall that the Peclet number is the proper equivalent to the Reynolds number; that is, Pe = Re*Pr.

1.1 Technical Approach and Task Description

Computational fluid dynamics (CFD) codes are increasingly relied upon for design, performance, and safety analysis of anticipated engineered systems. As computing power and availability increase, these codes are being used to predict physical phenomena on ever more refined spatiotemporal scales. As reliance upon these tools grows, it becomes critical to ensure that they do indeed describe the physical world to an acceptable level of accuracy. Validation and verification (V&V) of high resolution models of physical systems requires, however, comparisons with similarly finer-scaled experimental data. This, in turn, necessitates the use of 'modern' instrumentation and measurement techniques.

Many of the DOE laboratories are engaged in an effort to generate high resolution experimental data for the V&V of CFD tools used to predict fluid flow and heat transfer phenomena in advanced nuclear systems. The proposed work will be performed by a team of two universities, U. Idaho (UI) and U. Tennessee-Knoxville (UTK), and Argonne National Laboratory with both universities in close proximity to two additional DOE laboratories, INL and ORNL. The team plans to broaden a data base that can be applied towards code V&V specifically for liquid-metal based systems such as a sodium-cooled reactor. The team has a unique expertise base in both experimental and computational studies of liquid metal systems which includes fluid dynamics experiments using mercury, sodium, molten salts, water and gas as working fluids. The 'high' spatiotemporal nature of the data generally means enormous amounts of data. Thus the experimental (counterpart) challenge is the development and demonstration of spatiotemporal data generation, management and processing techniques and strategies. The proposed scope of work (SOW) facilitates comparisons between simulation tool predictions and the validation data. The three-year effort will focus on three primary objectives as follows; to:

- design and construction of two liquid-metal thermal-hydraulic (LM TH) separate effects experimental facilities at two universities, similar in scope, size (order of magnitude) and specifications to an existing DOE laboratory facility. Initial study on dual (parallel) jet, thermal mixing phenomena.
- identify and qualify advanced instrumentation for use in liquid metal coolants that provide higher-resolution spatio-temporal flow field data required for V&V, UQ and data management and standardization; also establish an accessible database. The databases will consist of large, time-correlated measurement data that characterize similar liquid-metal thermal-hydraulics in LMFRs.
- investigate, model and simulate thermal mixing of dual jets as a separate effects experiment and computationally, at additional scales of relevance to SFR flows. The CFD

study will essentially dictate the prototypic condition of the experiments; in addition, results of the simulation will be 'tuned' to spatio-temporal scales that 'match' the corresponding measurement of the convective field.

In terms of a generalized task, **Task 1** will consist of surveying the current state of knowledge work, select a commercial CFD package in order to design the separate effects experiments and scope the range of flow parameters realizable. The team will broaden DOE's computational and experimental efforts via development of instrumentation that will yield spatio-temporal velocimetric and thermometric data.

The selected reference (benchmark) thermal-hydraulic phenomena will be the thermal mixing of two, side-by-side, jets at similar to dissimilar velocities and temperatures. This has configuration has been selected for the following general and specific considerations:

1) understanding the thermal mixing of convectively dissimilar LM streams is key to SFR issues such as thermal striping and flow in plena.
2) flow of the simpler single jet (planar, axisymmetric, buoyant, isothermal) are well documented analytically, computationally and experimentally
3) thermal mixing of a triple-jet configuration in ordinary and low Pr-number fluids has been studied by Kimura and co-workers (2002) both experimentally and computationally, These studies are fairly recent, well-documented and the database is (likely) available. The flow is 'on average' symmetric with respect to the central jet.
4) thermal mixing of a dual-jet provides relevant complexity and an opportunity to investigate turbulence modeling, RANS, as well as LES and DNS approaches.

Scoping computational simulations using commercial CFD codes and an advanced DOE lab developed code will be completed prior to the finalization of the experimental design to identify potential flow instabilities that would limit the applicability of the data, aid in defining the state space for the test matrix, and assist in focusing the location and resolution of the instrumentation.

1.2 Separate Effects Test Facilities and Velocimetry

As noted, since isothermal and buoyant single-jets are well-documented and the thermal mixing of three parallel jets for both ordinary and low Pr-number fluids has been studied by Kimura, Nishimura and co-workers (2002, 2000 respectively) both experimentally and computationally, we plan to design and construct a separate effects test facility, initially configured to study two parallel jets with different velocities and temperature. A separate effects facility will be constructed at each participating university. In the current effort we will use two low Pr-number fluids, mercury (Hg) and sodium (Na); the former, since it is the fluid with an experiential base at ANL. Further, although Hg is toxic, its oxidation reaction does not pose a physical hazard and can be controlled and monitored by documented means. Lastly using both Hg and Na provides a means to investigate and compare the convective flow and heat transfer differences in liquid metals (LMs) due to approximate order of magnitude difference in Pr-number (~0.025 for Hg vs. 0.005 for Na); that is, an evaluation of both experimental and computational sensitivity and 'resolution' to small relative influences in thermal-physical properties.

The set-up will be similar in layout to an existing DOE laboratory sodium facility so that a common reference is maintained for the present and future collaborations; in fact, if possible connecting flanges and piping will be identical so that we create an option to exchange and share components amongst all three facilities. Thus inside a suitable confining volume with an auxiliary system similar to the existing DOE facility, we will design and configure two parallel jets, very similar to the triple-jet reported by Kimura et al. In fact, a very similar ultrasonic Doppler velocimeter will be used in our experiments in both sodium and mercury. In both liquid sodium and mercury, we will focus on generating spatio-temporal convective heat transfer data for detailed validation of turbulence dissipation and wall treatment models. Some point verification permanent magnet velocimetry probe measurements will also be conducted. A brief note on the principle of ultrasonic Doppler velocimetry is noted below.

1.3 Separate Effects Facility and Thermal Mixing of Two-Jets

Each university participant will design and construct a separate effects test facility, respectively planned for low Pr-number fluids, sodium and mercury. Other than the test section which will be specific to the proposed SOW, each university will adopt an auxiliary system (pump, tanks, fittings, piping, valves, etc.) to the extent possible that takes the DOE laboratory's system as the reference facility. The test section will consist of outer and inner enclosures with the 'annular' space serving as the return overflow to the auxiliary system. The two streams will be pre-conditioned via differential heating (resistance) and cooling (via liquid to gas heat exchanger) and differential electromagnetic (EM) pumping conditions. Per Kimura et al. we will also maintain the option to heat one stream relative to the other which we will keep at the bulk loop temperature. In order compare results, the temperature difference and velocity ratio between the heated (h) and unheated (c) jets will initially be, ΔT_{hc}=5°C, 10°C and R=($V_{cold,exit}/V_{hot,exit}$)=1.0 (isovelocity), 0.7, 0.5 respectively. The corresponding typical Reynolds number will be $Re_D=1.8 \times 10^4$, where D is the hydraulic diameter of the exit nozzle. Velocity measurement of single-jet and dual-jet arrangement will be taken by ultrasound Doppler velocimetry (UDV) while temperature data will be taken using a vertically traversed thermocouple array. Since UDV may be the only means by which higher fidelity spatiotemporal measurement can be obtained in LMs, we provide a short introduction below.

Table 1.1 Various Phenomena rankings identified by PIRT

Phenomena	Importance to Safety	Level of Knowledge
Steady State Intact Fuel and Fuel Changes	High	Medium
Transition to Natural Convective Cooling, Sodium Stratification	High	Medium
Thermal Response of Structures, Thermal Striping	High	Medium

Decay Heat Rejection, Radiation Heat Transfer from Vessels	High	Medium
Power Conversion Cycle, S-CO2 Accident Analysis	High	Low
Fuel Transient Behavior	Medium	Low
Severe Core Damage, Metal Fuel Motion, Dispersal and Morphology	High	Medium

In order to demonstrate multi-resolution instrumentation for fluid characterization applied to the problem of thermal mixing, an experimental convective loop featuring two fluid jets discharging into a reservoir of larger volume was designed, constructed and operated. The experimental apparatus has been designed per EHS standards of the Center for Advanced Energy Studies (CAES) to accommodate sodium. A safety design review using expert peer review by INL/BEA SMEs was completed. In preparation to experiments with sodium the apparatus, experimental procedures, and measurement technique were first validated using water. This work presents the results using water as the experimental fluid. ANL designed, constructed and experimented on thermal mixing of air jet at the MAX facility. In conjunction with these water experiments, computational fluid dynamic (CFD) simulations are also presented herein.

Sodium, although well suited as the heat transfer medium for the SFR, is chemically reactive water, air) and (optically) opaque. As such, sodium has presented engineered accessibility constraints relative to LWR operations and maintenance (O&M) and ISI technologies. Thus in terms of thermo-hydraulic measurements under normal conditions, and before/after off-normal (maintenance, unanticipated events) events, there have been limited sensing options. The opacity of sodium hinders conventional fluid testing techniques such as Laser Doppler Velocimetry (LDV) or any light-source based optical method, particle tracing, and (flow visualization) dye techniques. The melting temperature (~99C) and chemical reactivity in air also constrains the type of experiments that are possible to simulate flows.

In the majority of data collection methods currently used in SFR's, the coolant thermal-hydraulics is measured at only limited locations, and often in one stationary location, making it difficult to know or model the actual flow field within large areas. Some researchers are currently investigating the possibility of alternative velocity and temperature measurement systems with increased spatio-temporal resolutions in order to better model flow characteristics within pipes and larger convective regions. One example of this is Ultrasonic Doppler Velocimetry (UDV). By using an array of ultrasonic transducers as both emitter and receiver, a finer resolution can be produced for both velocity and temperature fields within a flow. The Doppler concept is used because the speed of sound is dependent on temperature, and the Doppler shift along the beamline divided into 'channels' can be recorded. The velocities are recorded in a similar manner. Acoustic methods, primarily ultrasonic, have been presented as a key measurement technology with applications in non-destructive testing, under-sodium (components) imaging, thermometry and velocimetry.

Other physical devices and the associated change in phenomena can be used to measure local velocities. Generally, there exists a limited number of point-, line- and volume-wise sensing/measurement methods with low-to-high resolution dependent on the inherent characteristic velocity in a medium (acoustical, light-based) or thermal/mechanical inertia. One method originally attributed to Mueller (XXXX) but developed by Kapulla et al (Kapulla, 2000) is called a permanent magnet probe (PMP), which is comprised of an annulus shaped permanent magnet with three thermocouples arranged throughout the sensor tip. A change in the magnetic intensity with change in flow past a permanent magnet induces a (measureable) current; thus the magnet can be any shape. The magnetic property is however temperature dependent and thus has to be measured. The differences in velocity are read and results compared to a calibrated model.

As further described, the current study is intended to yield a better qualitative understanding and quantitative means to measure the thermal hydraulic condition of thermal jet mixing under varied flow conditions through the design, construction and operation an university-based, smaller purposeful liquid metal flow loop ‘certified’ under near National Laboratory EHS standards. The method of thermal hydraulic characterization using UDV is applied here. A combined approach using CFD and experimental results is used to better understand the thermal mixing and convective heat transfer in jets.

Chapter 2. Literature Review

Acoustic attenuation in layers of materials, thermal mixing, jet behavior, CFD and meshing techniques, chemical interactions of materials, as well as mechanical design and fabrication were all considered in the design of the facility. Consequently, we bring these various concepts and technologies together to investigate these in relation to their particular role within the scope of this study.

2.1 Development ins Measurement Methods

To better understand the complex nature of fluid flows found in heat transfer and fluid mechanics applications, many measurement methods and techniques have been utilized. However, most measurement techniques are not applicable to liquid metals due to their opacity, temperature, chemical reactiveness, corrosiveness, and the frequent presence of electromagnetic fields. Methods capable of time resolution are especially desired so that real-time flow characteristics can be visualized. Magnetic flow meters (Cushing, 1964) (Sorrell, 1990) and hot-wire anemometers (Lock , 1968) (Tsuji, 1989) have been used extensively in the past, but only offer average and local velocity data, respectively. Various optical techniques with sufficient time resolution have been developed such as Laser Doppler Velocimetry (LDV) (Porta, 2002) (Hosokawa, 2009) and Particle Image Velocimetry (PIV) (Borowsky, 2006) (Deev, 2009) and are in common use today. Radiographic techniques have also been used for visualization of two-phase fluid flows encased in opaque materials such as pipes and containers (Koster, 1997). Table 2.1 provides a basic comparison of these measurement methods and a many other methods that are summarized by Eckert et al. (Eckert, 2007).

Table 2.1 Various Velocity Measurement Methods

Type	Pros	Cons
Hot-Wire Anemometry	Frequency response >100kHz, works in turbulent flows	Fragile, provides only local data, intrusive
Radiography	Ideal for pipe-flow visualization, non-intrusive	Safety concerns, high power requirement, potentially high attenuation, difficult setup
Laser Doppler Velocimetry	Non-intrusive, up to 50kHz frequency response	Only measures velocity profile perpendicular to lasers, complicated setup
Particle Image Velocimetry	Non-invasive, time resolution down to 110ns, spatial resolution ~0.5 – 1% of field of view	Expensive (~$100k-200k, depending on features), potentially dangerous, not ‘actual’ velocity field
Magnetic Flow Meter	High accuracy (~0.5% of reading), non-invasive, inexpensive (<$20,000)	Wafer-type only gives average velocity, Insertion-type gives point data

Vane – cup or miniaturized impeller	Relatively inexpensive, local velocity	Intrusive, one local velocity measurement at a time
Linear Displacement of a spring loaded plate	Relatively inexpensive, local velocity	Intrusive, one local velocity measurement at a time
Tube Anemometers	Small, local velocity, accurate to ~5mm/s in PbBi (Schulenberg, 2010)	Intrusive, not suitable for turbulent flow, one local velocity measurement at a time
Fiber Flowmeter	Local velocity	Intrusive, deflection needs to be measured by endoscope, one local velocity measurement at a time
Conductive Anemometer or Potential Difference Probes	Works in turbulent flows, local velocity	Intrusive, one local velocity measurement at a time
Permanent Magnet Probe (PMP) and Miniature PMP	High temperature functionality (970K), accurate up to ~1mm/s (Hayashi, 1990) (Kapulla, 2000) (Schulenberg & Stieglitz, 2010)	Intrusive, work in progress
Flow Tomography or Magnetoenecphal-ography (MEG)	Non-intrusive, Determine 3D velocity field	Requires electrodes at the fluid surface, work in progress
Contactless Electromagnetic Flowmeter [Priede]	Non-intrusive	Requires small magnetic field, work in progress

Another measurement method that has proved extremely useful in fluid flow visualization is an echographic technique, which utilizes ultrasonic sound waves. Ultrasound is defined as sound waves above the frequency detectable by the human ear (>20,000Hz). Ultrasonic (US) techniques can be extremely useful in heat transfer studies, because they can monitor fluids that can't be measured by optical methods (i.e. fluid flowing behind a container wall).

2.2 UltrasonicVelocimetry

In 1986, Takeda in collaboration with Met-Flow first introduced an ultrasonic Doppler shift detection device that was based on Meister's work on a blood flow meter in 1983. Meister's device was able to determine the time-dependent flow-rate of blood in a blood vessel by measuring the Doppler shift of an ultrasonic sound (US) wave, which is caused when the US wave contacts particles within the blood flow. Following further refinements, Takeda via Met-Flow, introduced the Ultrasound Velocity Profile Monitor (UVP), which was capable of

measuring the instantaneous velocity profile along the ultrasonic beam axis (Takeda, 1991), demonstrating that the UDV measurement technique measures in both time and space.

Takeda also provided initial validation of his ultrasonic Doppler shift detection device by investigating water in both Poiseuille and Taylor vortex flows (Takeda, 1986). Following the release of his UVP monitor, he validated his method for rotating flow (Takeda, 1991) within 5% accuracy for velocity and 1% for position. Many studies have been conducted with water to verify the UVP method including: Taylor vortex flows after sudden start (Takeda, 1990), oscillating pipe-flows (Teufel, 1992; Yamanaka, 1999), thermal striping and vertical planar jet (Tokuhiro, 1999), turbulent pipe flow (Alfonsi, 2001), and surface switching of a rotating fluid (Tasaka, 2008). A significant advantage UDV has over optical techniques such as LDV or PIV is the ability to analyze opaque fluid flows such as liquid metals. Additionally, in highly viscous flow where intrusive probes disturb the flow the UVP could be placed outside the flow container (Takeda, 1999).

Takeda first validated the UVP method for opaque fluids in 1987 for liquid mercury (Takeda, 1987). Among others, Eckert and Gerbeth have extensively studied a number of opaque fluids ranging from eutectic alloys to liquid sodium with the UVP (Eckert and Gerbeth, 2002; Eckert, 2003; Zhang, 2005; Eckert, 2007). Eckert et al. additionally explored high-temperature applications with various liquid metals by utilizing wave guides (Eckert, 2002). Several comparative studies have been made between ultrasonic and optical measurement methods. Both Takeda and Tokuhiro compared LDV and UDV techniques with the general conclusion that LDV offers slightly more accurate results while sacrificing setup and operational ease [Takeda, 1992; Tokuhiro, 1999]. UDV and PIV methods were also juxtaposed by Sano et al. in a water thermal turbulence study. They found a correlation coefficient greater than 0.9 between the two methods, which increased as the velocity range increased (Mashiko, 2005).

In using the UDV method, or any experimental measurement method, special care must be taken to ensure that the ultrasonic transducers function properly. The transducers used here are vulnerable to elevated temperatures and the sodium environment. A protective metal jacket is used to protect the transducers from the harsh sodium environment and elevated temperatures. The effect of this jacket on the ultrasonic beam requires careful consideration, as it must travel through multiple layers of different mediums.

2.3 Acoustic Transmission through Multiple Layers

As with any measurement method, UDV instruments have limits of appropriate application. A notable challenge is that most ultrasonic transducers are limited to about 60°C. Developments in materials and manufacturing have led to some commercially available high temperature transducers that are capable of operating at temperatures up to 150°C and 250°C. However, these high temperature transducers are much more expensive and the common 60°C transducers have been used here. This necessitates the design and fabrication of a protective jacket that will enable the transducer to operate at elevated temperatures and protect it from the harsh sodium environment. Another limitation is that acoustic signals tend to be weak compared to the power required to produce the signal. This is true in most

acoustic phenomena. For example, the efficiency of speakers may be only 1% to 2%. Consequently, the signal tends to attenuate rapidly when different material layers are introduced between sensor and test medium. Because of material compatibility issues with sodium, the proven compatible and material of choice for shielding against liquid sodium is stainless steel. If appropriate coupling materials are used to acoustically connect the transducer, while still providing insulation to the transducer, a large portion of the signal can be transmitted. The degree to which this transmission occurs is described by a transmission coefficient (T_i). It is important to note that for measurable levels of sound to return to the device, the wave must be transmitted through each layer twice.

It was initially assumed that the transducers required a layer of insulation due to the elevated temperatures. As the system was analyzed, it was realized that results were unsuitable for the given parameters; specifically, porous media is generally formed with a large percentage of volume filled with air and so, good insulators are generally very poor acoustical transmitters. Mohammadi et al. investigated transmission loss through a triply layer panel. The triply layer panel had two solid layers with a middle layer of air or liquid. Theoretical models were compared with experimental results, and Mohammadi concluded that for a middle layer of air and a frequency above 780 Hz there is high transmission loss of the acoustic wave (Mohammadi, 2009). This means for the present research with the use of 4MHz transducers air gaps will not allow for effective acoustic transmission. Mohammadi also demonstrated that fluid density is an influential parameter in the transmission loss values. Different fluids with similar densities produce similar results.

Eckert et al. (2007) investigated the issue of acoustic transmission through stainless steel while studying sodium flow through a square duct under a magnetic field. Eckert determined that there are three major requirements for effective acoustic transmission. These are 1) effective coupling between the transducer face and the solid barrier, e.g., stainless steel wall, 2) proper barrier thickness for maximum transmission, and 3) effective wetting (coupling) between the barrier and the fluid of interest (Eckert 2002). All three of these requirements are related in the fact that in order for there to be effective transmission of sound waves through layers of different materials the difference in the acoustic impedances between each layer must be minimized. In order to minimize the impedance between layers, or maximize the transmission coefficient, Eckert uses the equation below.

$$T_i = \frac{1}{\sqrt{1 + \frac{1}{4}\left(m - \frac{1}{m}\right)^2 sin^2 \frac{2\pi d}{\lambda}}}$$

where T_i is the transmission coefficient, m is the ratio of acoustic impedances between layers; in this case liquid sodium and steel, d is the thickness of the steel plate, and λ is the wavelength in the plate. It should be mentioned that this equation assumes that the steel plate and incident wave are perpendicular to each other. In Eckert's experiment he coupled the transducer face to the steel plate using silicon grease. He also assumed that the impedance of the silicon grease ($Z_{gr} = 1 * 10^6\ Ns/m^3$) and liquid sodium ($Z_{Na} = 2 * 10^6\ Ns/m^3$) were approximately the same. This is a valid assumption because the impedance of both sodium and grease are equally small compared to that of stainless steel ($Z_{st} = 45 * 10^6\ Ns/m^3$).

Using the above equation Eckert determined the plate thickness, d, which maximized the transmission coefficient, T_i, was 2.21mm. The transmission coefficient as calculated above is plotted for different materials in Figure 2.1.

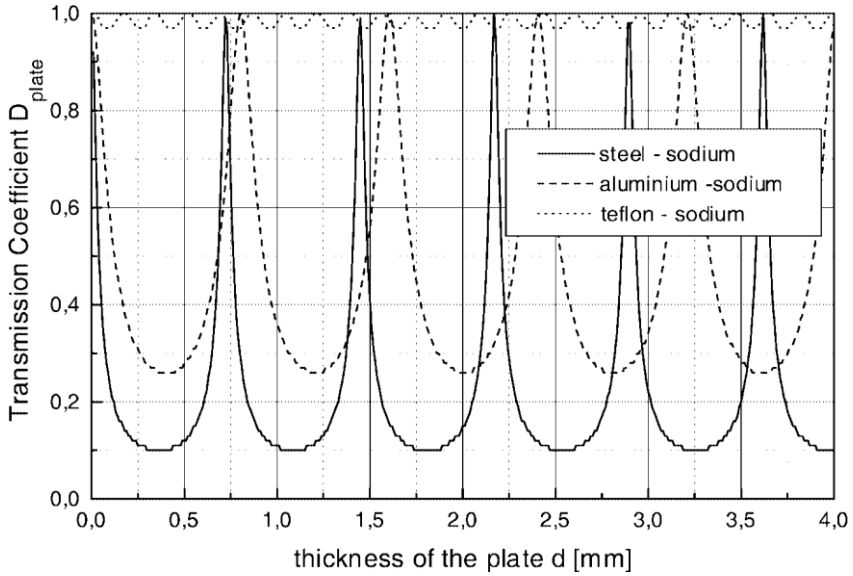

Figure 2.1. Eckert plot of ultrasonic transmission coefficient (Eckert, 2002)

Due to the large impedance of stainless steel the resonance peaks are very strong and narrow. Outside of the peaks only about 10% of the wave is transmitted through the steel plate.

In this research it is proposed to use an array of transducers to provide a planar mapping of both temperature and velocity within the flowing sodium. As noted earlier, it is critical to achieve a high T_i. This can be achieved by coupling the transducer to the protective jacket wall using gel or grease, and by properly sizing the jacket wall. Theoretically, it is possible to have nearly perfect transmission through an appropriately sized wall. However, as seen in Figure 2.1 the very narrow resonance peaks make it difficult to obtain with reasonable manufacturing tolerances. Still, it is possible to have near 90% transmission with reasonable tolerances.

2.4 Basic Jetting Flow Characteristics

Much has been documented on the subject of jet flow and jet behavior under many flow conditions. The submerged jet is the area of focus and emphasis in this research. Figure 2.2, below, is a diagram of a simple submerged jet. A submerged jet is a laminar and/or turbulent jet that spreads into a larger (finitely large) medium of the same fluid at rest. The outer boundary of the jet is defined as the point where the velocity with respect to the jet axis, x-axis, is zero. Eddies are formed in the region along the jet boundary. These eddies result in mass entrainment into the jet and subsequently result in the transfer of momentum and energy across the boundary. They also form a region of finite thickness where there is a continuous distribution of velocity, temperature, and particle concentration, if there exists a concentration gradient. This is the turbulent jet shear layer or mixing layer (Tennekes & Lumley, 1973).

In the initial stages of development, the jet consists of two mixing layers (on either side if planar) separated by a core of irrotational flow. At the jet exit the shear layer has zero thickness. As the flow continues to develop the two mixing layers merge into a single, larger layer. There is a short transition region where the velocity profiles change slightly with axial distance. After the short transition region the velocity profiles become similar in shape and only change in magnitude. This is the fully developed or self-preserved region (Tennekes & Lumley, 1973). The shear layer will continue to grow as the jet slows and the surrounding fluid is entrained. The static pressure remains constant at each flow cross-section and relative to the external fluid. This results in a constant momentum condition at each flow cross-section. All of this leads to the broadening of the jet velocity profile and decreasing velocity magnitude with increasing distance from the virtual jet source as indicated in the Figure 2.2.

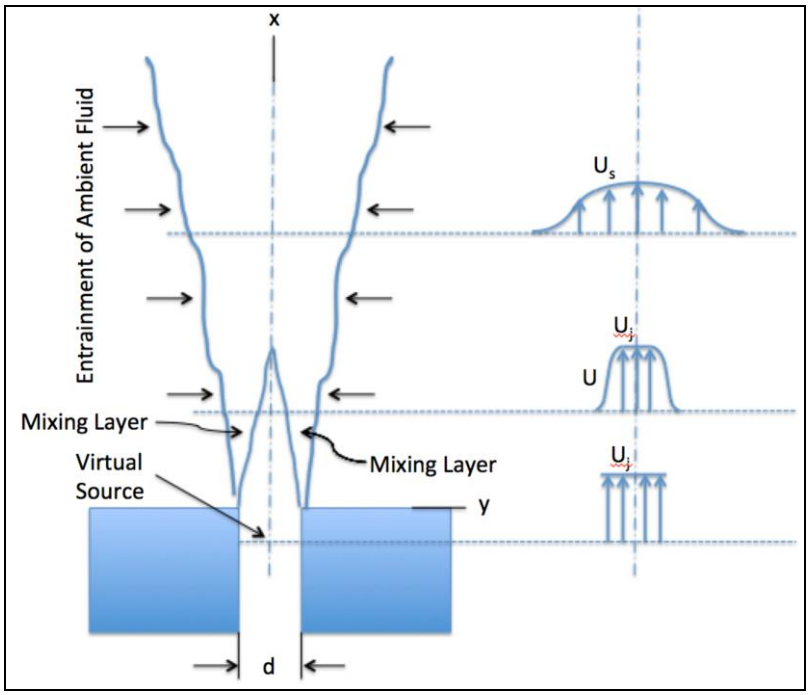

Figure 2.2 Submerged jet flow

Many experimental investigations have been conducted to demonstrate an idealized turbulent jet shear flow. One investigation that has been conducted, and that has particular importance to the current study, was performed by Tokuhiro (1999). Tokuhiro experimentally captured submerged jet flow behavior using the LDV and UDV methods in a single water jet injected vertically into a larger pool volume of water, and compared the results with experimental results presented by others. Two plots from Tokuhiro's work help to visualize the dispersion of momentum axially and transversely. An ideal jet is characterized by the decay of its centerline velocity with respect to axial distance from the jet exit, and the jet half radius also along its axial distance; see Figure 2.3 and Figure 2.4 respectively. The nearly constant velocity magnitude region in Figure 2.3 between z/d equal to 0 and 4 show the core region. The constant positive slope at z/d greater than ~4 shows that as axial distance increases the magnitude of the velocity decay increases, or in other words, the magnitude of the centerline velocity decreases. Based on the centerline velocity decay along the axial component and the

jet half radius, the width of the jet when the velocity is half of the maximum, the thermal-hydraulic flow development and flow regions were characterized. We note the fortunate circumstance that the same UDV instrument (Met-Flow) that supported Tokuhiro's experimental UDV work supports the current work.

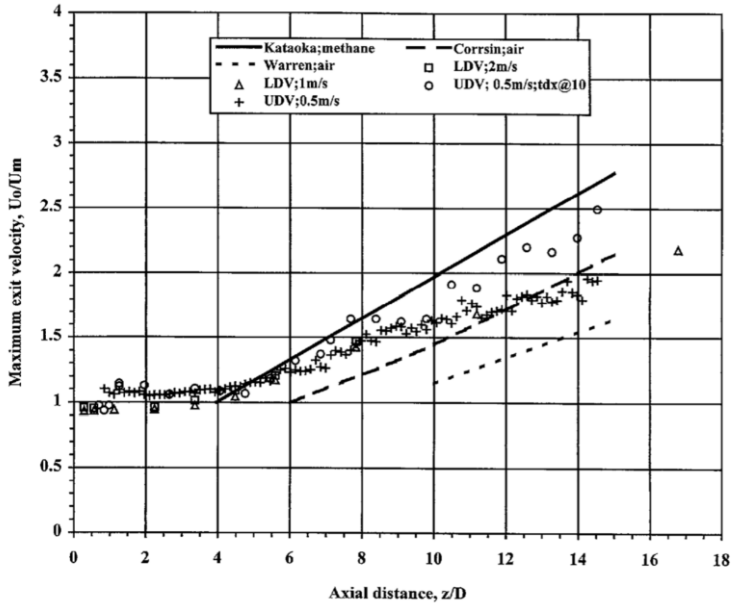

Figure 2.3. Centerline velocity decay vs. axial distance (Tokuhiro, Experimental Investigation of a Vertical Planar Jet by Ultrasound and Laser Doppler Velocimetry, 1999)

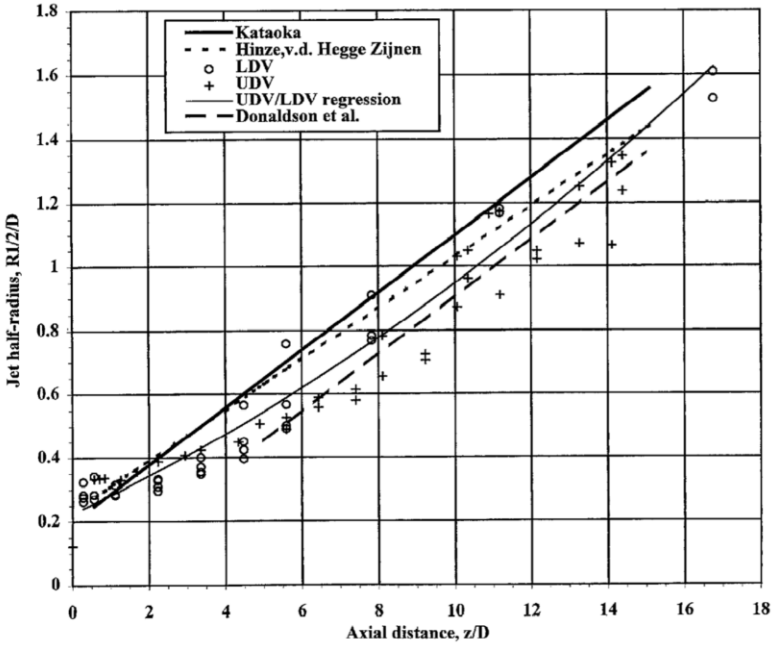

Figure 2.4. Jet half radius vs. axial distance (Tokuhiro, Experimental Investigation of a Vertical Planar Jet by Ultrasound and Laser Doppler Velocimetry, 1999)

Parallel vertical jets dispensing into still surroundings of a larger volume tend to merge into a quasi-single jet at a certain downstream location of these jets. That is, if they are in proximity of each other at the exit. The mixing of parallel jets of different temperatures and velocities play an important role in the design and operation of sodium cooled nuclear reactors. The interaction of these turbulent jets can be a complete mixing of the fluids, however, the incomplete mixing of these jets leads to the thermal striping phenomena. Thermal striping is a potential safety concern to the long term operation of a SFR due to the thermal stresses on structures from poorly mixed streams of coolant flowing from the core. Thermal striping occurs at different locations in the reactor assembly, but mainly at the interface of the core cover plate and upper instrument structure (UIS). Figure 2.5 shows the 'next generation' Japan Sodium Fast Reactor (JSFR) reactor vessel and internals with the flow conditions at the reactor core exit enlarged and to the side. In an effort to economize the design, more components are located internal to the pool. This reduces the coolant volume (for a given vessel) and increases the stipulated flowrate (and velocity) of coolant through the core. The typical design characteristics of the JSFR were used as a reference prototype design in this research, and characteristic outlet parameters are summarized in Table 2.2.

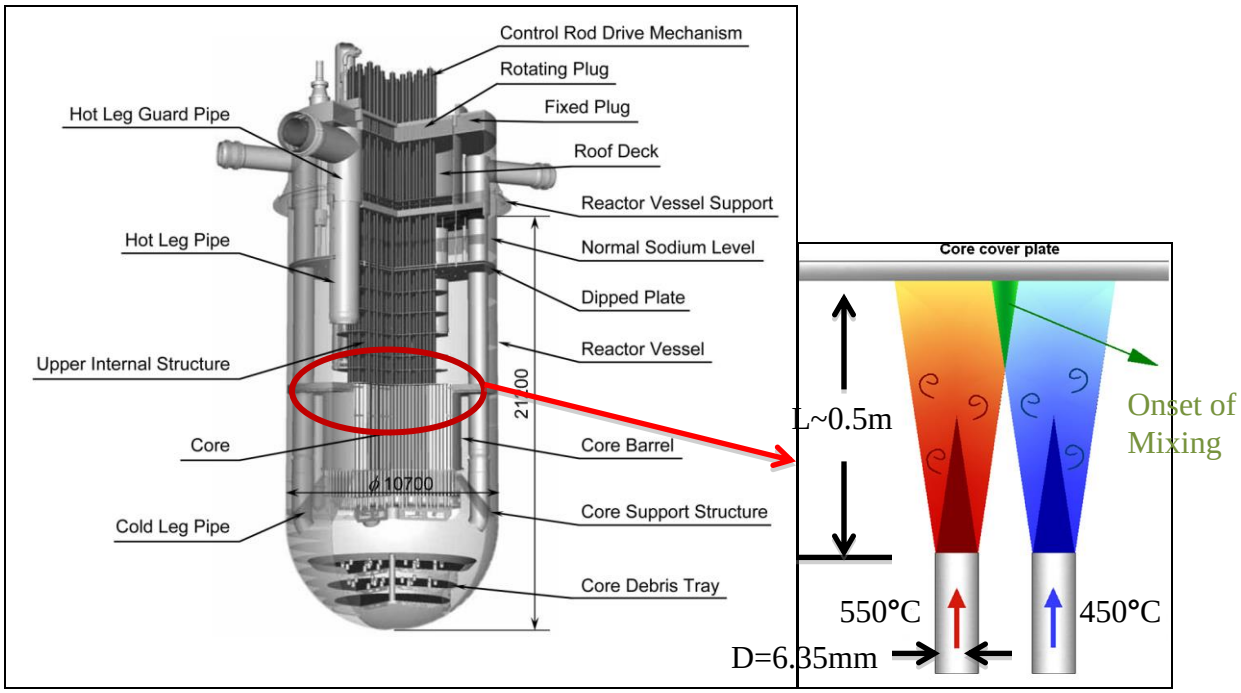

Figure 2.5. JSFR reactor vessel and internals

Table 2.2. Characteristic outlet conditions at core exit of prototype SFR (Omotowa, 2013)

Parameter	Values
Outlet temperature (K)	773
Outlet velocity (m/s)	2.3-5
Inner diameter of flow channel (mm)	6.5

Durve et al performed a numerical study of mixing in parallel jets and an important summary of what is currently known on the subject (Durve, 2011). Much of the discussion in this section is referenced from their work.

Early studies by Miller and Comings in 1960 and Tanaka in 1970 and 1974 showed the basic flow and entrainment mechanisms. The general flow field of two parallel jets they describe is shown in Figure 2.6. Three important regions of the flow field were identified, namely, the converging region, the merging region, and the combined region. The converging region is from the jet exit to what is known as the merge point, the point where the two inside shear layers of each jet merge together.

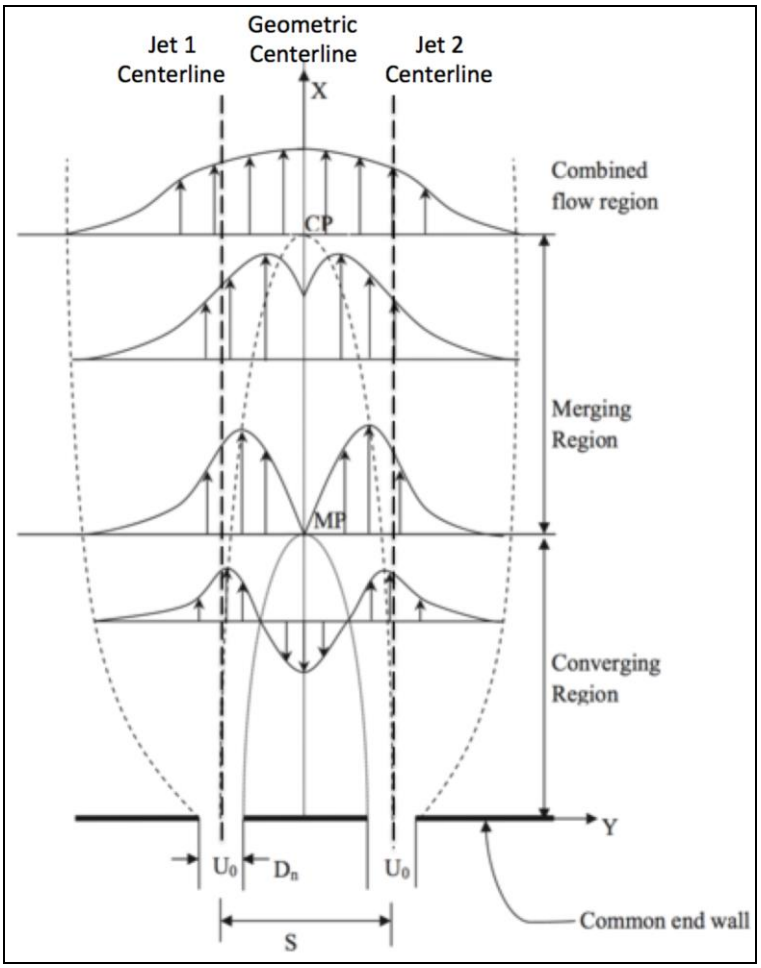

Figure 2.6. General flow field of two parallel jets

MP identifies the merge point in Figure 2.6. At the jet exit the high fluid velocities lead to entrainment of fluid in the shear layer of the jets. In the region between the two jets there is a high entrainment rate, which leads to low pressures in the region. Therefore, the jets are drawn toward each other. At the merge point the velocity in the axial direction of flow is theoretically zero. The highest pressure in the flow field also occurs at the merge point. The high pressure is responsible for redirecting the flow in the axial direction and a partial reversal of the flow in the converging region between the jets.

Following the converging region is the merging region. The merging region begins at the merge point and continues to the combine point. Mixing between the two jets occurs in the merging region. The combine point is defined as the point where the axes of the two jets merge, and the two jets begin to resemble a single, self-similar jet. The combined point is also where the maximum velocity in the primary flow direction on the axis of symmetry occurs. CP identifies the combine point in Figure 2.6. The combined region is downstream from the combined point.

The profiles of the mean velocity and static profiles along the flow field were investigated by Marsters in 1977 and Elbanna et al in 1983. They measured the mean velocity profiles of each jet and found them to be self-similar in the converging and combined regions. The spreading rate of two-jet flow in the combined region also measured similarly to a single planar jet. Elbanna and Sabbagh in 1987 studied the effect of jets with different velocities. They showed that the jet with the slower exit velocity was drawn toward the jet with the higher exit velocity. A sub-atmospheric pressure region is established at the entrance region between both jets, and the higher entrainment rate on the faster jet causes the slower jet to shift towards the faster jet. They also observed that this attraction of the weaker jet to the stronger jet shifts the merge point upstream.

Anderson and Spall in 2001 studied the ability of standard k-ε turbulent model and Reynolds Stress Model (RSM) to predict the two-jet flow field. Anderson and Spall used experimental data collected by hot wire anemometry and found that both turbulence models could accurately predict the location of the combine point, but over-predicted the mean velocity profiles in the combined region by 3-5%. Durve et al also compared experimental results with simulations from the previously mentioned investigators and found that the locations of the merge point and combined point varied considerably between the investigators.

Spall in 2002 used the standard k- ε model to study the effect of buoyancy on the merge point. The buoyancy effect was investigated by injecting two jets of the same temperature into a tank filled with fluid at a lower temperature. Spall showed that a small change in the buoyancy has a considerable effect on the merge point. Increasing the buoyancy causes the merge point to shift downward in the axial direction, or closer to the jet exit. The maximum temperature difference between the jets and the tank fluid was ~15 K.

Suyambazhahan et al in 2007 used similar simulations as Spall to study the effects of Reynolds number, nozzle spacing, and buoyancy on the fluctuations of the temperature and velocity fields. The buoyancy was found to have a significant effect on the velocity fluctuations even at high Reynolds numbers (9,000-12,000). It was also observed that increasing the jet spacing, s/d=15 to s/d=60, resulted in a decrease in the frequency of the velocity fluctuations but an increase in the amplitude of the velocity fluctuations.

Other researchers have focused more on the thermal mixing phenomena and the effect of the presence of additional jets. Tokuhiro and Kimura focused more specifically on the thermal mixing phenomena by using a three parallel jet system, where the two outside jets were heated to a higher temperature that the middle jet to simulate SFR outlet flow. They made

velocity profile measurements using ultrasonic velocimetry, while temperature measurements were made using thermocouples. It was observed that when the velocity of the outside jets was increased it delayed the onset of mixing. It was also shown that when the temperature difference between the outside jets and the middle jet was increased from 5 K to 10 K the buoyancy forces tend to suppress the turbulent temperature flucuations (Tokuhiro & Kimura, 1999). Other investigators have used these results to conduct numerical studies in an effort to understand the thermal mixing phenomena.

Nishimura et al used the standard k- ε model and Low Reynolds number Stress Flux model (LRSFM) to carry out numerical simulations to predict thermal mixing. They discovered that the LRSFM could predict mean profile quatities of flow. However, the k- ε model consistently underpredicted the amount of mixing. Both turbulent models overpredicted the values of the temperature fluctuations. They also noticed that the periodic jet oscillations contribute to the overall mixing (Nishimura, 2000).

Later, Kimura et al used the experimental results previously attained with Tokuhiro and conducted a numerical study using a k- ε model, a LRSFM, and direct numerical simulation (DNS). They showed that LRSFM could predict the temperature fluctuations from flow instability, but could not predict the overall mixing phenomena. The only model that was able to predict the overall mixing was through DNS (Kimura, 2002).

Chandran et al continued to investigate the effect of multiple jets on the thermal mixing phenomena by using a numerical 10-jet water model. They used the Reynolds stress model to forecast the temperature fluctuations near the solid structures in a LMFBR core. They used seven 'hot' jets in a row, corresponding to jets coming from the core fuel zone, followed by three 'cold' jets corresponding to jets coming out of the blanket zone. In the case where the velocity of the hot jets and the cold jets were equal the maximum temperature fluctuations near the solid structures was observed. As the velocity ratio, $V_{hot}/V_{cold,}$ was increased the location of the maximum temperature fluctuations shifted toward the cold jets. Beyond a velocity ration of 1.0, the temperature fluctuations reduce as the velocity ratio increases (Chandran, 2011).

2.5 Literature Review Summary

The above works have focused on investigating improved methods and instruments for collecting flow velocity data, and determining the basic flow characteristics of two parallel jets, the thermal mixing phenomena of three and more jets, and identifying the critical factors influencing mixing. The next step in continuing to research the thermal mixing of jets with application to SFR R&D is to build an apparatus that is capable of generating detailed mixing data by using improved instrumentation, and to characterize thermal mixing in terms of dimensionless parameters in an effort to 'quantify' mixing in each mixing region.

Chapter 3: Experimental Setup and Measurement Methods (fix figure references in text)

3.1 SEPARATE EFFECTS TEST FACILITIES and VELOCIMETRY

Isothermal and buoyant single-jets are well-documented and the thermal mixing of three parallel jets for both ordinary and low Pr-number fluids has been studied by Kimura, Nishimura and co-workers both experimentally and computationally, we proposed to design and construct a separate effects test facility, initially configured to study two parallel jets with different velocities and temperature. An isothermal jet is here defined as a jet at a given temperature flowing into a larger volume at the same temperature; positively or negatively buoyant jet respectively at higher and lower temperature than the volume into which they flow into.

The work proposed designing, construction and operating separate effects experiments using two low Pr-number fluids, mercury (Hg) and sodium (Na); the former, since it is the fluid of choice at SNS and the latter as coolant for the SFR. Further, though toxic, its oxidation reaction does not pose a physical hazard and can be controlled and monitored by documented means. Lastly using both Hg and Na provides a means to investigate and compare the convective flow and heat transfer differences in liquid metals (LMs) due to approximate order of magnitude difference in Pr-number (~0.025 for Hg vs. 0.005 for Na); that is, an evaluation of both experimental and computational sensitivity and 'resolution' to small relative influences in thermal-physical properties.

The set-up will be similar in layout to an existing DOE laboratory sodium facility so that a common reference is maintained for the present and future collaborations; in fact, if possible connecting flanges and piping will be identical so that we create an option to exchange and share components amongst all three facilities. Thus inside a suitable confining volume with an auxiliary system similar to the existing DOE facility, we will design and configure two parallel jets, very similar to the triple-jet t arrangement shown in Figure 1 by Kimura et al. In fact, a very similar ultrasonic Doppler velocimeter will be used in our experiments in both sodium and mercury. In both liquid sodium and mercury, we will focus on generating spatio-temporal convective heat transfer data for detailed validation of turbulence dissipation and wall treatment models.

3.2 Separate Effects Facility and Thermal Mixing of Two-Jets

Each university participant will design and construct a separate effects test facility, respectively planned for low Pr-number fluids, sodium and mercury. Other than the test section which will be specific to the proposed SOW, each university will adopt an auxiliary system (pump, tanks, fittings, piping, valves, etc.) to the extent possible that takes the DOE laboratory's system as the reference facility. We propose this so that the three institutions can 'exchange' components and test sections under the present and future collaborations. Cursory details of the experimental apparatus is shown in Figure 3.1. The test section will consist of outer and inner enclosures with the 'annular' space serving as the return overflow to the auxiliary system (see Fig. 3.1). The two streams will be pre-conditioned via differential

heating (resistance) and cooling (via liquid to gas heat exchanger) and differential electromagnetic (EM) pumping conditions. Per Kimura et al. we will also maintain the option to heat one stream relative to the other which we will keep at the bulk loop temperature. In order compare results, the temperature difference and velocity ratio between the heated (h) and unheated (c) jets will initially be, ΔT_{hc}=5°C, 10°C and R=($V_{cold,exit}/V_{hot,exit}$)=1.0 (isovelocity), 0.7, 0.5 respectively. The corresponding typical Reynolds number will be Re_D=1.8 x 10^4, where D is the hydraulic diameter of the exit nozzle. Velocity measurement of single-jet and dual-jet arrangement will be taken by ultrasound Doppler velocimetry (UDV) while temperature data will be taken using a vertically traversed thermocouple array. Since UDV may be the only means by which higher fidelity spatiotemporal measurement can be obtained in LMs, we provide a short introduction below.

One purpose of this project was to build a small yet purposeful liquid sodium loop capable of generating thermal mixing data from two, submerged, parallel jets. Much work was done to construct such an apparatus that could facilitate a two-jet system wherein fluid flow might be analyzed in a safe, convenient and effective manner. The main parts of the apparatus are the test section, the instrumentation tank, transfer tanks, instrumentation movement, and piping network. Other critical items were the data acquisition system (DAQ), user interface, and gas, pressure and electrical systems. The design of the apparatus was based off sodium to be the experimental fluid. Sodium is referenced throughout this chapter as the operating fluid, however, only water data has been collected in the apparatus. The operating procedure is the same for any fluid. This chapter summarizes the design, setup, and operation of the liquid flow loop and the methods used to generate mixing data. For greater detail on each component in the loop and the operating procedure, reference Appendix A.

3.3 Test Apparatus Arrangement and Control

The loop consists of a Lower Transfer Tank (LTT), an Upper Transfer Tank (UTT), and an Instrumentation Tank. The instrumentation tank is divided in two sections. The upper portion is the instrument area and the lower is the test section. The test section contains the weir, where all the measurements take place. Figure 3.1 below shows the basic loop components and arrangement.

Two parallel jets are created within the weir assembly in the test section through the use of gravity and pressure. Gravity drives sodium from the UTT down through the piping and up through the bottom of the weir. Pressure drives sodium from the LTT through the piping in up through the bottom of the weir. The two jets penetrate a quiescent reservoir of sodium inside the weir. The sodium is allowed to spill over the top of the weir into the outer area where it can be drained back into the LTT. The two jets are 6.35mm in diameter (D=6.35mm) and are spaced two jet diameters (s=2D) center to center.

Figure 3.2 is a picture looking from the instrument area down into the weir. The experimental measurements are taken in the circular region of the weir. The rectangular portion of the

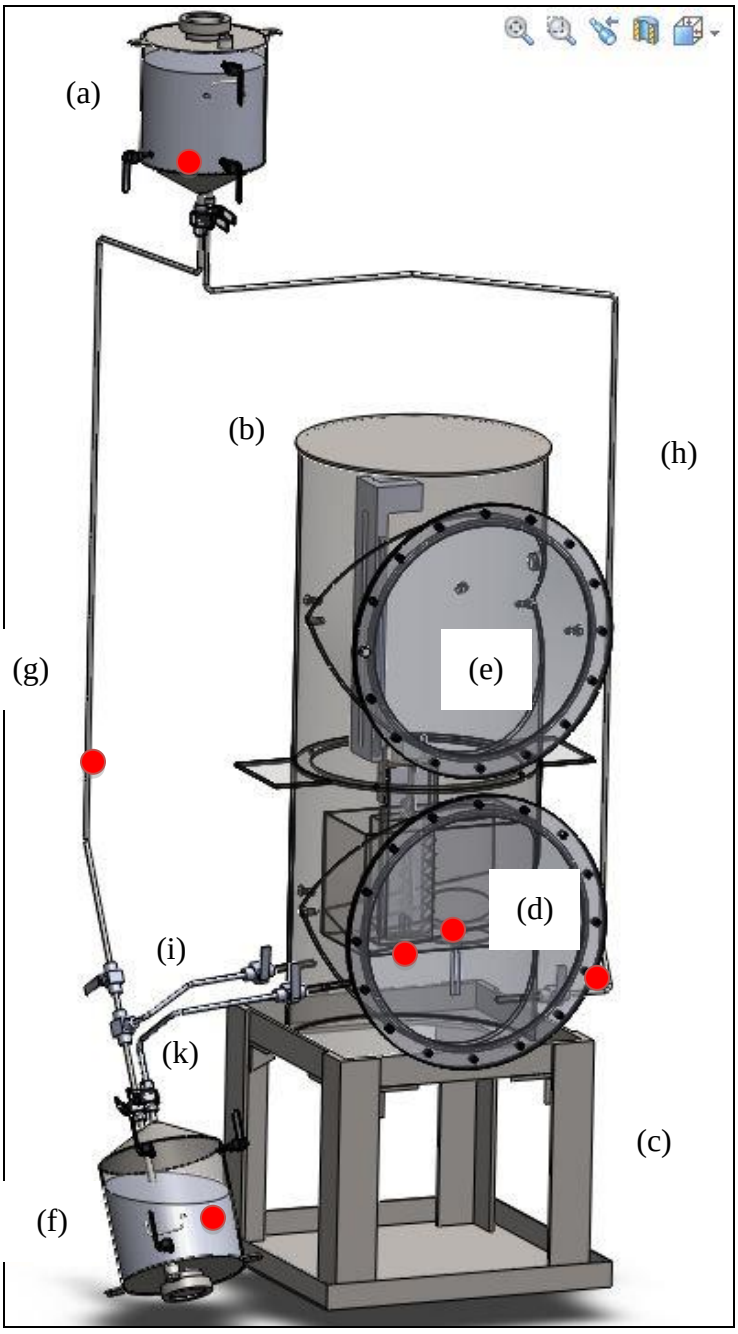

Figure 3.1. Basic elements of sodium loop; (a) Transfer Tank (expansion tank), (b) Instrumentation Tank, (c) Support Base, (d) Test Section (Weir Assembly), (e) Instrument Area/Multiple Transducer Cooling Jacket, (f) Transfer Tank (Dump Tank), (g) Transfer Line, (h) Gravity Jet, (i) Pressure Jet, (k) Drain. Red dots indicate the location of control thermocouples.

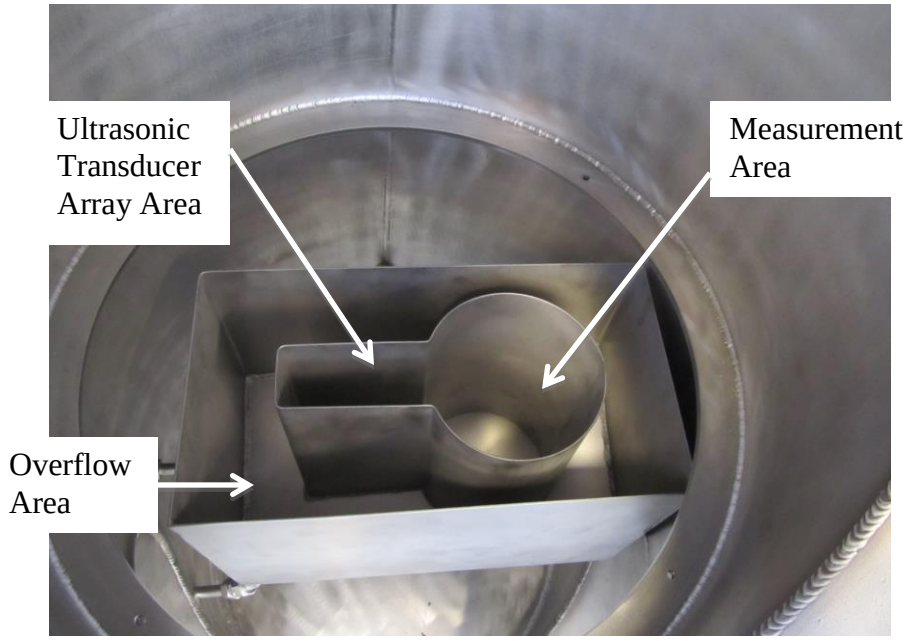

Figure 3.2. View of weir assembly from above.

weir allows an array of ultrasonic transducers to be lowered into the reservoir of sodium in the weir and capture the velocity profile.

The test procedure always begins with liquid sodium in the LTT. This means prior to initiating the test procedure the LTT must heated to melt and heat the sodium to the desired test temperature. Remotely actuated valves, see Figure 3.3, control the flow of sodium within the loop. To begin, the LTT is pressurized and the transfer valve is opened and sodium is allowed to flow from the LTT up into the UTT and timed. When the desired amount of time has passed and sodium is in the UTT the transfer valve is closed. Next, the both the gravity jet valve and the pressure jet valve are opened and both jets are allowed to flow into the weir and measurements are taken. When the when the velocity and temperature measurements have been recorded the jet valves are closed and the LTT is vented to relieve the pressure. Then the drain valve is opened and the sodium from the weir overflow is drained back into the LTT and the process is repeated. The pressure inside the LTT controls the velocity of the pressure jet. This provides the ability to change the velocity of the pressure jet and create the velocity ratios of 0.3 to 1.0 between the two jets. The pressure is monitored by a pressure gauge on the gas inlet to the LTT, and controlled by a throttle valve.

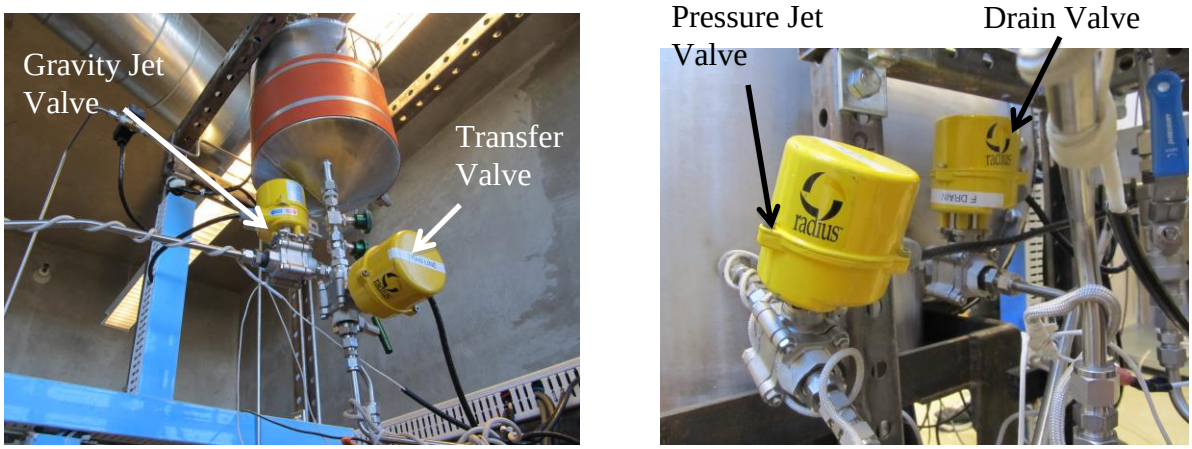

Figure 3.3. Remote actuated valves for (a) transfer line and gravity jet, and (b) pressure jet and drain.

A necessary feature of the loop to operate with sodium is to maintain an inert atmosphere. A gas manifold provides a central location to control the atmosphere inside the apparatus, and control the gas flow and pressures throughout the loop, see Figure 3.4.

Temperature controllers and k-type thermocouples are used to control and monitor the temperatures throughout the loop. The red dots shown in Figure 3.1 are the locations where thermocouples are installed to control the process temperature. Temperature control is important to maintain each jet at the correct temperature and create the temperature difference between the jets. The LTT and UTT have independently controlled heaters, so the temperature of either jet may be increased or decreased. In this study the temperature of the UTT is held constant and the temperature of the LTT is adjusted to create a temperature difference of 10°C to 30°C between the jets.

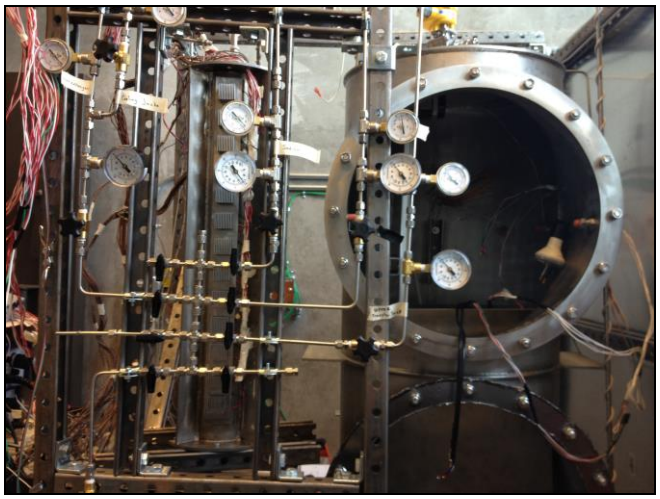

Figure 3.4. Front view of gas manifold, pressure and flow gages.

Experimental temperature readings within the weir are recorded also using k-type thermocouples, a National Instruments DAQ, and Labview software. Thirty thermocouples are available inside the instrument tank for experimental temperature readings and five other

thermocouples are available for process control. Figure 3.5 shows the thermocouple penetrations into the instrumentation tank and temperature controllers. Figure 3.6 shows unenclosed thermocouples connecting to the terminal blocks that are connected to the DAQ.

The Met-Flow 4MHz ultrasonic transducers used for collecting the velocity data are lowered into and raised from the test section by an electric linear actuator. The transducers are mounted at a 20-degree angle from the horizontal inside the protective cooling jacket; see Figure 3.7. The cooling jacket is made of stainless steel and provides a protective barrier between the sodium and the transducers. It was suggested (Tokuhiro, personal reference)

Figure 3.5. Thermocouple Penetrations on Instrumentation Tank and temperature controllers

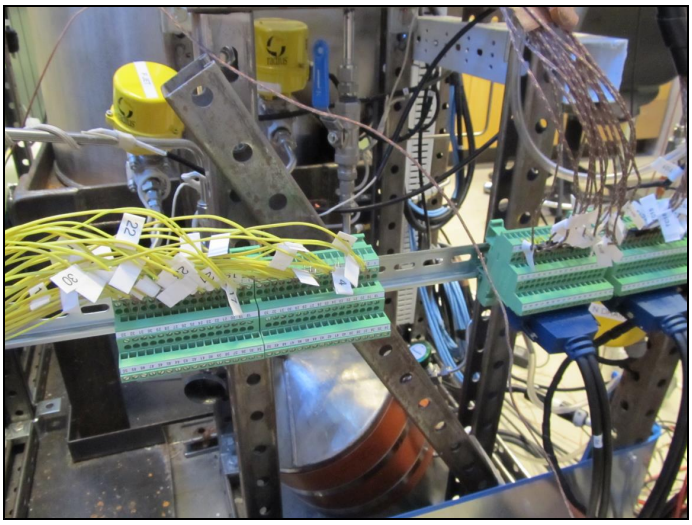

Figure 3.6. Thermocouple terminal blocks and connection to DAQ

Figure 3.7. Transducer Cooling Jacket on Linear Actuator

that the Joule-Thomson effect could be used to cool the transducers. Simply, as a gas expands, the average distance between molecules grows. Because of intermolecular attractive forces, expansion causes an increase in the potential energy of the gas. If no external work is extracted in the process and no heat is transferred, the total energy of the gas remains the same because of the conservation of energy. The increase in potential energy thus implies a decrease in kinetic energy and therefore in temperature. The cooling jacket exhausts the gas flowing through it into the instrument area of the apparatus.

The Joule-Thomson coefficient is the rate of change of temperature with respect to pressure in a Joule-Thomson expansion process (constant enthalpy). Figure 3.8/ 7 shows the Joule-Thomson coefficient for argon gas expanding to atmospheric pressure. With a starting temperature about 20°C the Joule-Thomson coefficient is approximately 0.4. This means a pressure drop of about 2 atmospheres, for example, will yield a 1°C temperature drop in addition the forced convective cooling.

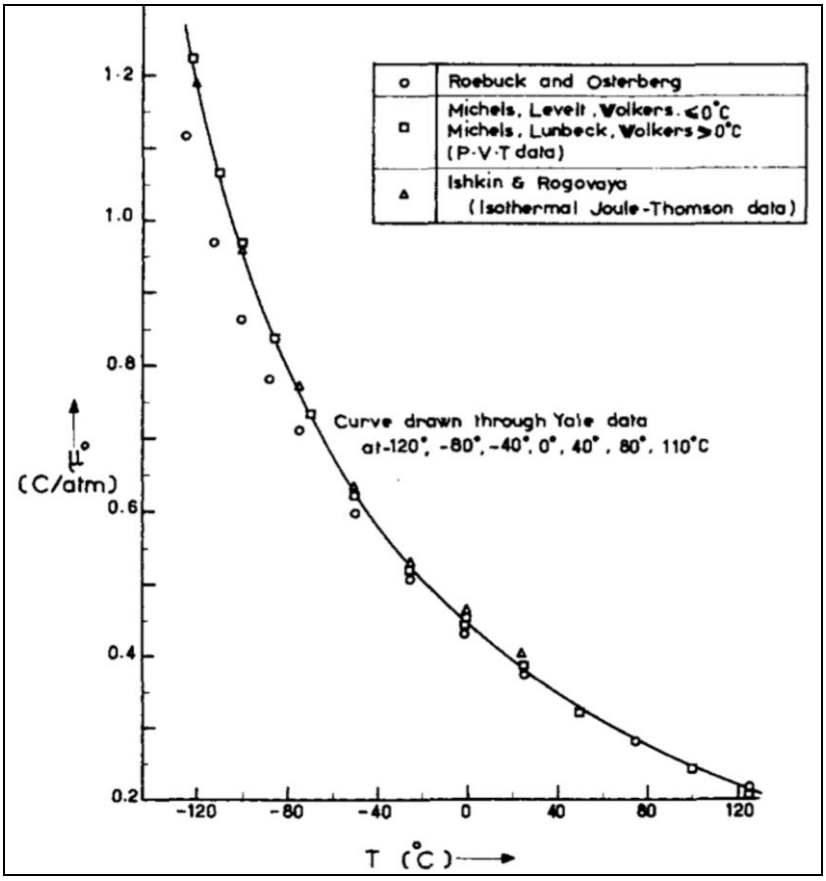

Figure 3.8/ 7. Experimental Joule-Thomson coefficients at zero pressure for argon (Strakey, 1974)

3.4 Ultrasonic Velocity Profile Method

The UVP monitor instrument used in this research was manufactured by Met-Flow S.A. (Met-Flow, 2002), and consists of three components: the measurement probe, the main unit (Figure 3.9), and the user interface. The measurement probe is a small (typically ~8mm diameter) piezoelectric transducer and is connected to the main unit by a magnetically shielded cable. Electrical signals from the transducer are processed and digitized by the main unit. These signals are then sent to a computer from the main unit by the user interface software, where the data is stored and analyzed.

Figure 3.9. UVP-DUO monitor main unit (Met-Flow, 2002)

The Met-Flow UVP Monitor Model UVP-DUO and the 4 MHz transducer is employed in the present research, and the user's guide gives a good summary of how the UVP works and how to use it. To explain the UVP measurement process, Equations 1-9, provided below (Met-Flow, 2002) are used. This transducer is a piezoelectric device that emits a plane wave. Piezoelectric transducers convert electric pulses into mechanical waves and can convert mechanical waves into electric pulses. They achieve this by electrostriction. Electrostriction is a property of dielectric materials. When an electric field is applied the molecules in the material align with the electric field causing the material to have a minute change in dimension, creating a mechanical wave. The transducer also consists of various other layers and components, and is shown in Figure 3.10/ 8.

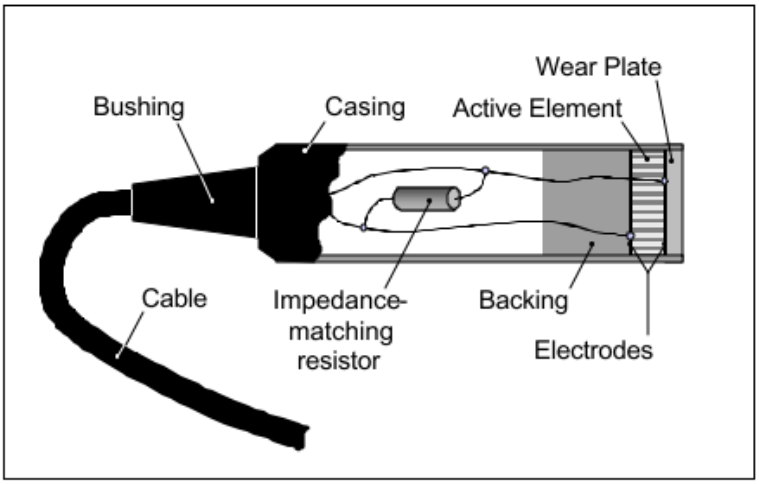

Figure 3.10/ 8. Cross-section of Ultrasonic Transducer (Met-Flow, 2002)

The piezoelectric transducer first emits an ultrasonic wave burst into the fluid (similar to a speaker) and then switches to a receiving mode (similar to a microphone). As the ultrasonic pulse propagates through the medium, it encounters various particles suspended in the medium, and a portion of the ultrasonic wave energy is scattered by the particles and reflected back towards the transducer. The transducer receives this echo after a time delay defined by Equation 1,

$$t = \frac{2x}{c} \tag{1}$$

Where, t time delay between transmitted and received signals [s]

x distance of particle from transducer [m]

c speed of sound in the medium [m/s]

The functionality of ultrasonic velocity profiling is based on Doppler shift theory. Consequently, it is important to know the rate at which sound propagates in the medium of interest, the velocity and position of the transmitter/receiver, and the reaction of the particulate imaged to pressure wave impingement. A sound wave that impinges a moving particle is partially reflected back towards the source. The frequency of the reflected sound wave is shifted. This shift in frequency is termed the Doppler shift or effect. The Doppler effect is a well-known phenomenon that can be demonstrated as a siren of constant frequency approaches and then recedes from a given location. As the velocity of the object changes relative to the point, the sum of the object's speed and the speed of sound are different before and after, yielding a difference in pitch. This change in frequency can be measured and ultimately provide not only the velocity of the moving particle but also the direction of the movement. Thus, the velocity magnitude and direction, indicated by the sign of the Doppler shift frequency, of the scattering particle can be determined by Equation 2 as,

$$\frac{v}{c} = \frac{f_d}{2f_0} \tag{2}$$

Where, v velocity of particle along acoustic axis of transducer [m/s]
c speed of sound in the medium [m/s]
f_d Doppler shifted frequency [Hz]
f_0 emitted frequency [Hz]

It is important to note the presence of the '2' above in Equation 9. This is due to the fact of two Doppler shifts, one from the relative motion of the scattering particle to the source, and the other from the relative motion of the scattering particle to the observer. Thus, if the UVP instrument can measure the Doppler shift frequency, f_d and the time delay, t, both the position (Equation 1) and velocity (Equation 2) of the scattering particle can be measured.

If this same principle is applied along the emitted beam line of the transducer then independent velocity measurements at discrete locations can be made. The transducers used here produce a nearly cylindrical beam with only a spread of two degrees over one meter. The sound beam is divided into discrete volumes called channels and these channels each represent a position in the flow where the velocity can be calculated. Figure 3.11 and Figure 3.12 show general transducer measurement principles and window. The width and thus, the spatial resolution of each channel is defined in Equation 3 as,

$$w = c\frac{n}{2f_0} = \frac{n\lambda_0}{2} \tag{3}$$

Where, w width of each channel [m]
c speed of sound in the medium [m/s]
n number of cycles per pulse [-]
f_0 emitted frequency [Hz]
λ_0 wavelength of emitted frequency [m]

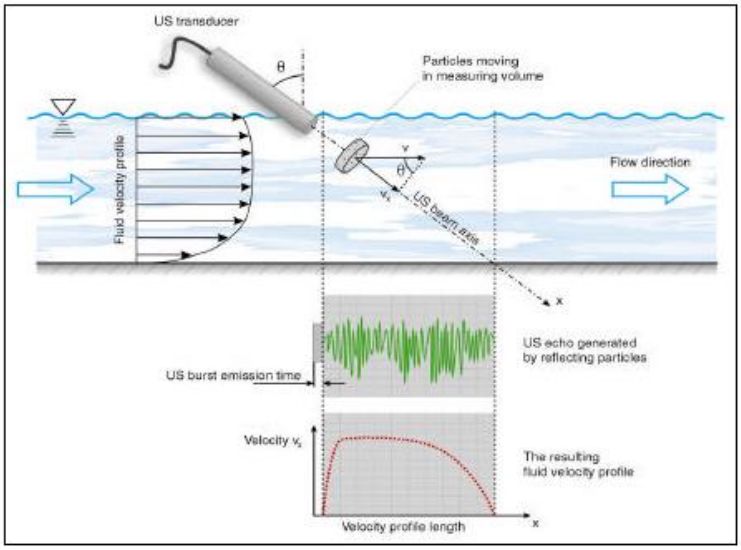

Figure 3.11. Transducer Measurement Principle and Profile (Met-Flow, 2002)

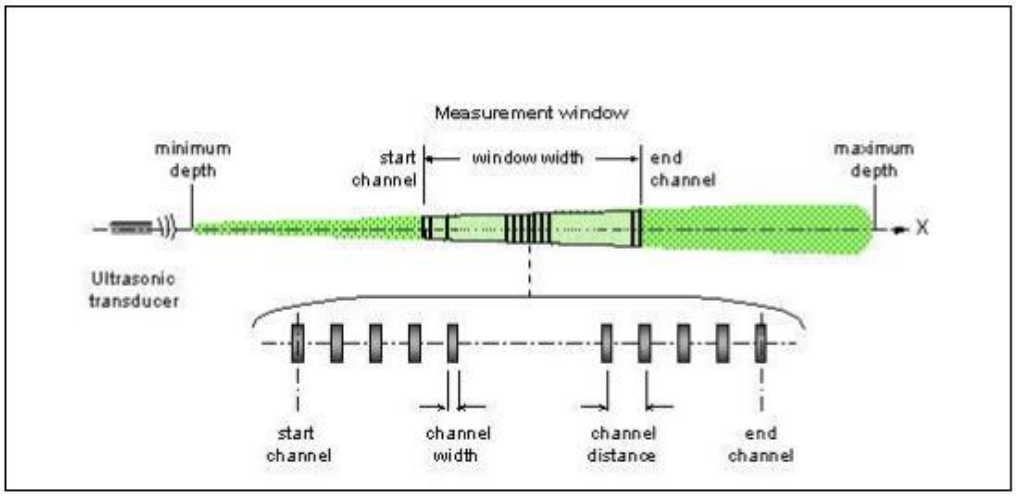

Figure 3.12. Transducer Measurement Window (Met-Flow, 2002)

Each measurement channel is equally spaced along the measurement axis and bounded by the measurement window as shown in Figure 3.12. The channel distance is defined as the center-to-center distance between two adjacent channels. During measurements, it is important to avoid channel overlapping, which occurs when the channel distance is set smaller than the channel width. The UVP instrument has the capability of operating with 10 to 2048 channels, starting with channel 1 and ending with N_{ch}. The measurement window length is defined as the distance from the center of channel 1 to the center of N_{ch} and is given by Equation 4 as,

$$W = (N_{ch} - 1) * channel\ distance \quad (4)$$

Where, W measurement window length [mm]
N_{ch} selected number of channels

A maximum depth is required because a new ultrasonic burst cannot be emitted until the previous pulse echo returns from the furthest measurement channel (N_{ch}). Thus, the maximum measurable depth that can be measured with the transducer is limited by the pulse repetition frequency, F_{prf}, as follows,

$$P_{max} = \frac{c}{2F_{prf}} \tag{5}$$

Where, P_{max} maximum measurable depth [m]
c speed of sound in the medium [m/s]
F_{prf} number of cycles per pulse

To measure the Doppler shift frequency, echo signals from each channel are oversampled in order to ensure accuracy. However, it must be noted that increasing the sampling time also decreases the time resolution. The maximum measurable velocity range is limited by the Nyquist theorem, which states that the desired maximum measurable frequency must be one-half of the sampling frequency,

$$f_{Dmax} = \frac{F_{prf}}{2} \tag{6}$$

this limits the measurable velocity range in Equation 7 to be,

$$V_{range} = \frac{cF_{prf}}{2f_0} \tag{7}$$

Combining Equations 5 and 7 then gives Equation 8,

$$V_{range} = \frac{c^2}{4f_0 P_{max}} \tag{8}$$

and finally, Equation 9, the velocity resolution,

$$\Delta V = \frac{V_{range}}{N_{DU}} = \frac{V_{range}}{256} \tag{9}$$

Where, ΔV velocity resolution [m/s]
N_{DU} number of 'Doppler units'

The number of 'Doppler units' (N_{DU}) is so defined in Equation 9 because the UVP digital signal processor uses an 8-bit word to distinguish velocity values during measurement, thus making a total of 256 possible bit combinations.

It is important to note that the ultrasonic velocimetry measurements are not direct measurements of the fluid velocity. Instead ultrasonic velocimetry relies upon the interaction of ultrasonic sound waves with particles in the fluid flow field. The critical assumptions

made with this measurement approach are that the particulate (tracer particles) returning echoes follow the motion of the fluid, and that they differ in their acoustic impedance from the fluid medium. Large impedance differences between two substances ensure a large reflection coefficient. The characteristic acoustic impedance is defined in Equation 10. If the fluid does not have enough reflectors to give an echo that represents the flow, tracer particles must be added (Takeda, 1991). The tracer particles must be larger than a quarter of the wavelength ($\lambda/4$) to ensure they work well as a reflector. For a 4MHz transducer the minimum recommended tracer particle size in water is 93μm (Met-Flow, 2002). The particles also need to be distributed over the entire volume and match as closely as possible the density of the fluid to make sure they flow with the fluid without altering the flow (Eckert, 2008), i.e., there exists a no-slip condition between the relative motion of the particle and the fluid. It is also important that the speed of sound and the measurement frequency are set to match the fluid being measured, the temperature of the fluid, and the type of transducer.

$$Z_0 = \rho c \tag{10}$$

Where, Z_0 acoustic impedance [kg/m^2-s]
ρ density of the medium [kg/m^3]
c speed of sound in the medium [m/s]

In this project Expancel 80 was used as tracer particles in the water. These particles have an average diameter of 80μm, which for a 4MHz transducer works well as a reflector.

3.5 Experimental Cases

The experimental apparatus is used to gather velocity profiles for seven different cases and temperature profiles for four different mixing cases. An early CFD scoping study compared experimentally realizable flows for Hg and Na. Table 3.1 shows the flow conditions for each of the seven cases. The four temperature profiles are taken for each of the four velocity ratios with a temperature difference of 30°C. The velocity ratio, V_r, is defined as the velocity of the cold jet divided by the velocity of the hot jet. Again, the operating procedure and UVP monitor settings for each experimental case can be found in Appendix A.

Table 3.1. Test Case Flow Conditions

Test Case Number	Velocity Ratio, V_r	Temperature Difference, ΔT
Case 1	1	0
Case 2	0.7	0
Case 3	0.5	0
Case 4	0.3	0
Case 5	0.7	10
Case 6	0.5	20
Case 7	0.3	30

Chapter 4: Thermal Mixing Analysis using CFD

4.1 University of Tennessee – Knoxville Contributions

The University of Tennessee – Knoxville's Prof. A. Ruggles served as co-PI and with his students contributed to the project. Besides a review of validation and verification (V&V) standards, they conducted thermal jet mixing and visualization experiments in support of CFD work. UTK and UI jointly used COMSOL as our common CFD tool.

4.1.1 Initial CFD Scoping Studies using COMSOL

One of the objectives of this was to provide detailed measurements of the thermal mixing of two vertical jets, experimentally but the team realized the utility of computational fluid dynamics (CFD) simulations for the initial scoping studies during the project. Since water, sodium and mercury-based experiments were planned and the latter two working fluids are optically opaque, we used CFD to characterize the anticipated thermal mixing flows. Using COMSOL CFD (version 3.5 and onward) and the provided turbulence models, verification (correctness) of the CFD software was first verified for a single-, isothermal jet configuration for which there exists relevant velocity data using laser and ultrasonic Doppler velocimetries (Tokuhiro, 1999). Although agreement is not outstanding in Figure 4.1 below, this is attributed to limitations of the standard k-ε turbulence model.

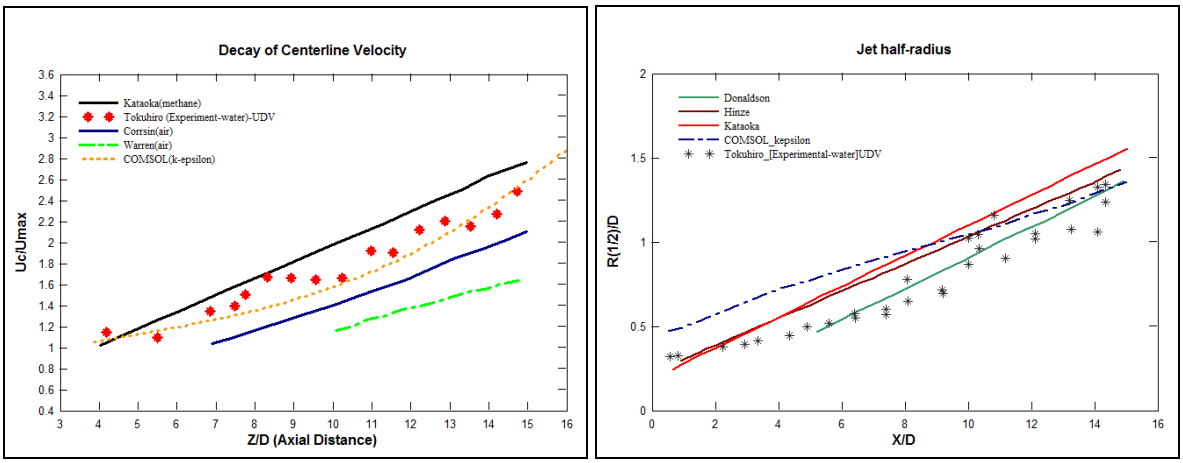

Figure 4.1a and b. Decay of the Centerline Velocity versus Axial Distance and Jet Half Radii versus Axial Distance. (Tokuhiro 1999)

Based on these results, a CFD-based scoping study to forward the design of the experiment and overlapping dimensionless parameter was carried out.

4.1.2 Review of Validation and Verification Standards

The AIAA, ASME, NRC, NEA and NIST approaches to V&V are reviewed with emphasis on common elements and discussion of differences in intent. The AIAA, ASME, and NEA standards and guidelines apply specifically to CFD. The NIST standard as applicable to fire modeling using the Fire Dynamics Simulation (FDS) large eddy simulation CFD code as

adopted by the USNRC is reviewed. The CSAU methodology was developed for reactor system simulations during anticipated transients and hypothetical accidents. CSAU is well established in the US nuclear safety community for providing best estimate simulation outcomes, with quantified uncertainties for prescribed confidence intervals.

The use of peer review, as suggested in the ASTM method for assuring the theoretical basis is correct, and as implemented in NEA and CSAU to develop a PIRT often has a broader impact than just assuring the correct models are in the simulation. The panel of experts used in developing the PIRT also provides a political base should outcomes be contested later. In the case of NRC CFD applications, the process of adjudication ultimately may decide the acceptance of a simulation outcome.

Code verification establishes that the code accurately solves the mathematical model incorporated in the code. Solution verification estimates the numerical accuracy of a particular calculation. It is assumed that code verification is successfully performed prior to the solution verification process. Grid refinement studies are critical to the solution verification process. However, grid refinement offers only an estimate of the error associated with discretization. In the case of using a CFD code in a predictive role, errors in the representation of geometry, boundary condition or initial condition cannot be discovered using these approaches. Input checking must be used, along with judgment and experience. Input for a complicated simulation may be quite large, with many portions of the input generated using tools like an automated grid generator, perhaps accepting files from a computer aided design program to establish geometry, and a graphical user interface. All these tools offer opportunities to introduce errors to the input.

Modern quality assurance programs have successfully reduced errors and faults in complicated manufacturing environments, and these methods could be adapted to CFD use in critical applications. The NEA best practices document advocates use of QA methods as an umbrella over the V&V activities outlined here, but the methods were not detailed or tailored to CFD simulation. Several quality assurance approaches specific to software development exist, but are not treated further here.

Experience with large complicated system codes such as RELAP5 and TRAC indicates that continued use of a code for a family of applications, in conjunction with a user group actively reporting problems and suggesting enhancements, can lead to continuous improvement of a code if the information is properly managed. This approach to collecting data from the field to guide improvement is part of modern quality assurance methods in manufacturing industries, and could be formalized in CFD development. Most of the major CFD vendors offer venues for such information exchange, either in user groups and/or in conferences. The source code for many of the commercial CFD products is not available to users, so the code custodians must implement appropriate changes. An open source code can benefit from user feedback and from constant code

4.2 University of Idaho, CFD and Scaling in Thermal Jet Mixing

4.2.1 Scaling Approach

The design of separate effect thermo-fluid experiments such as the turbulent mixing are often based on preservation of common dimensionless parameters such as Re_D , Pr, and Pe, where,

$$Re_D = \frac{UD}{\vartheta} \text{ (inertia to viscous forces)} \quad (1)$$

$$Pr = \frac{\vartheta}{\alpha} \text{ (momentum to thermal diffusivity)} \quad (2)$$

$$Pe = \frac{UD}{\alpha} = Re_D Pr \text{ (thermal energy convection to conduction)} \quad (3)$$

While the scaling parameters[2] (equations 1 to 2) do describe the global characteristic of the turbulence induced mixing, they do not provide any information about the local turbulence characteristics. In addition, they do not correlate the associated length and time scales of the thermal-hydraulics to the energy transport within the system.

In order to achieve similitude in separate effect and integral turbulent mixing in large volumes, detailed consideration needs to be given to transport mechanism, geometric, kinematic and dynamic similarities.

The relative impact of scaling on the thermal-hydraulic mixing phenomena is therefore analyzed. For a pool-type SFR design, the associated scales of relevance to the impingement of the unmixed streams to the interface of components, include the vertical length-scale (~0.5m) between the core exit and the UIS and the lateral length-scale between the core exit and the IHX, pump or hot leg pipe (see Figure 4.2).

[2] Traditional global dimensionless parameters used to characterize liquid metal thermal-hydraulic flows. The parameters also guide in the integration of separate effect tests to integral and full-scale conditions.

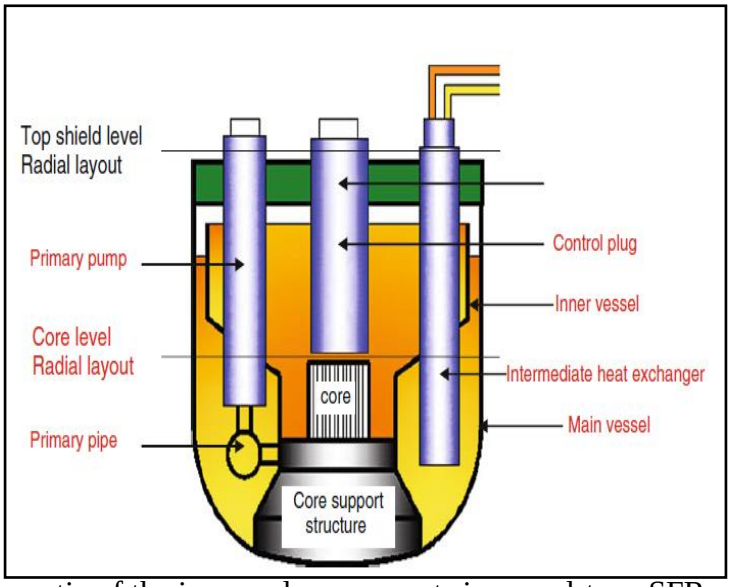

Figure 4.2: Schematic of the in-vessel components in a pool-type SFR configuration

Based on existing advanced SFR designs, the average core out-let velocity and temperatures are 2.3 m/s to 5 m/s and 500℃ (773K) respectively. Also, temperature difference at the exit of core sub-assemblies could be as high as 60℃. With reference to current SFR designs, co-location of several large internal components into the reactor vessel displaces the coolant. Hence, less inventory of sodium and a resulting increase in nominal flow through the high power density core. High core exit velocities also pose additional surface gas entrainment safety challenges as wake regions develop at the free surface around the components. Such entrainment into the core has a potential to impact the kinetics of the reactor operations.

Given the above considerations, CFD is used as a tool to evaluate the impact of scaling on the pool-type SFR design and provide insight into the mixing phenomena. The lack of thermal mixing impacts the scaled design of the SFR pool and its in-pool, col-located components. Identified length scales include: the jet diameter '*d*', the spacing between multiple jets '*s*', and the axial distance between the core exit and the upper core structures '*h*', e.g. UIS. Parametric studies are also performed to evaluate the impact of kinematic ratios at core exits into the upper plenum pool. To understand the dynamics of the transport mechanism and quantification of the convective mixing in the upper plenum, a test matrix (see Table 4.1) representing different core outlet flow conditions was modeled and simulated using COMSOL CFD with liquid sodium as the working fluid.

Table 4.1: Numerical representation of different core outlet flow conditions in a SFR*

		Temperature Difference (ΔT) Between Dual Jets (K)							
		0	**5**	**10**	**20**	**30**	**40**	**50**	**60**
Velocity Ratio (V_c/V_h)*	**0.1**	**X**	**X**	**X**	**X**	**X**	**X**	**X**	**X**
	0.3	**X**	**X**	**X**	**X**	**X**	**X**	**X**	**X**
	0.5	**X**	**X**	**X**	**X**	**X**	**X**	**X**	**X**
	0.7	**X**	**X**	**X**	**X**	**X**	**X**	**X**	**X**
	1	**X**	**X**	**X**	**X**	**X**	**X**	**X**	**X**

V_c *and* V_h are velocities of cold and hot jet representing fuel and blanket zones respectively where temperature of the hot jet 'T_h' is kept constant at 773K representative of the fuel-subassembly outlet condition and temperature of the cold jet 'T_c' representing blanket-zone subassembly temperature is varied accordingly.

In summary, parametric studies has been performed to reveal the relative impact poorly mixed streams to the scaling and design of the SFR pool and in-pool, co-located components such as IHX, UIS, and pump.

Chapter 5. Experimental Results

5.1 UTK. Thermal Mixing and Visualization Experiments in Water

One of the objectives of this was to provide detailed measurements of the thermal mixing of two vertical jets, experimentally and as predicted and complemented by computational fluid dynamics (CFD) simulations. In that both sodium and mercury-based experiments are not amenable to flow visualization,

The research calls for test sections to be created for separate effects tests. The data from the tests could then be compared to simulations of the experiment in a V&V effort to determine the accuracy and effectiveness of the code. The environment for the thermocouple rake in this project is twin jet mixing. The test area involved will have two turbulent water jets that are injected parallel to each other at two different temperatures. This creates a turbulent mixing region. The test tank is shown in Figure 5.1 and a close up of the jets is shown in Figure 5.2. In this figure, colored dye was added to the feed water for each jet allowing it to be visualized.

The system was designed so that each jet has its own pump and inlet reservoir tank. This makes running with each jet at a different temperature possible. When one jet is hotter than the other, thermal energy is mainly transmitted via turbulent mixing particles, because of this the temperature profiles during thermal mixing can be measured, and compared with CFD simulation outcomes. This test section was designed to take three types of measurement: a thermocouple rake for thermal mixing data, an ultrasound probe for velocity measurements, and optical measurements of velocity and fluid mixing using various approaches through the clear walls.

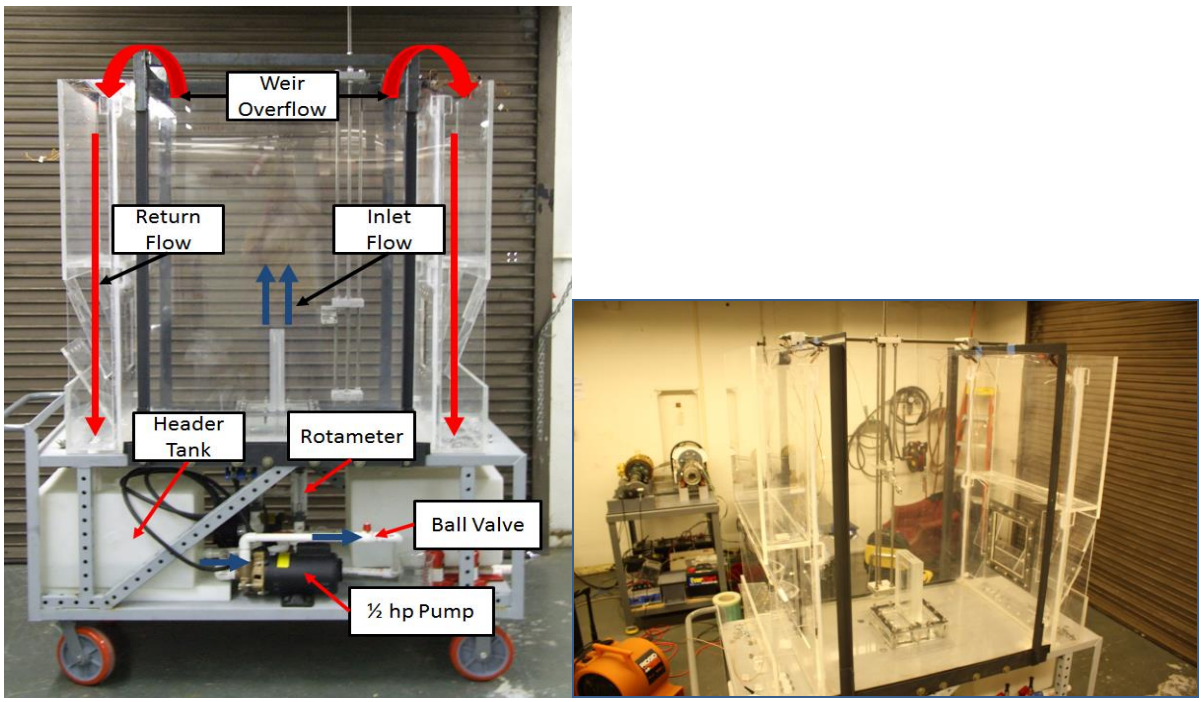

Figure 5.1 Full frontal view of the UTK water experiment and a close-up view.

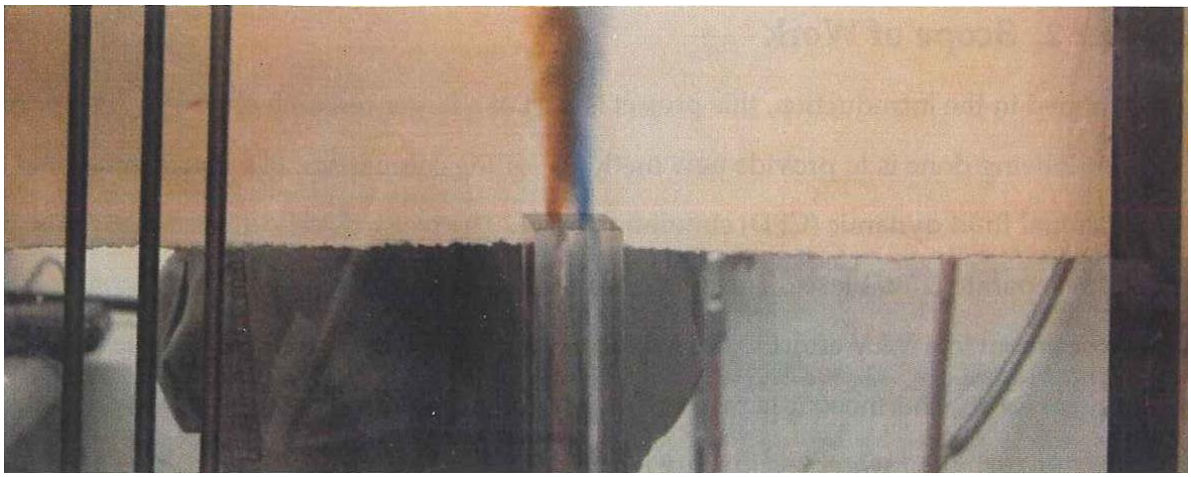

Figure 5.2. Close-up view of the flow visualization of two water jets (dyed).

5.2 UTK Mercury Experiments

Some small-scaled experiments using mercury were also conducted by UTK.

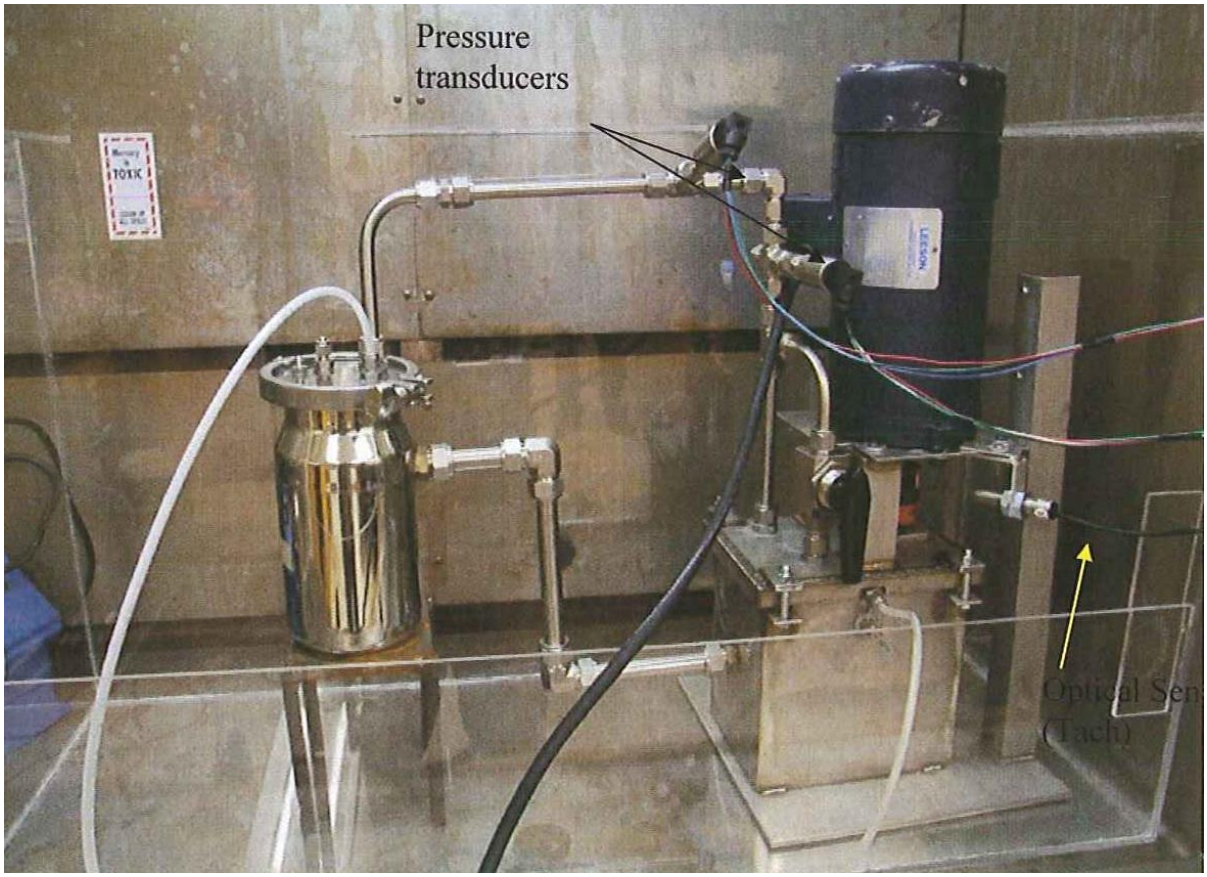

Figure 5.3. Photo of the UTK 3 liter Hg heat transfer loop (shown without the heat transfer components). The loop from Eagle stainless uses He cover gas, pressure transducers and a Leeson pump monitored by an optical sensor.

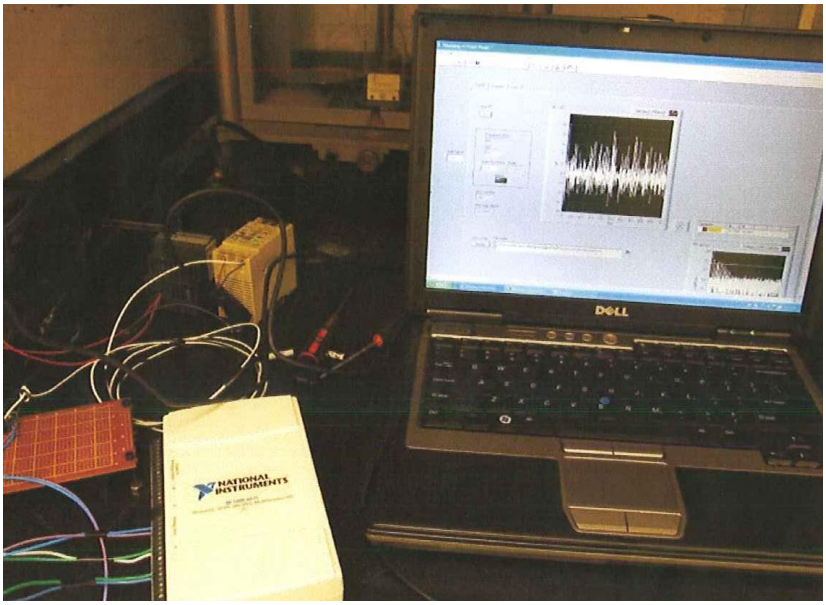

Figure 5.4. Photo of the ultrasonic transducer power unit, laptop with Labview and National Instruments' USB-based data acquisition system.

5.2 Thermal Mixing and Visualization Experiments in Water

Each of the experimental cases is presented below. Additionally, a single jet case is also presented as a benchmark case compared to the UDV work of Tokuhiro. In support of the overall objective of this project Omotowa generated CFD results for each test case using Comsol (Omotowa, 2013). A comparison between the CFD results and the experimental data is made at the geometric centerline between the jets. To test and demonstrate the capabilities of the apparatus and the measurement techniques, water testing has been completed and only the water testing results are presented here. Unfortunately, the local institutions did not support moving forward on carrying out sodium experiments. The CFD results are presented using sodium jets while the experimental data is presented using water.

An overview on the centerline behavior of two-jet mixing and the radial profiles at various axial locations (along z direction) are given here as this describes the thermal mixing phenomena of interest. Figure 5.5 shows the focus areas for the experimental measurements. Please note that the figure is adapted from the general flow field of two-jet mixing from Durve et al. (2011).

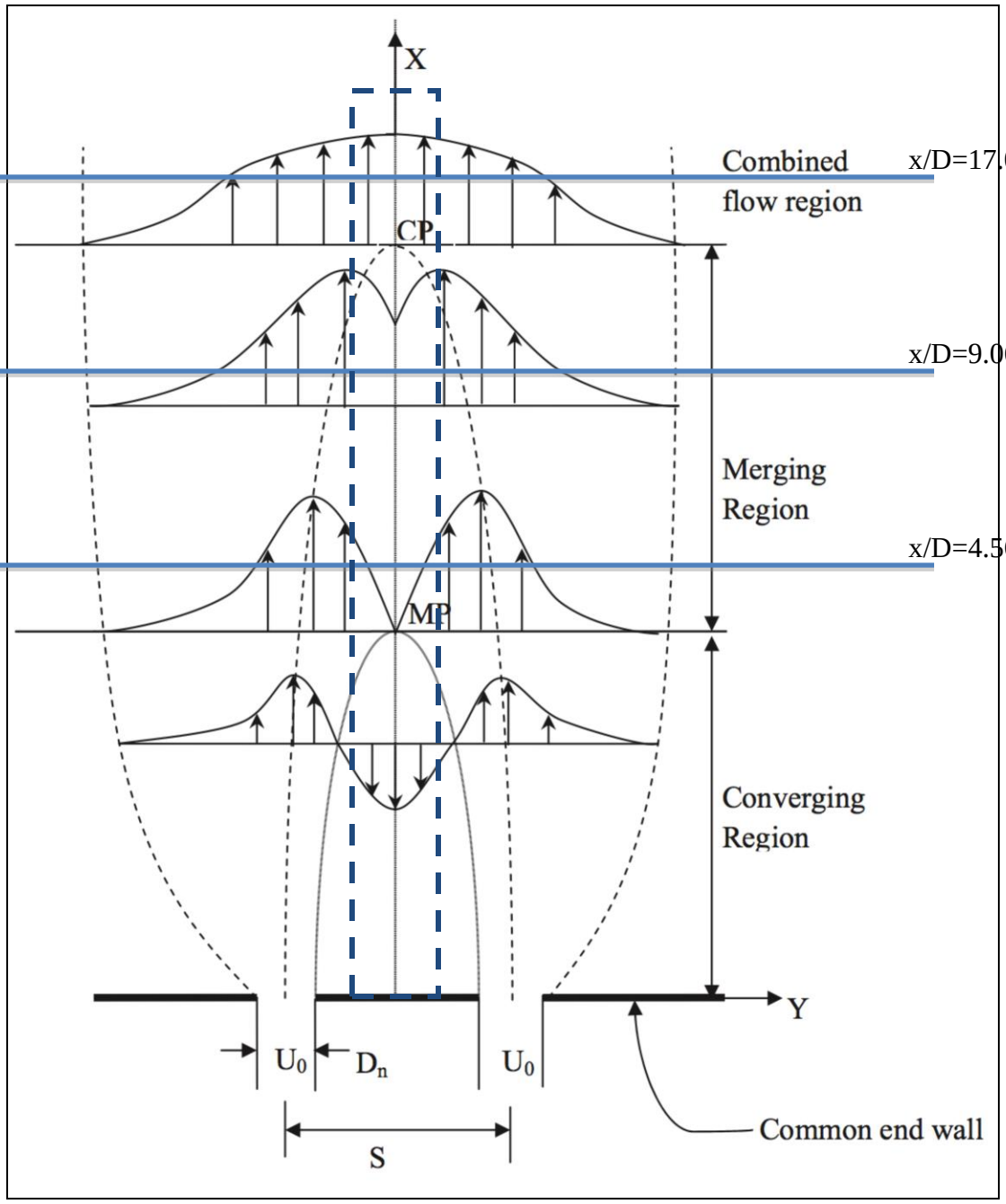

Figure 5.5. Two jet mixing behavior areas of interest.

5.3 Benchmark Single Jet Test

Single jet velocity data was taken and compared to Tokuhiro single jet data to benchmark the UVP instrumentation (Tokuhiro, 1999). It can be seen from Figure 5.6 that there is good agreement between Tokuhiro results and the UVP measurements taken in the test apparatus by Seaver (2013). This demonstrates the capability of the experimental setup and the UVP technique to generate and capture characteristic jet flow behavior.

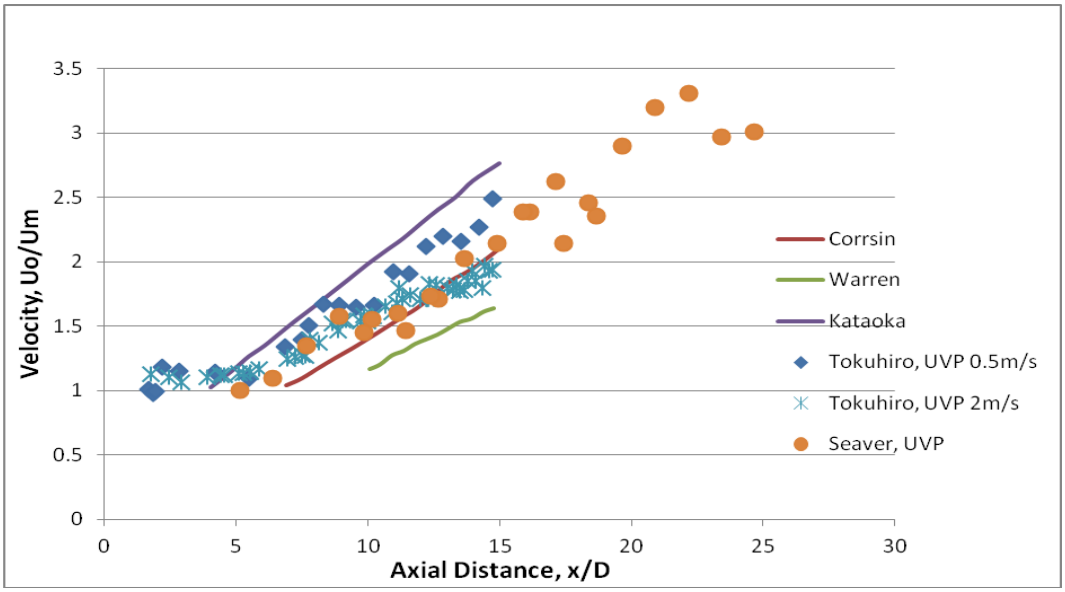

Figure 5.6. Single Jet Centerline Velocity Decay

5.4 Twin-Jet Test Cases

Figure 5.7 shows the two jet velocity profiles for experimental case 1 (V_r=1, ΔT=0°C). Case 1 is considered another benchmark and baseline case for two-jet flow. As such, the radial velocity profile and the normalized RMS (RMS*) velocities are also presented; see Figure 5.8 and Figure 5.9 respectively. The velocity profiles in Figure 5.7 agree with the profiles presented by Durve et al in Figure 2.6. The two jets are strong and pronounced close to the jet exit and merge point. As the flow develops downstream the maximum velocity decreased until the jets become fully combined and only a single jet velocity profile remains (self-similar profile). The peak velocity of each jet does not show as the same velocity in the figure because of the angle of the probe. The x/D dimension is the axial distance of the US beam at the geometric centerline. Thus, the first (left) jet is slightly higher (downstream) axially and the second (right) jet is slightly lower (upstream) axially.

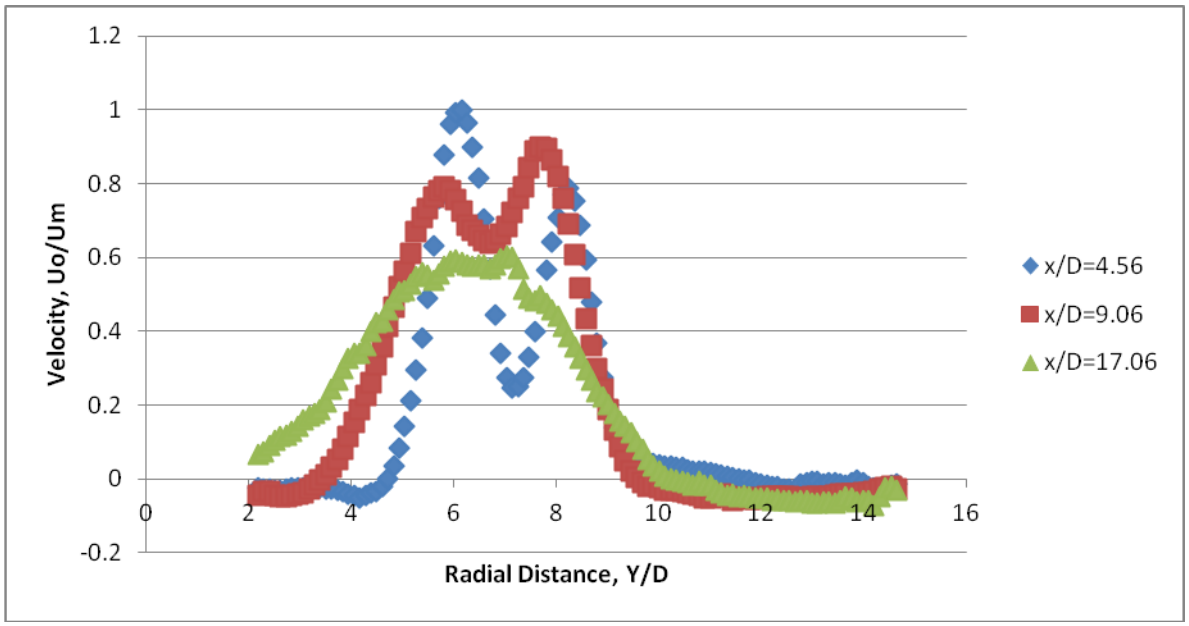

Figure 5.7. Case 1 velocity profiles at different axial positions.

Figure 5.8 shows the normalized radial velocity profile of the two-jet flow field at three different axial locations. The radial velocity profiles also demonstrate the widening of the profile as the flow develops downstream.

Figure 5.9 shows the experimental case 1 RMS* velocity profile at different axial locations. The spike in RMS* velocity at approximately 11 Y/D is due to the reflection of the UV wave off the side of the weir.

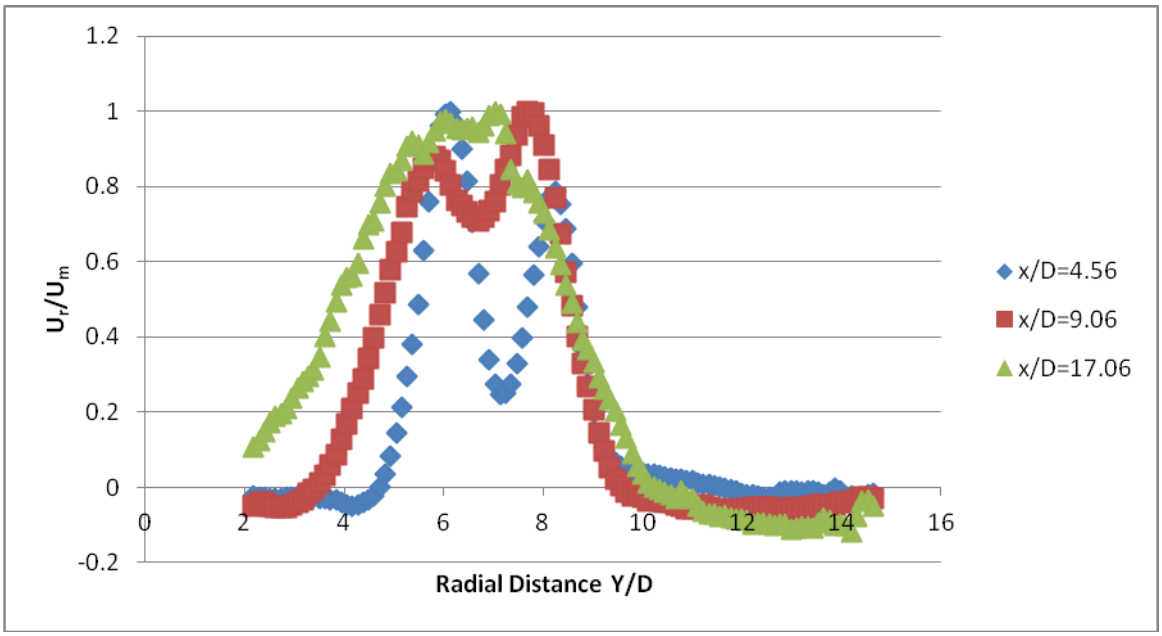

Figure 5.8. Case 1 Radial Velocity Profile at Different Axial Positions.

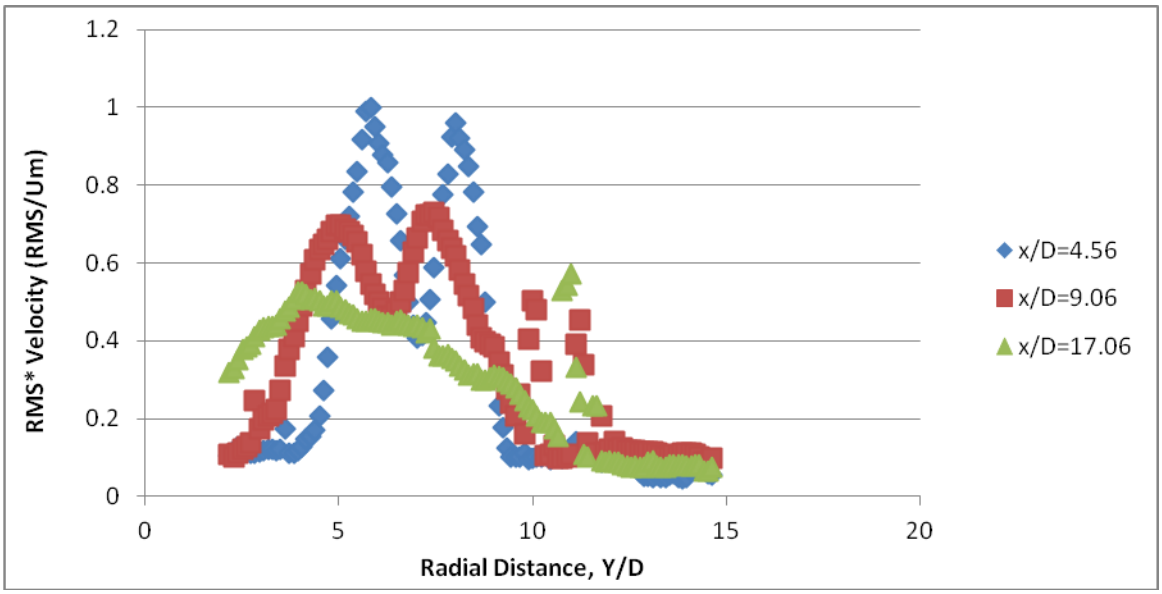

Figure 5.9. Case 1 RMS* velocity

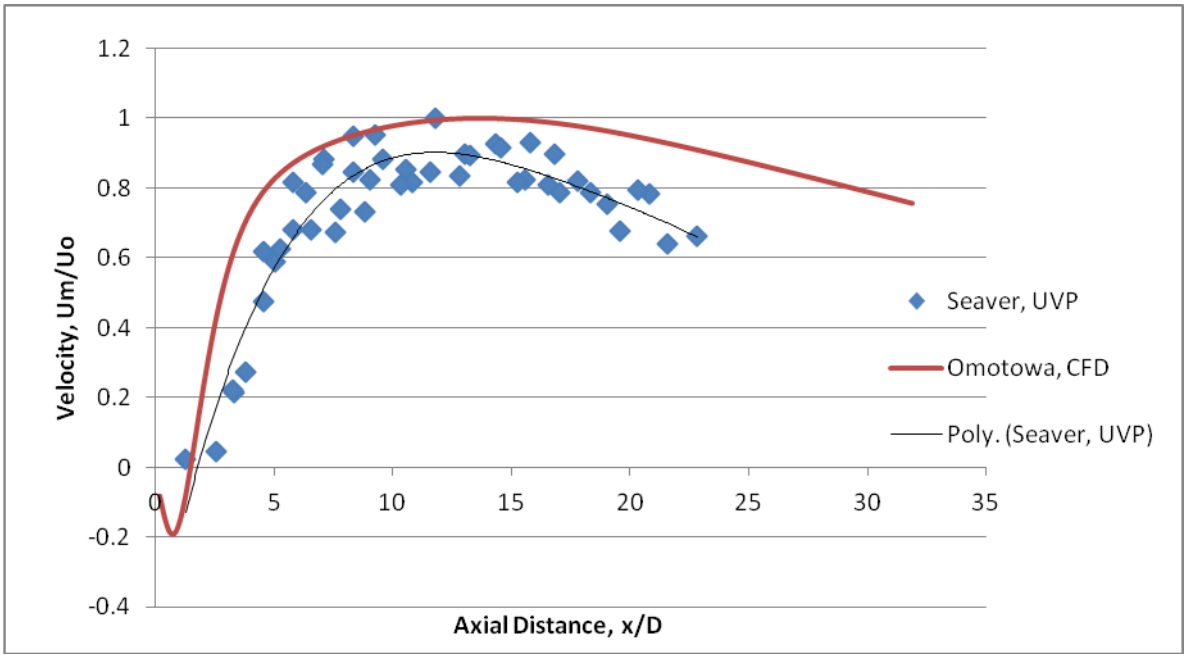

Figure 5.10. Case 1 Centerline Velocity Decay (V_r=1.0, ΔT=0°C)

Figure 5.10 presents the experimental axial velocity decay versus the CFD axial velocity decay along the geometric centerline for experimental case 1. The experimental data agrees with the CFD results. The merge point is identified where the value of the centerline velocity is equal to zero. The combine point is where the centerline velocity is at its maximum. The CFD results agree with the experimental results in identifying the axial position of both points. The centerline velocity decay is the major jet flow characteristic used here to compare and understand momentum mixing and thermal-hydraulic jet behavior.

Figure 5.11 through Figure 5.16 present the experimental axial velocity decay versus the CFD axial velocity decay along the geometric centerline for the other experimental cases. The experimental data trend agrees largely with the CFD trend in all cases. The velocity values are generally less than the CFD results.

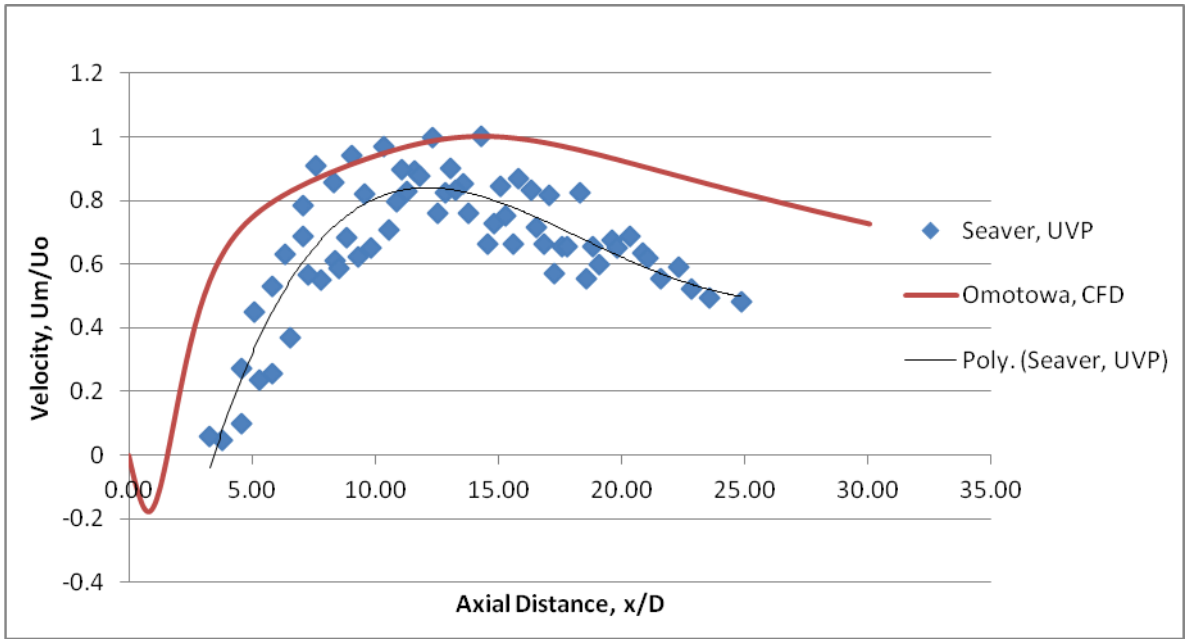

Figure 5.11. Case 2 Centerline Velocity Decay (V_r=0.7, ΔT=0°C)

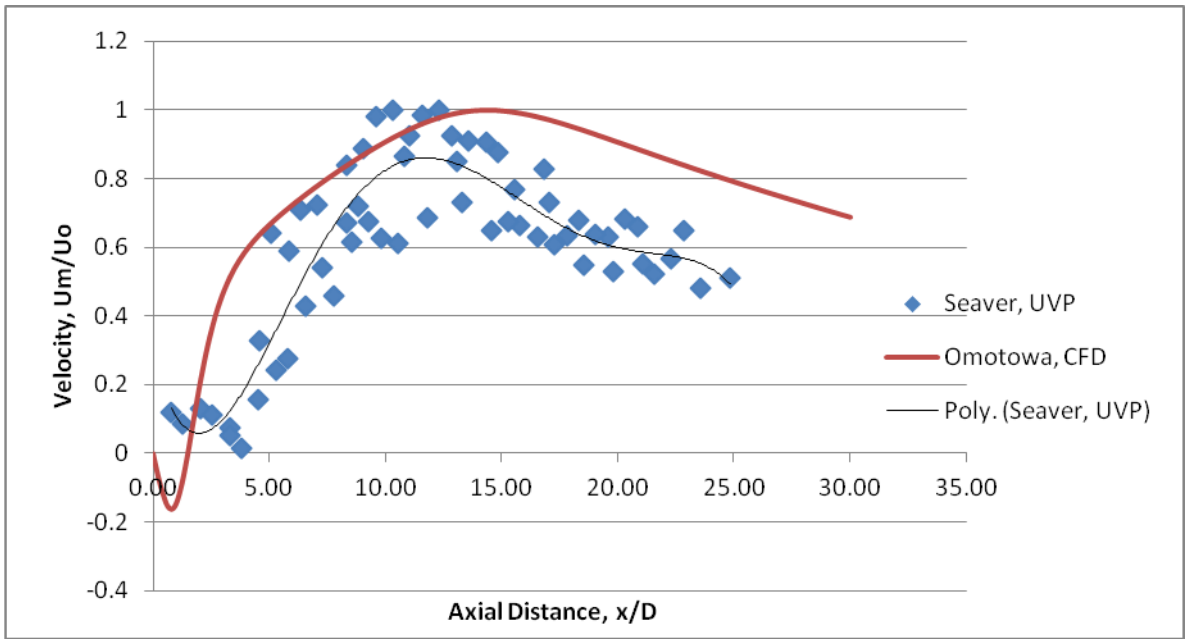

Figure 5.12. Case 3 Centerline Velocity Decay (V_r=0.5, ΔT=0°C)

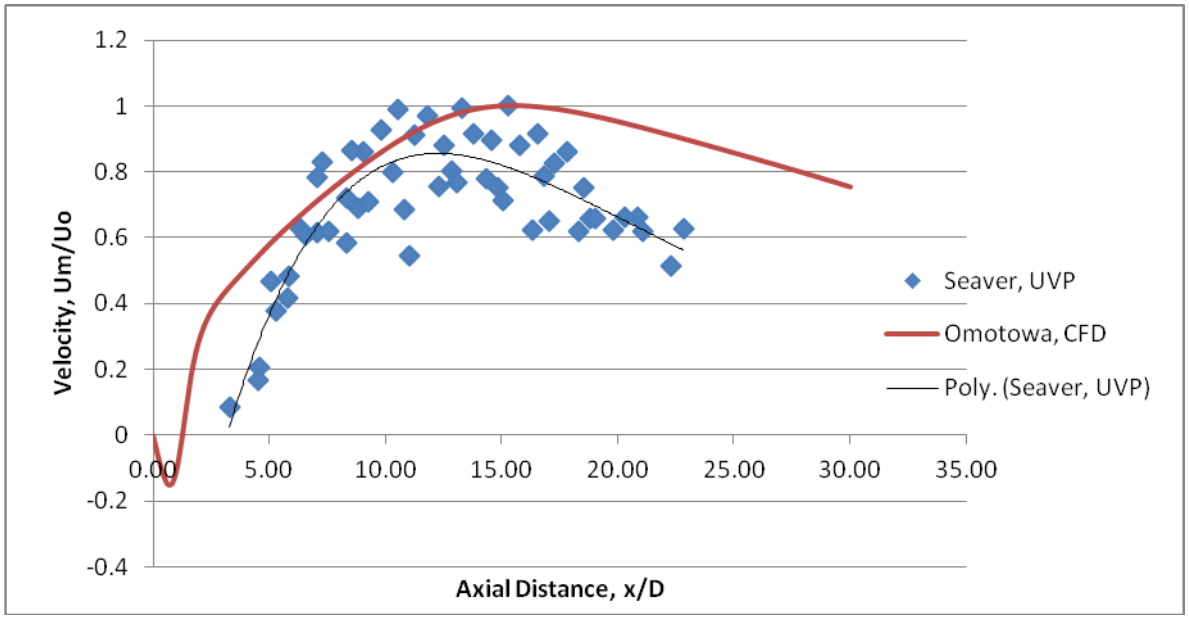

Figure 5.13. Case 4 Centerline Velocity Decay (V_r=0.3, ΔT=0°C)

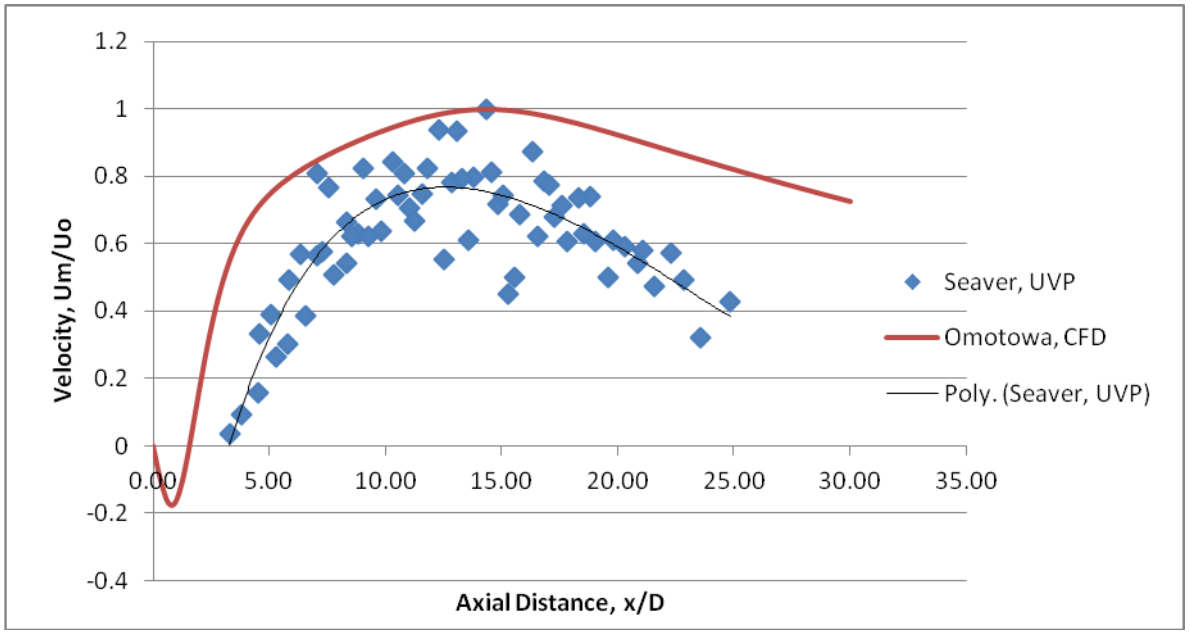

Figure 5.14. Case 5 Centerline Velocity Decay (V_r=0.7, ΔT=10°C)

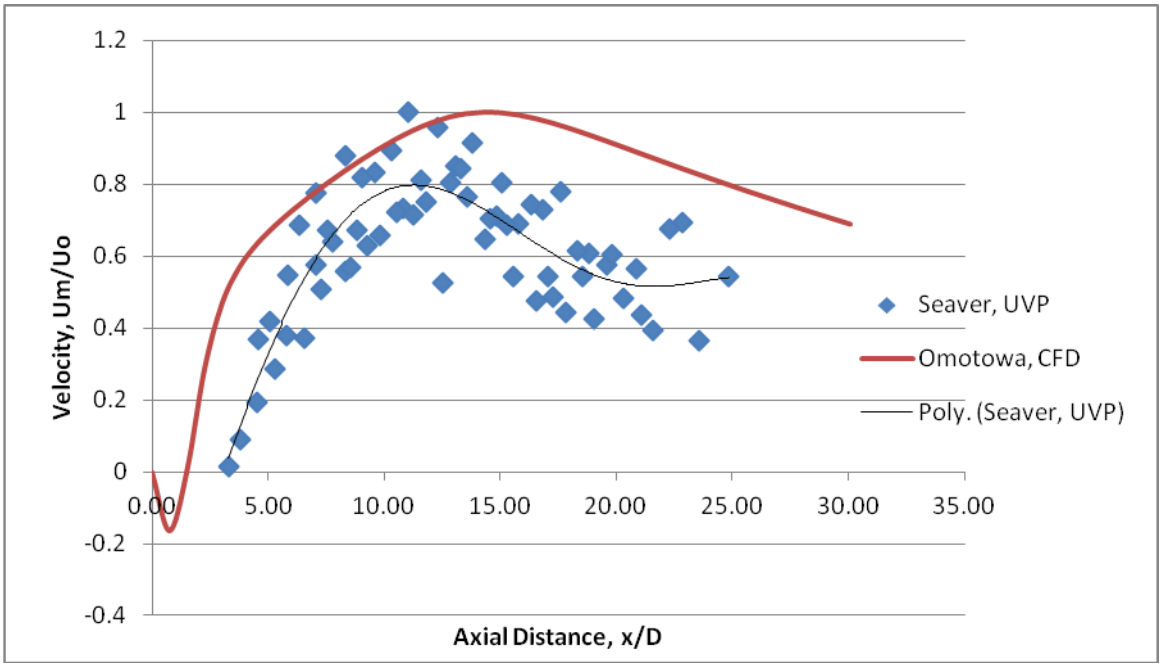

Figure 5.15. Case 6 Centerline Velocity Decay (V_r=0.5, ΔT=20°C)

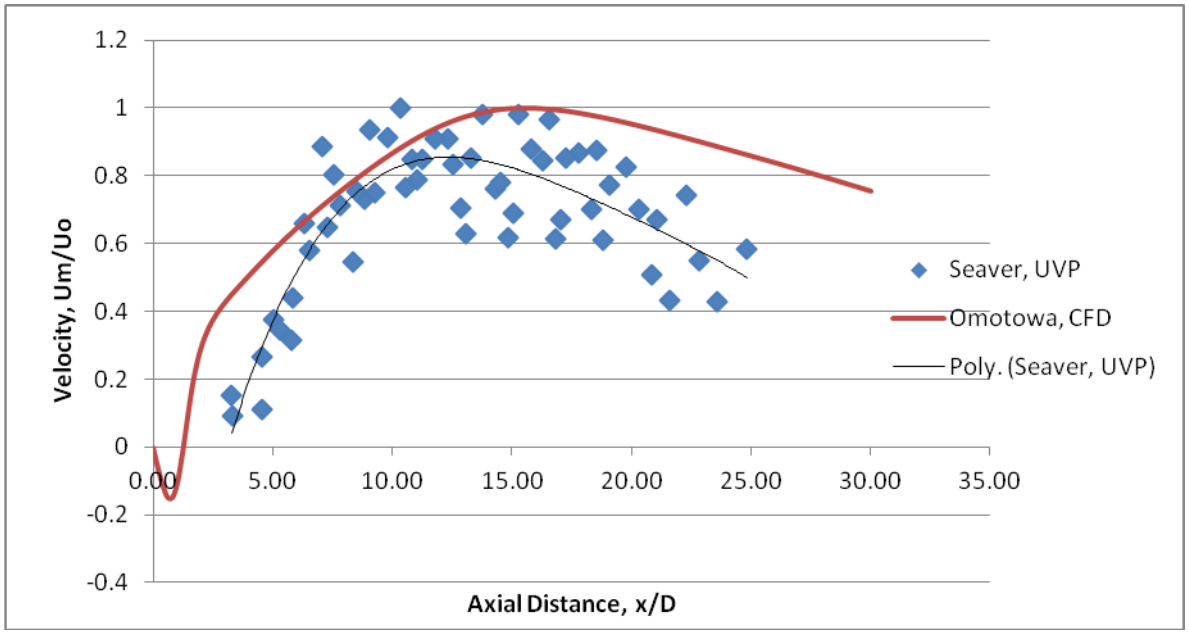

Figure 5.16. Case 7 Centerline Velocity Decay (V_r=0.3, ΔT=30°C)

5.5 Combined Velocity Plots

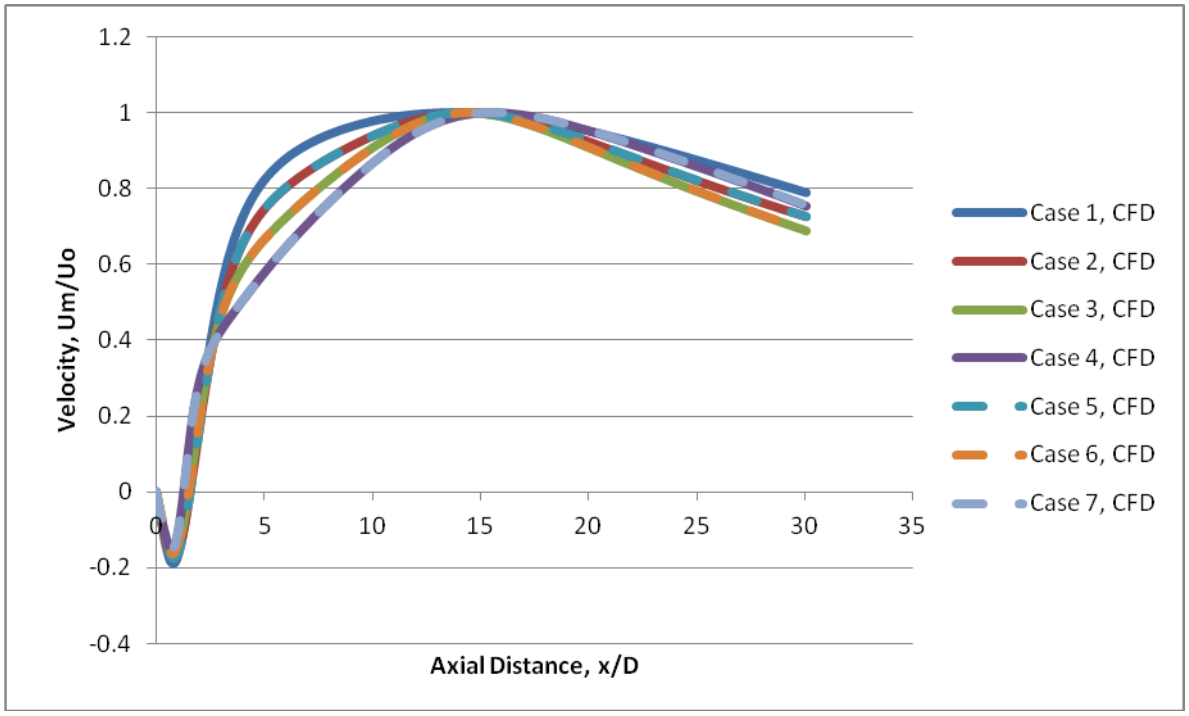

Figure 5.17. All Cases CFD Centerline Velocity Decay

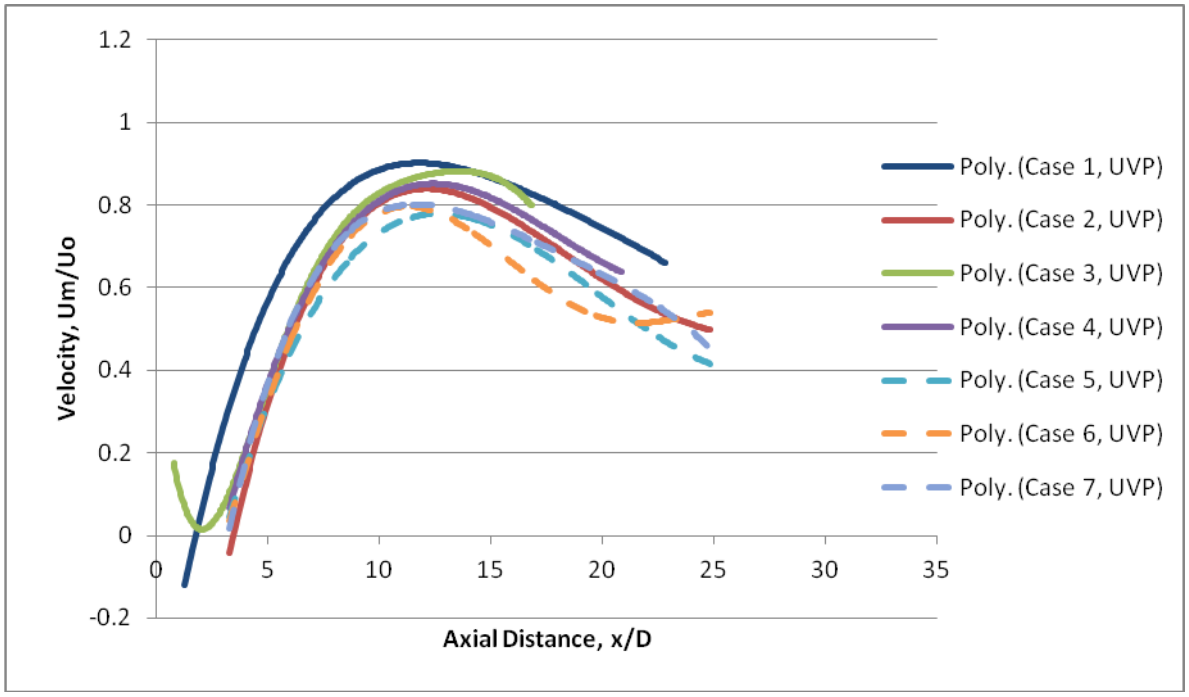

Figure 5.18. All Cases Experimental Centerline Velocity Decay

Figure 5.17 and Figure 5.18 present the centerline velocity decay for all the test cases for the CFD results and for all the experimental results, respectively. The merge point and the combine point are virtually unchanged in their axial location between cases. The agreement

between the experimental data and the CFD results is important because it demonstrates the UVP technology capability of capturing detailed flow characteristics and also helps validate the computational method.

5.6 Temperature Measurements

Figure 5.19 presents the CFD geometric centerline temperature profiles with a temperature difference of 30°C for velocity ratios from 1.0 to 0.3.

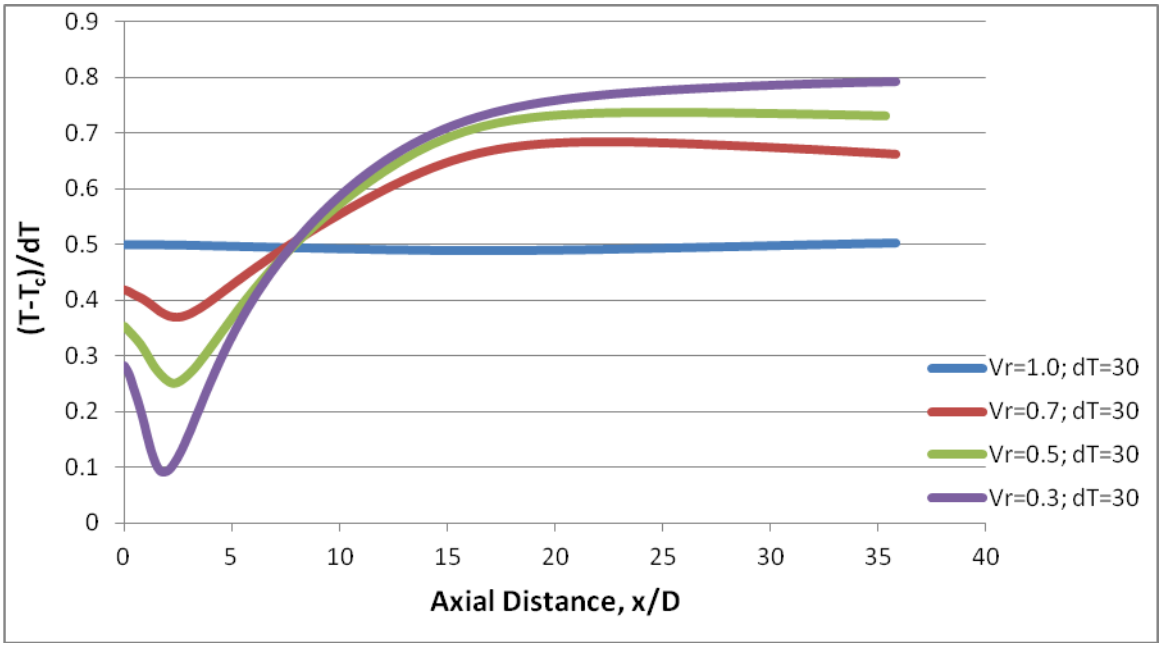

Figure 5.19. CFD Normalized Centerline Temperature (Omotowa, 2013)

The experimental geometric centerline temperature profiles are shown in Figure 5.20. The profile trends agree with the CFD trends. Much of the variance in the temperature measurements is due to the thermocouple arrangement in the test section. The thermocouple rods were placed side by side along the geometric centerline in the same plane as the two jet axes. This puts one rod closer to one jet or the other, hence, the oscillation in the variance of the measurements. The CFD trend shows a decreasing initial centerline temperature as the velocity ratio decreases. The experimental trend shows an increasing initial temperature as the velocity ratio decreases. This trend occurred experimentally because each of the temperature profile velocity cases were recorded one after the other with decreasing velocity ratio. Therefore, the bulk temperature of the test section was rising with each test and resulted in the initial temperatures to measure higher each time.

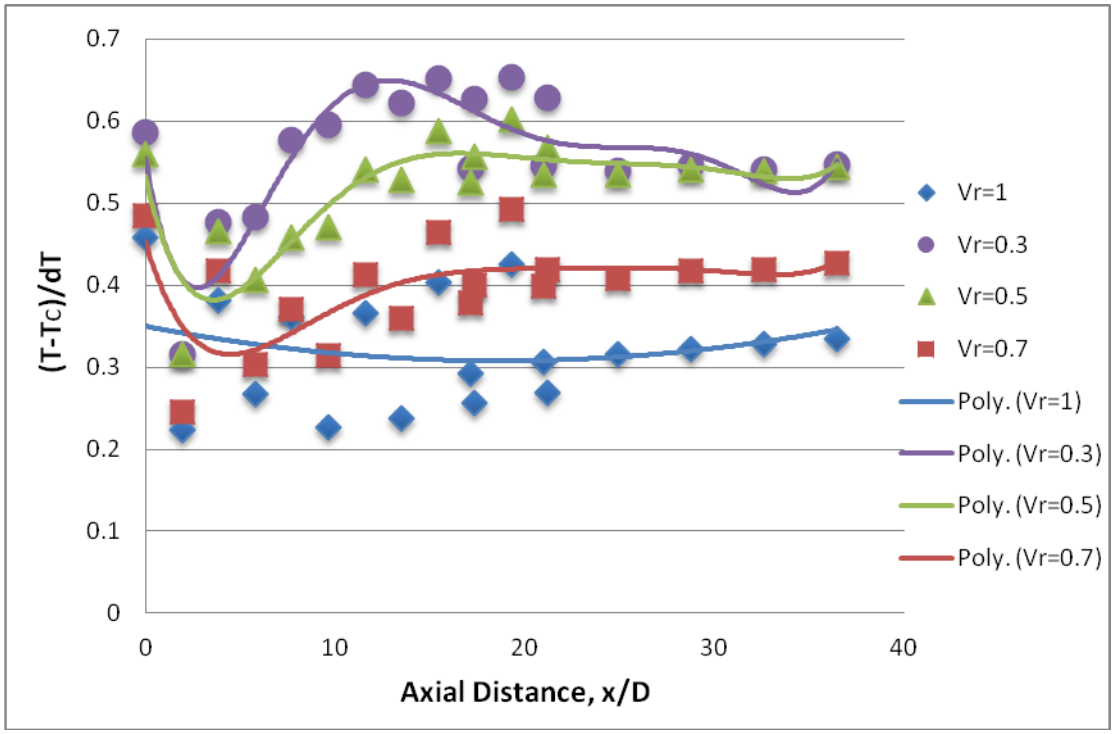

Figure 5.20. Experimental Normalized Centerline Temperature

The clear and consistent temperature decrease until approximately x/D=3 and then the increase until a maximum and asymptotic approach to the mean temperature can be seen and agrees with the CFD results. This agreement between experimental and computational results is important to validate the CFD results. These CFD results are now used to further understand the thermal-hydraulic behavior of vertical twin-jets.

Chapter 6. Discussion of Results

6.1 University of Idaho. CFD Modeling and Simulations

Modeling and simulation of thermal mixing for an anticipated SFR core outlet thermal-hydraulics configuration with COMSOL Multiphysics has been computationally investigated as a separate effect test. Considerations have been given for the inclusion of additional scales (geometric and kinematic) other than the global dynamic similarities (Re and Pe) in order to have a good representation of the convective mixing in small and large scale designs.

6.2 Baseline Thermo-fluid Simulation: Iso-velocity and Iso-thermal

A baseline thermo-fluid simulation with sodium is representative of similar velocities (2.3 m/s) and temperatures (773K) across both jets. This gives a basis for thermal-hydraulic comparison for the parametric studies at different flow conditions as highlighted in Table 3.1. Maintaining the same nozzle diameter (D=6.35mm) and geometric ½ axial length-scale ($l = 0.5$) of a full-scale upper plenum, the equivalent $\mathrm{Re_D}$ and Pe are $5.2 * 10^4$ and $2.29 * 10^2$ respectively. Figure 6.1 shows the instantaneous velocity surface field for the steady-state simulation and also the representation of the idealized lateral velocity profile . Figure 6.2 displays the streamwise velocity decay along the geometric centerline from a representative simulation.

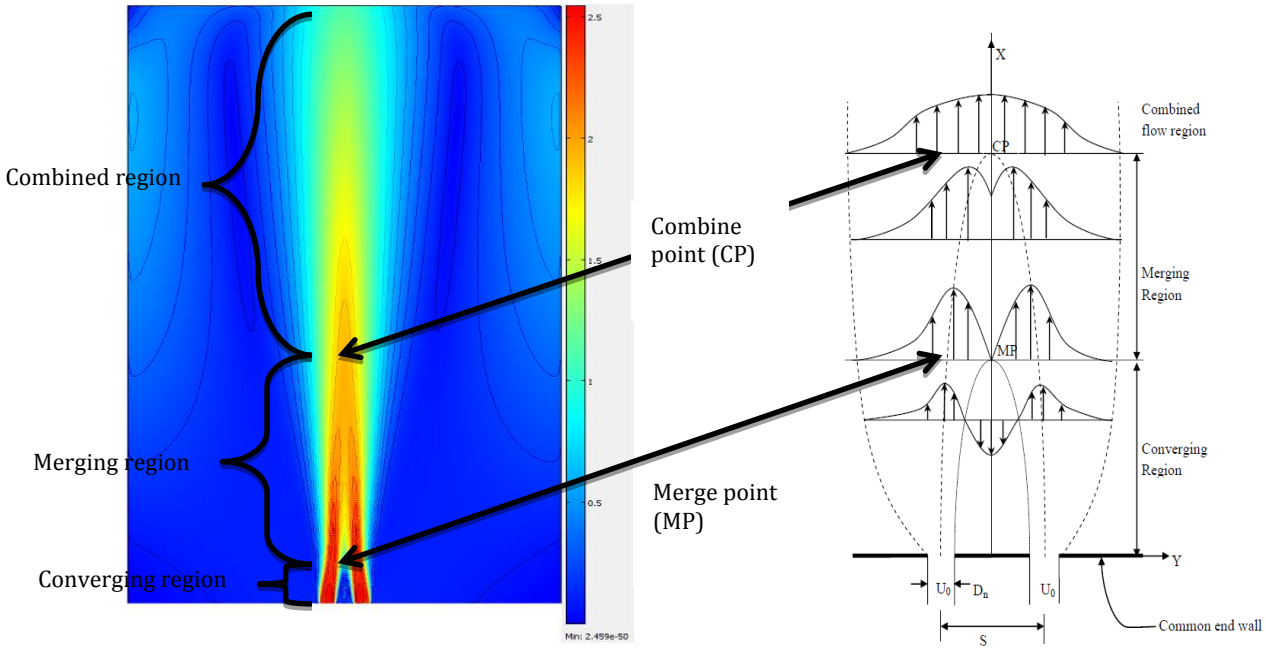

Figure 6.1: Instantaneous velocity surface plot and flow field for isothermal dual-jets

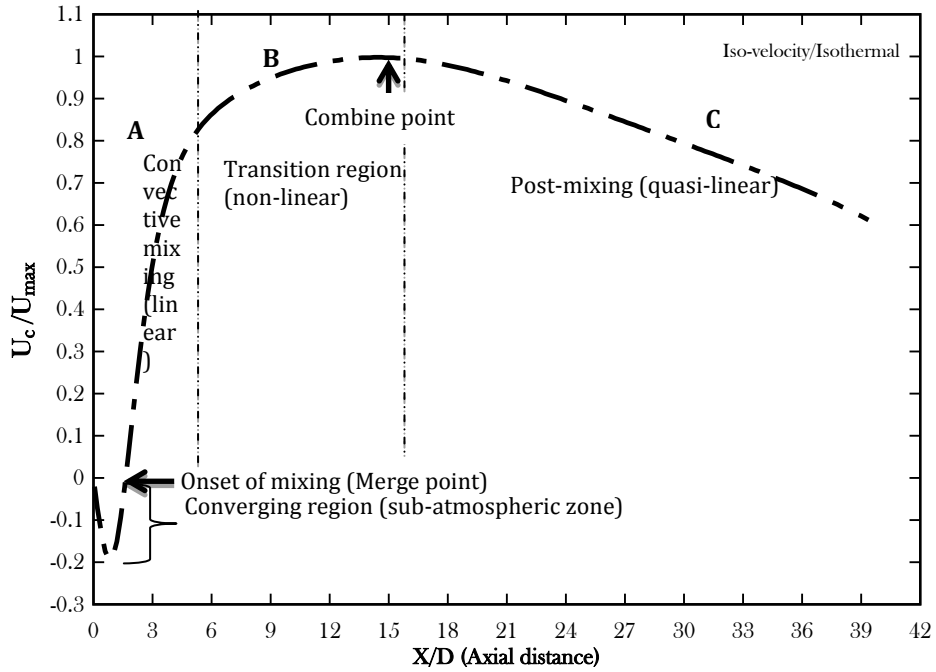

Figure 6.2: Regions along the geometric centerline velocity decay of parallel dual-jets

In Figure 6.2, the axial distance and velocity along the geometric centerline were non-dimensionalized by using the jet diameter and maximum centerline velocity respectively. Comparing the flow pattern in Figures 6.1 and 6.2, there is an equal entrainment rate (2.3m/s) across both jets. This creates a sub-atmospheric region with reverse flow near the entrance region between both jets. This explains the converging region (negative velocity) between $0 < \frac{X}{D} < 1.6$. At $\frac{X}{D}$= 1.6, the velocity along the geometric centerline is zero and the inner shear layers of both jets begin to merge, i.e. merge point. This represents the onset of mixing between both streams. The merging region ($1.6 < \frac{X}{D} < 14.2$) is where the most convective mixing takes place. This peaks at the combine point ($\frac{X}{D} = 14.2$) which equally represents the maximum velocity along the geometric centerline. At $\frac{X}{D} > 14.2$ (post-mixing region), the dual-jets gradually become self-similar (acting like single jet). However, any existing ΔT between the jet gradually dissipates as transverse heat transfer takes place.

6.3 Effect of Temperature on Sodium Turbulent Mixing

The velocity field was kept the same but the temperature difference at the inlet across both jets was varied ($5K < \Delta T_{hc} < 50K$) because besides velocity, the two streams are expected to be at different temperatures. Though the temperature difference between multiple jets at the exit of different sub-assemblies could be as high as 150K, the thermo-fluid simulations were limited to $\Delta T_{hc} < 50K$ mainly because up to $\Delta T_{hc} = 50K$, no significant thermal effect was observed on the velocity field (see Figure 6.3. Figure 6.3 shows the geometric centerline velocity decay for several iso-velocity but non-isothermal thermo-fluid simulations.

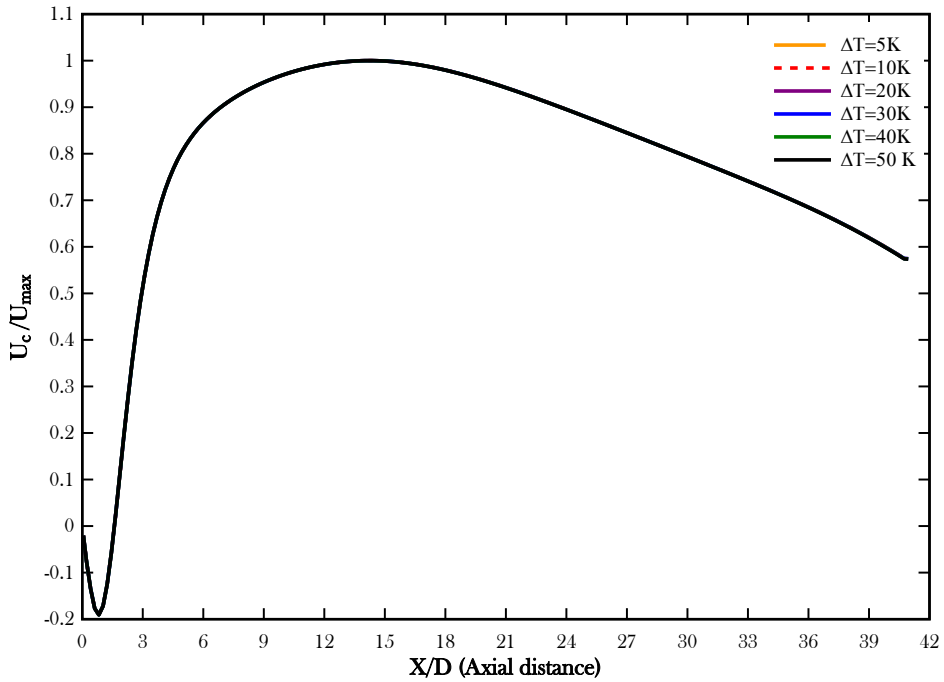

Figure 6.3: Effect of ΔT_{hc} across both jets on the streamwise centerline velocity decay

In Figure 6.3, no noticeable difference (less than 0.5%) was observed as a result of temperature difference (ΔT_{hc}) on the convective mixing regime ($1.6 < \frac{X}{D} < 14.2$) because all the centerline profiles over-lay each other. It hence shows that the jet flow is momentum or inertially-controlled and buoyancy effects are negligible. The momentum dominated analysis was further confirmed with the Richardson number (Ri) ranging between $1.70 \times 10^{-5} < Ri < 1.69 \times 10^{-4}$.

Figure 6.4 illustrates the centerline thermal mixing for different ΔT_{hc}. The centerline thermal field profile for $5K < \Delta T_{hc} < 50K$ shows that a homogenous mixture was not obtained even at 5K.

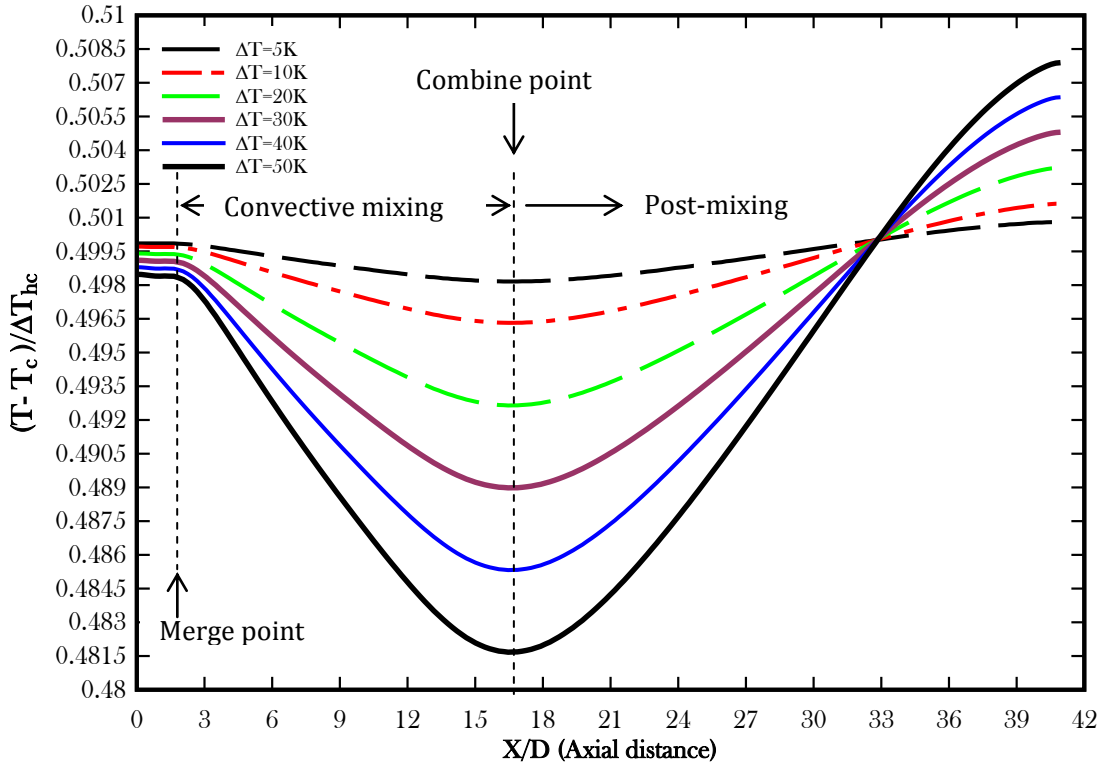

Figure 6.4: Thermal mixing along the geometric centerline for non-isothermal dual-jets

On the y-axis of Figure 6.4, the difference between the instantaneous temperature and the temperature of the cold jet is non-dimensionalized by the temperature difference between hot and cold jet. From Figure 6.4, the onset of thermal mixing corresponds with the onset of momentum mixing at $\frac{X}{D} \sim 1.6$. There is however a slight shift in the combine point at $\frac{X}{D} \sim 16.8$ as compared to $\frac{X}{D} \sim 14.2$ for the velocity field. Beyond $\frac{X}{D} \sim 16.8$, the convective mixing is small compared to the transverse heat transfer after the jets merge. Hence, the temperature gradually increases beyond $\frac{X}{D} \sim 16.8$. Since temperature is a scalar, thermal mixing is facilitated by mixing of the transverse momentum. However, transverse momentum is smaller than its axial counterpart. Hence, there is a slight spatial lag that corresponds to the minimal point of thermal mixing relative to momentum mixing.

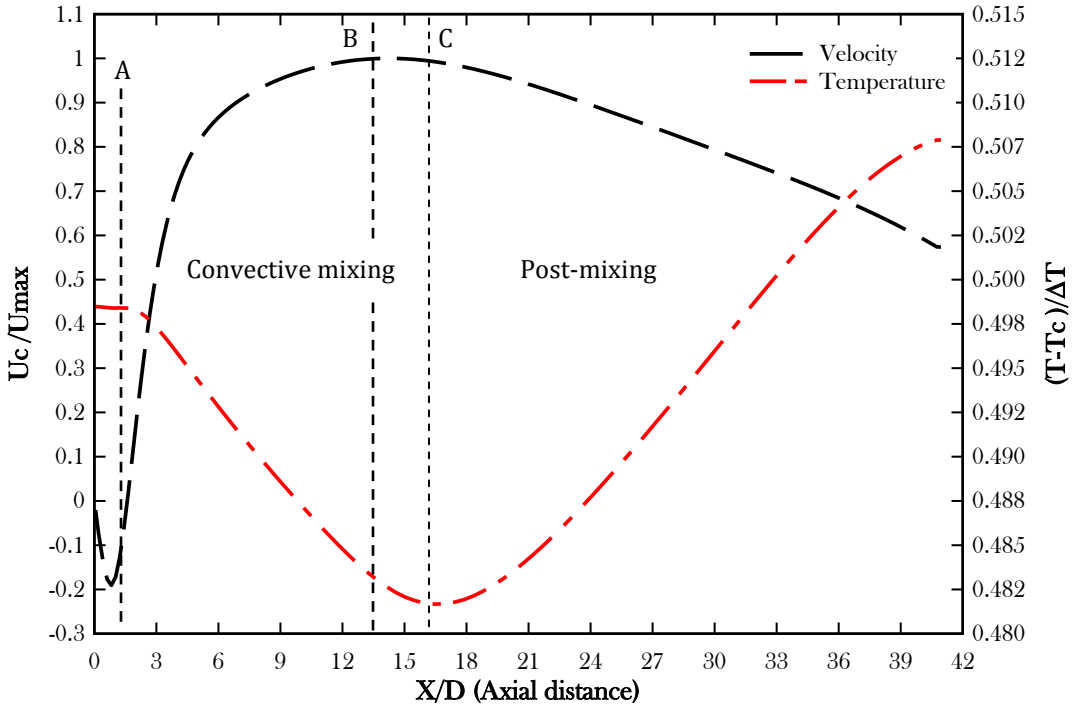

Figure 6.5: Streamwise velocity and temperature profiles for non-isothermal ($\Delta T = 50K$) and iso-velocity (2.3 m/s) dual-jets. Point "A" represents the merge point, "B" represents the completion of momentum mixing while "C" represents the peak thermal mixing

Figure 6.5 incorporates an element of Figure 6.3 and Figure 6.4, and gives a comparison of the geometric centerline of the thermal and velocity fields. From Figure 6.5, it can be deduced that thermal mixing and momentum mixing are both initiated at same merge point ($\frac{X}{D} \sim 1.6$). However, it is observed that the peak momentum mixing occurs at $\frac{X}{D} \sim 14.2$ while peak thermal mixing is essentially achieved further downstream at $\frac{X}{D} \sim 16.8$.

Figure 6.6 shows the prediction of the temperature field across the test loop at different axial locations along the flow field. As it would be expected, the temperature gradient is highest close to the jet exit (X/D=1.6) and gradually decreases downstream (X/D=41) after to thermal mixing and radial dissipation.

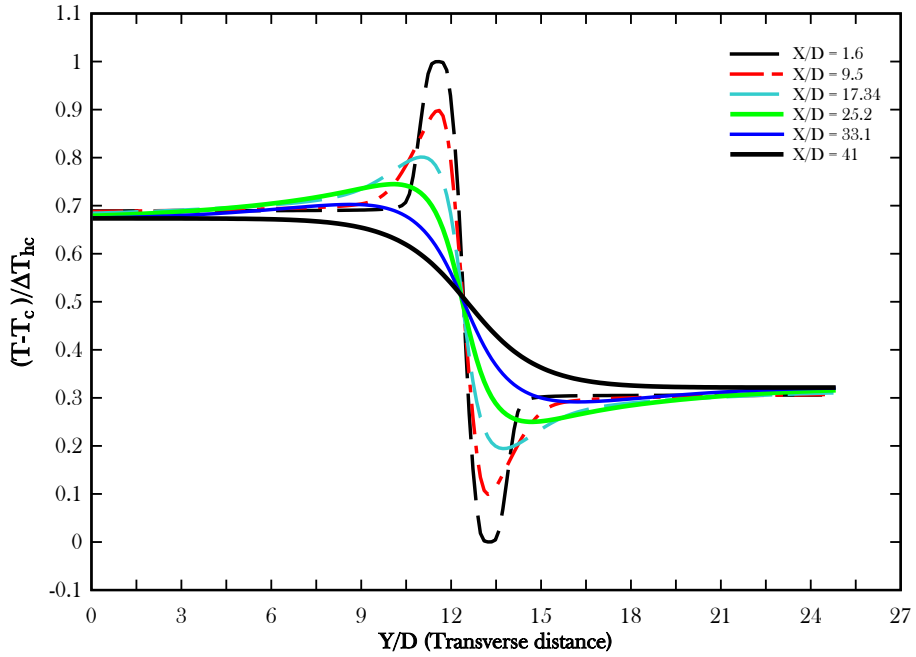

Figure 6.6: Spanwise temperature profile across the flow field at different elevations for $\Delta T = 50K$ and $Vratio = 1$

6.4 Effect of Velocity Ratios on Thermal Field

Convective mixing was also quantified under scenarios where the core exit velocities in different core sub-assemblies varied. Based on the matrix in Table 3.1, simulations were performed for velocity ratios $0.1 < \frac{U_c}{U_h} < 1$. For non-isothermal jets (ΔT_{hc}=10K), Figure 6.7 shows the velocity contour plots for (U_c/U_h) = 0.5, 0.7, 1.

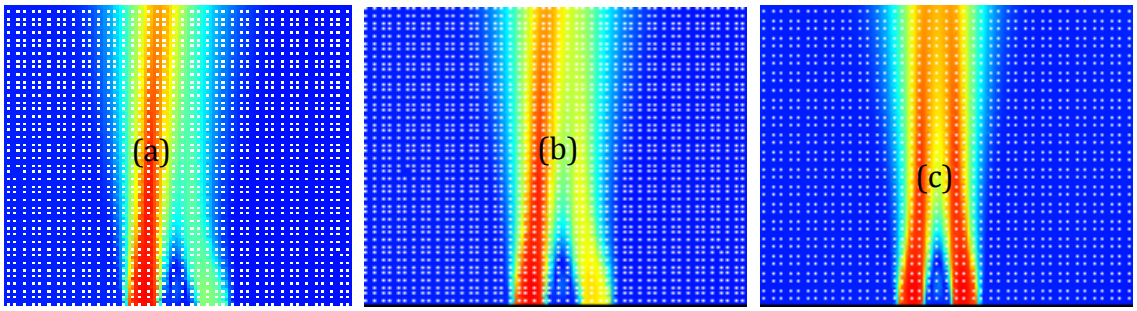

Figure 6.7: Velocity field plots for different velocity ratios at $\Delta T = 10K$ showing the different merge points (a) $\frac{U_c}{U_h} = 0.5$ (b) $\frac{U_c}{U_h} = 0.7$ (c) $\frac{U_c}{U_h} = 1$

Figure 6.7 therefore shows a slightly modified flow trajectory for different jet velocity ratios. It is observed that the lower velocity jet (right jet) merges with the higher velocity jet (left jet) slightly closer to the jet entrance. This is largely due to the higher entrainment rate of the surrounding fluid by the higher velocity jet. Figure 6.8 shows the centerline temperature for

the different velocity ratios and reveals the effect of velocity ratios across the jet streams on thermal mixing.

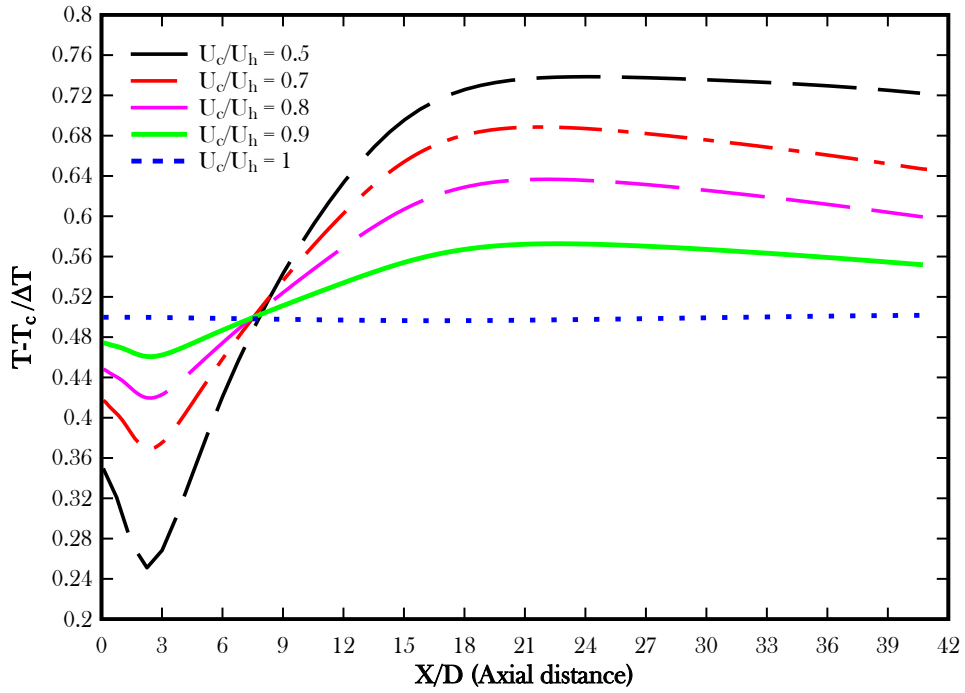

Figure 6.8: Influence of velocity ratios on non-isothermal field ($\Delta T = 10K$)

Though with lower velocity ratios, the onset of mixing occurs earlier, Figure 6.8 shows that $\frac{U_c}{U_h} < 1$ are not favorable to turbulent mixing between the two jets. An explanation for this is because a much lower pressure zone is established due to different entrainment rates between the jets with $\frac{U_c}{U_h} < 1$ as compared to $\frac{U_c}{U_h} = 1$. As a result, the respective jets are entrained in a non-symmetric manner. Hence the mixing rate at the onset of mixing is lower and less thermal mixing is achieved.

6.5 Effect of Jet Spacing

Studies to investigate an optimum jet spacing that will be most appropriate to enhance turbulent mixing were performed. For the dual jet under review, Figure 6.9 highlights the onset of mixing (merge point) in the instantaneous surface velocity field plots for S/D =2, 5 and 7.

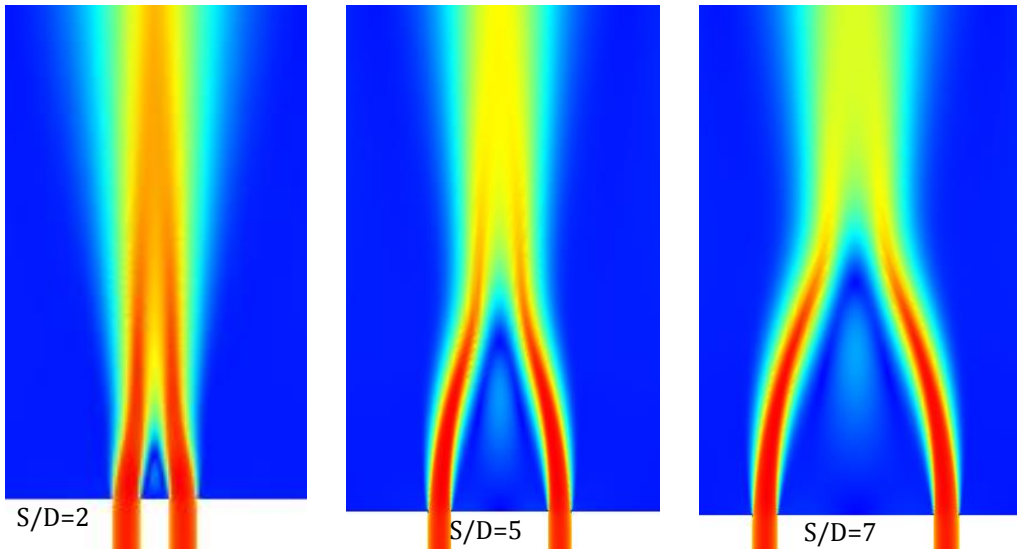

Figure 6.9/ 4-9/ 6-1: Instantaneous velocity field for isothermal (773K) and iso-velocity (2.3m/s) dual jets for S/D =2, 5 and 7 respectively

Comparative plots of the centerline velocity decay for each of the jet-spacing thermo-fluid simulations (S/D=2, 3, 5 and 7) are shown in Figure 6-23. A visible shift further downstream of the onset of mixing is noticeable with increasing spacing between both jets (see Figure 6-23). Based on the results from Figure 6-23, Figure 6-24 establishes a correlation that relates the jet-spacing to the onset of mixing for two parallel jets.

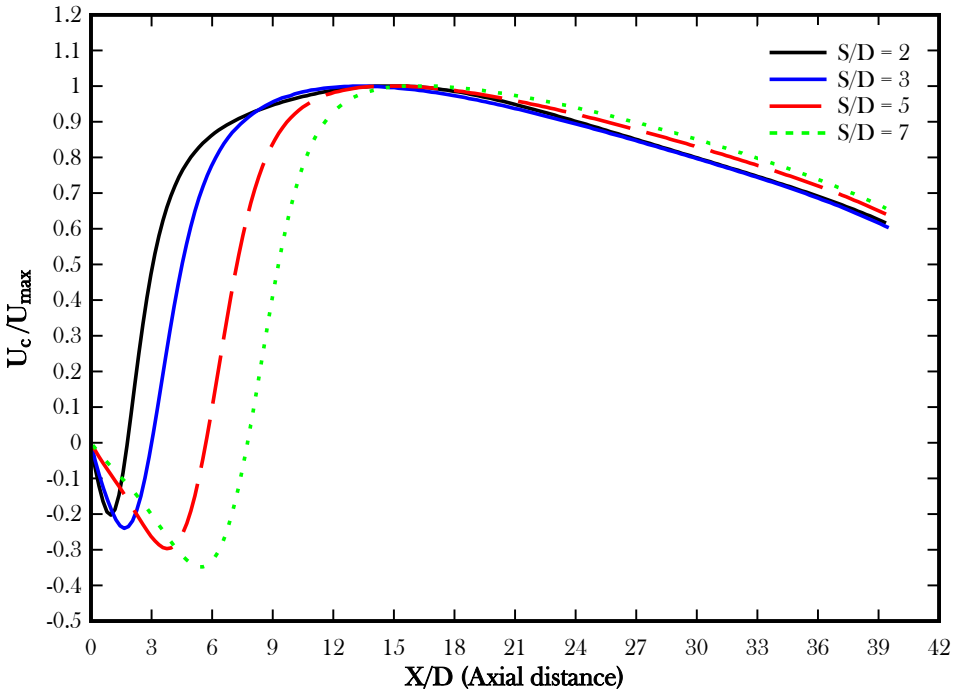

Figure 6.10/ 4-10/ 6-2: Influence of jet-spacing on turbulent mixing of two parallel jets at T=773K and U=2.3m/s

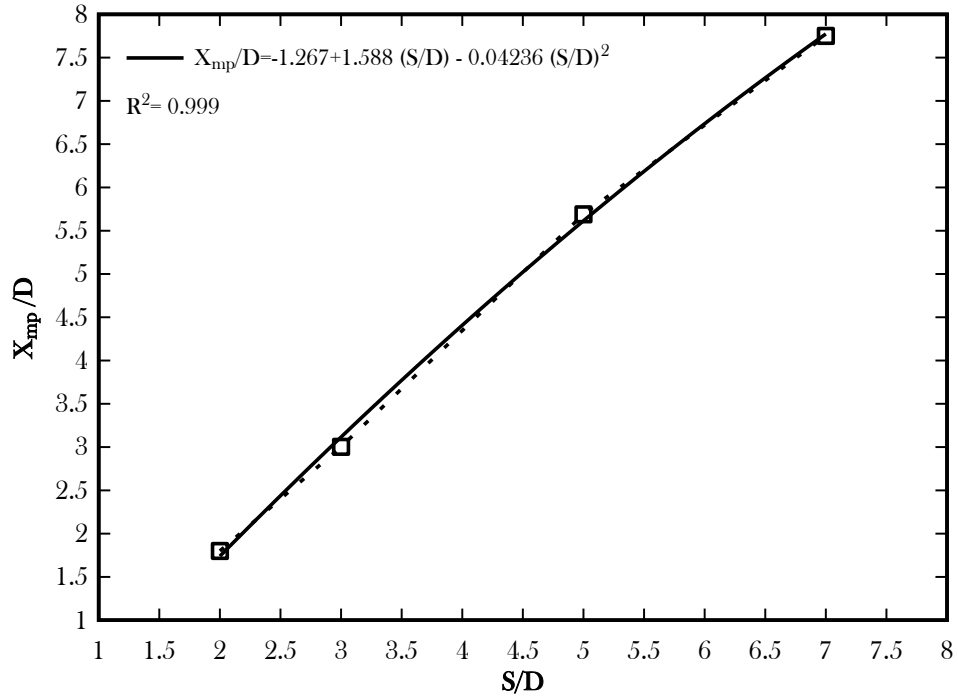

Figure 6.11/4-11/ 6-3: Correlation between jet-spacing and onset of mixing for two isothermal (773K) and iso-velocity (2.3m/s) jets.

Figures 6-23 and 6-24 therefore show that at some threshold spacing between both jets, less and almost no mixing will be achieved. Hence, each of the jets will essentially behave as a single-jet. For an optimized turbulent mixing system, the S/D=2 facilitates the most thermal mixing. Lack of thermal mixing beyond the core exit therefore has significant impact on the scaling of the SFR pool (height and width), and major in-pool components (UIS, IHX and pump). For the design of larger scale or integral test facility, there will be need to simulate the realized lack of thermal mixing and its scaling impact on IHX and pump performance.

6.6 University of Idaho Experimental Results versus CFD

The CFD results used in this chapter are from work by Omotowa using the Comsol software in support of this project (Omotowa, 2013). In Figure 5.17 the axial distance and the velocity along the geometric centerline of the seven test cases are shown together. Comparing the flow patterns in all cases it can be seen that the entrainment rate across both jets creates a sub-atmospheric region between them near the jet exit that results in a flow reversal. This explains the converging region, which occurs between $0 < x/D < 1.6$ for the iso-velocity case (case 1). At approximately x/D=1.6 the velocity is zero and the inner shear layers of both jets begin to merge. This is the merge point and represents the onset of mixing between the jets. The merge point is virtually unchanged with increasing velocity ratio between the jets. The merging region is represented from $2 < x/D < 14.2$. This is where most of the convective mixing takes place. The centerline velocity peaks at around x/D=14.2, which is the combine point. The combine point is also unchanged with increasing velocity ratio. At $x/D > 14.2$ the two jets gradually become self-similar, however, there still exists a temperature difference between the jets until it dissipates through transverse heat transfer.

There is no noticeable difference in the velocity fields between cases 2 and 5, cases 3 and 6, and cases 4 and 7, but a temperature difference does exist between the jets. It is also seen in Figure 5.17 that a temperature difference of up to 30°C produces no noticeable effect on the velocity profile. Omotowa found that for a temperature difference of 50°C still did not produce a noticeable effect in the thermo-fluid simulations. This indicates that the jet flow is momentum or inertial-controlled and buoyancy effects are negligible.

In Figure 5.19 the centerline velocity temperature profiles for the four temperature cases are presented together. From Figure 5.19 the onset of thermal mixing corresponds to the onset of momentum mixing at x/D=1.6.

Chapter 7. Conclusions

The thermal striping phenomenon is a potential safety concern to the long term operation of the SFR due to the thermal stresses accumulated on structures and components from the impingement of poorly mixed streams of coolant flow from the reactor core. In pool-type Sodium Fast Reactors (SFR) the regions most susceptible to thermal striping are the upper instrumentation structure (UIS) and the intermediate heat exchanger (IHX). This thermal-cyclic load is undesirable in terms of the long term operational safety of the SFR. For the anticipated configuration, the provided length scale for thermal mixing is short. Thus, we sought to experimentally and computationally (CFD) understand thermal mixing using four different fluids (air, water, Na and Hg). The impact of scaling was also considered.

The thermal mixing phenomenon was simulated using two vertical jet at different velocities and temperatures as prototypic of two adjacent channels out of the core. Owing to the uncertain commercial availability of an electromagnetic pump, the loop was uniquely designed with one stream gravity-driven, the other pressure-driven from a lower storage tank. Thermal jet mixing of anticipated flows at different temperatures and velocities were investigated. Velocity profiles are measured throughout the flow region using Ultrasonic Doppler Velocimetry (UDV), and temperatures along the geometric centerline between the jets were recorded using a thermocouple array. CFD simulations, using COMSOL, were used to initially understand the flow, then to design the experimental apparatus and finally to compare simulation results and measurements characterizing the flows.

The experimental results and CFD simulations showed that the flow field (without UIS, and thus unrestricted) is characterized into three regions with respective transitions, namely, convective mixing, (flow direction) transitional, and post-mixing. Both experiments and CFD simulations supported this observation. For the anticipated SFR conditions the flow is momentum dominated and thus thermal mixing is limited due to the short flow length associated from the exit of the core to the bottom of the UIS. This means that there will be thermal striping at any surface where poorly mixed streams impinge; rather unless lateral mixing is ‘actively promoted out of the core, thermal striping will prevail. Furthermore we note that CFD can be considered a ‘separate effects (computational) test’ and is recommended as part of any integral analysis. To this effect, poorly mixed streams then have potential impact on the rest of the SFR design and scaling, especially placement of internal components, such as the IHX that may see poorly mixed streams.

Finally, due to lack for infrastructural support for carrying out sodium experiments, only water experiments were realized in, an otherwise, sodium-approved experimental apparatus. It remains available to interested parties. .

References

University of Tennessee - Knoxville V&V paper refs

Standard for Verification and Validation in Computational Fluid Dynamics and Heat Transfer, ASME V&V 20-2008, American Society of Mechanical Engineers, 2008.

Test Uncertainty, ASME PTC19.1-2005, American Society of Mechanical Engineers, 2005.

Guide for the Verification and Validation of Computational Fluid Dynamics Simulation, AIAA G-077-1998, American institute of Aeronautics and Astronautics, 1998.

AIAA Committee on Standards for Computational Fluid Dynamic: status and plan, Cosner, R. R, Oberkampf, W. L., Rumsey, C.L., Rahaim, C.P. and Shih, T.I., AIAA 2006-0889.

Terminology for Model Verification Credibility, Schlesinger, S. Simulation, Vol. 32, No. 3, 1979, pp. 103-104.

Standard Guide for Evaluating the Predictive Capability of Deterministic Fire Models. ASTM std. E1355-05a, ASTM 2005.

Verification & Validation of Selected Fire Models for Nuclear Power Plant Applications, NUREG-1824, U.S. NRC with the Electric Power Research Institute (EPRI) and National Institute of Standards and Technology (NIST). 2007.

An Overview of the Code Scaling, Applicability and Uncertainty Evaluation Methodology, B.E. Boyack, I. Catton, R.B. Duffey, P. Griffith, K.R. Katsma, G.S. Lellouche, S. Levy, U.S. Rohatgi, G.E. Wilson, W. Wulff, N. Zuber. J. Nuclear Engineering and Design, Vol 119, No. 1, 1990, pages 1-16.

Best Practice Guidelines for the Use of CFD in Nuclear Safety Applications, Committee on the safety of nuclear installations, NEA/CSNI/R(2007)5.

University of Idaho References

U.S. Atomic Energy Commssion. (1970). *A Study of Piping Materials for Sodium Piping in LMFBR Plants.* Technical Report 228,

Alfonsi, G. (2001). Analysis of Streamwise Velocity Fluctuations in Turbulent Pipe Flow with the Use of an Ultrasonic Doppler Flowmeter. *67*, 137-142.

Arimatsu, T., Wada, S., Kikura, H., Aritomi, M., & Mori, M. (2004). Development of Flow Rate Measurement on Open Channel Flow Using Ultrasonic Doppler Method. *Proc. of 4th International Symposium on Ultrasonic Doppler Method for Fluid Mechanics and Fluid Engineering.* Sapporo.

Böck, H. (n.d.). *Module 11 Liquid Metal Fast Breeder Reactors (LMFBR)*. (A. o. Universities, Producer) Retrieved from http://www.ati.ac.at/fileadmin/files/research_areas/ssnm/nmkt/11_LMFBR.pdf

Borowsky, J., & Wei, T. (2006). Simultaneous Velocimetry/Accelerometry Measurements in a Turbulent Two-Phase Pipe Flow. *Experiments in Fluids , 41*, 13-20.

Cengal, Y. A., & Boles, M. A. (2008). *Thermodynamics An Engineering Approach* (6th Edition ed.). McGraw Hill.

Chandran, R. K., Banerjee, I., Padmakumar, G., & Reddy, K. S. (2011). Investigation of Thermal Striping in Prototype Fast Breeder Reactor Using Ten-Jet Water Model. *Heat Transfer Engineering , 32* (5), 369-383.

Cissel, D. W., Coelman, L. F., Pancner, F. O., Smith, F. A., & Tevebaugh, A. D. (1970). *Guidelines for Sodium Fire Prevention, Detection, and Control.* Argonne National Laboratory (ANL-7691), Report of the Ad Hoc Committee on Sodium Fires.

Cushing, V. (1964). Magnetoelectric Flowmeter. *The Review of Scientific Instruments , 35.4*, 496-499.

Deev, A. V., Rasheed, T., Welsh, M. C., Khan, M. M., & Rasul, M. G. (2009). Measurement of Instantaneous Flow Velocities in a Concentric Reducer Using Particle Image Velocimetry: Study of Scale Deposition. *Experimental Thermal and Fluid Science , 33*, 1003-1011.

Durve, A., Patwardhan, A. W., Banarjee, I., Padmakumar, G., & Vaidyanathan, G. (2011). Numerical Investigation of Mixing in Parallel Jets. *Nuclear Engineering and Design , 242*, 78-90.

Eckert, S., & Gerbeth, G. (2008). Velocity Measurements in Liquid Metal Flows Using the Ultrasonic Doppler Method: Examples and Perspectives. *Proc. 6th International Symposium on Ultrasonic Doppler Methods for Fluid Mechanics and Fluid Engineering*, (pp. 1-6). Prauge, Czech Republic.

Eckert, S., & Gerbeth, G. (2002). Velocity Measurements in Liquid Sodium by Means of Ultrasound Doppler Velocimetry. *Experiments in Fluids , 32*, 542-546.

Eckert, S., Cramer, A., & Gerbeth, G. (2007). Velocity Measurement Techniques for Liquid Metal Flows. *Magnetohydrodynamics-Historical Evolution and Trends* , 275-294.

Fanning, T. H. (2007). *Sodium as a Fast Reactor Coolant.* U.S. DOE/U.S NRC.

Hayashi, H., Becker, A., & Evans, J. W. (1990). Toward a Probe for Velocity Measurement in Molten Metals at High Temperature. *Metallurgical and Materials Transactions , 830.4*, 623-630.

Hosokawa, S., & Tomiyama, A. (2009). Multi-Fluid Simulation of Turbulent Bubbly Pipe Flows. *Chemical Engineering Science , 64*, 5308-5318.

Ichimiya, M., Hill, R., Roglans, J., Fiorini, G.-L., Hahn, D., Abram, T., et al. (2006, May). R&D Program Plan for the Sodium Fast Reactor (SFR). (S. P. Committee, Compiler)

Idaho National Laboratory. (n.d.). *Experimental Breeder Reactor-1*. Retrieved from www.inl.gov/ebr/

Kale, R. D., & Rajan, M. *Developments in Sodium Technology.* Indira Gandhi Centre for Atomic Research, Kalpakkam, India.

Kapulla, R., Sigg, B., Horanyi, S., & Hudina, M. (2000). Local Velocity Measurements in a Thermally-Stratified Sodium Mixing Layer Using a Permanent-Magnet Probe. *Experimental Thermal and Fluid Science , 20*, 115-136.

Kimura, N., Nishimura, M., & Kamide, H. (2002). Study on Convective Mixing for Thermal Striping Phenomena (Experimental Analysis on Mixing Process in Parllel Triple-Jet and Comparisons between Numerical Methods). *JSME International Journal , 45* (3), 592-599.

Knebel, J. U., Krebs, L., Muller, U., & Axcell, B. P. (1998). Experimental investigation of a confined heated sodium jet in a co-flow. *Journal of Fluid Mechanics , 368*, 51-79.

Knief, R. A. (2008). *Nuclear Engineering: Theory and Technology of Commercial Nuclear Power.* American Nuclear Society.

Koster, J. N. (1997). Visualizing Convection and Solidification in Metallic Alloys. *JOM* , 31-35.

Lock, G. S., & Trotter, F. J. (1968). Observations on the Structure of a Turbulent Free Convection Boundary Layer. *International Journal Heat Mass Transfer , 11*, 1225-1232.

Mashiko, T., Segawa, T., Sano, M., & Tsuji, Y. (2005). Simultaneous Measurements of Velocity Fields in Thermal Turbulence by USV and PIV. *Flow Measurement and Instrumentation , 17*, 107-112.

Meister, J. J. (1983). Mesure par echographie Doppler et modelisation theorique de l'effet de troubles cardiaques sur la pression et le debit arteriels. *These No. 504* .

Met-Flow. (2002). *User's Guide UVP Monitor Model UVP-DUO* (Vol. Release 5).

Mohammadi, N., & Mahjoob, M. J. (2009). Transmission Loss of Multilayer Panels Containing a Fluid Using Progressive Wave Model: Comparison with Impedance Progressive Model and Experiments. *C.R. Mecanique , 337*, 198-207.

Moore, G. (2008). Retrieved 2013, from Wikipedia: http://en.wikipedia.org/wiki/File:LMFBR_schematics2.svg

Nave, R. (2013). (G. S. University, Producer) Retrieved May 22, 2013, from HyperPhysics: http://hyperphysics.phy-astr.gsu.edu/hbase/nucene/fasbre.html#c4

Nishimura, M., Tokuhiro, A., Kimura, N., & Kamide, H. (2000). Numerical Study on Mixing of Oscillating Quasi-Planar Jets with Low Reynolds number Turbulent Stress and Heat Flux Equation Models. *Nuclear Engineering and Design , 202*, 77-95.

Nuclides and Isotopes, Chart of the Nuclides 16th Edition, KAPL. (2002). Lockheed Martin.

Obayashi, H., Tasaka, Y., Kon, S., & Takeda, Y. (2008). Velocity Vector Profile Measurement Using Multiple Ultrasonic Transducers. *Flow Measurement and Instrumentation , 19.3-4*, 189-195.

Omotowa, O. A. (2013). *Scaling Approach and Thermal Hydraulic Analysis in the Reactor Cavity Cooling System of a High Temperature Gas-Cooled Reactory and Thermal Jet Mixing in a Sodium Fast Reactor.* Dissertation, University of Idaho, Nuclear Engineering in the College of Graduate Studies.

Porta, P. A., Cutin, D. P., & McInerney, J. G. (2002). Laser Doppler Velocimetry by Optical Self Mixing in Vertical-Cavity Surface-Emitting Lasers. *IEEE Photonics Technology Letters , 14.12*, 1719-1721.

Schulenberg, T., & Stieglitz, R. (2010). Flow Measurement Techniques in Heavy Liquid Metals. *Nuclear Engineering and Design , 240* (9), 2011-2087.

Sorrell, F. Y., Curtin, T. B., & Feezor, M. D. (1990). An Electromagnetic Current Meter-Based System for Application in Unsteady Flows. *IEEE journal of Oceanic Engineering , 15.4*, 373-379.

Strakey, J. P., Bennett, C. O., & Dodge, B. F. (1974). Joule-Thomson Coefficients of Argon-Carbon Dioxide Mixtures. *AlChE Journal , 20* (4), 803-814.

Takeda, Y. (1991). Development of an Ultrasound Velocity Profile Monitor. *Nuclear Engineering and Design , 126*, 277-284.

Takeda, Y. (1987). Measurement of Velocity Profile of Murcury Flow by Ultrasound Doppler Shift Method. *Nuclear Technology , 79* (1), 120-124.

Takeda, Y. (1999). Ultrasonic Doppler Method for Velocity Profile Measurements in Fluid Dynamics and Fluid Engineering. *Experiments n Fluids , 26.3*, 177-178.

Takeda, Y. (1986). Velocity Profile Measurement by Ultrasound Doppler Shift Method. *International Journal Heat and Fluid Flow , 79.1*, 313-318.

Takeda, Y., Kobashi, K., & Fischer, W. E. (1990). Observation of the Transient Behaviour of Taylor Vortex Flow between Rotating Concentric Cylinders after Sudden Start. *Experiments in Fluids , 7* (4), 313-318.

Tasaka, Y., Yano, K., & Jima, M. (2008). Ultrasonic Investigation of Flow Transistion in Surface Switching of Rotating Fluid. *Sixth International Symposium on Ultrasonic Doppler Methods* , 159-162.

Tennekes, H., & Lumley, J. (1973). *A First Course in Turbulence.* The Massachusetts Institute of Technology.

Teufel, M., Trimis, D., Lohmuller, A., Takeda, Y., & Durst, F. (1992). Determination of Velocity Profiles in Oscillating Pipe-Flows by Using Laser Doppler Velocimetry and Ultrasonic Measuring Devices. *Flow Meas. Instrum , 3* (2), 95-101.

Tokuhiro, A. (1999). Experimental Investigation of a Vertical Planar Jet by Ultrasound and Laser Doppler Velocimetry. *Journal of Nuclear Science and Technology , 36* (6), 540-548.

Tokuhiro, A., & Kimura, N. (1999). An Experimental Investigation on Thermal Striping Mixing Phenomena of a Vertical Non-buoyant Jet with Two Adjacent Buoyant jets as Measured by Ultrasound Doppler Velocimetry. *Nuclear Engineering and Design , 188*, 49-73.

Tschaepe, L. (2012). *Liquid Jet Experiments and Simulations for a Verification and Validation Study.* Dissertation for the Doctorate of Philosophy, University of Tennessee, Knoxnille.

Tsuji, T., & Nagano, Y. (1989). Velocity and Temperature Measurements in a Natural Convection Boundary Layer Along a Vertical Flat Plate. *Experimental Thermal and Fluid Science* , 208-215.

US DOE Nuclear Energy Research Advisory Committee and the Generation IV Int. Forum. (2002). A Technical Roadmap for Generation IV Nuclear Energy Systems. *GIF-002-00* .

Yamanaka, G., Kikura, H., Takeda, Y., & Aritomi, M. (1999, September 20-22). Flow Measurement on Oscillating Pipe Flow Near the Entry Using UVP Method. *Second International Symposium on Ultrasonic Doppler Methods* , 21-24.

Zhang, H., Zhao, H., Mousseau, V., & Szilard, R. (2009). *Design Considerations for Economically Competitive Sodium Cooled Fast Reactors.* ICAPP. INL/Con-08-14889.

University of Tennessee – Knoxville Theses

Peters, S.P., Thermocouple temperature measurements for twin jet thermal mixing, MS Thesis, University of Tennessee – Knoxville, December 2011.

Tschaepe, L.P., Liquid jet experiments and simulations for a verification and validation study, Ph.D. Thesis, University of Tennessee – Knoxville, January 2012.

University of Idaho Theses

Omotowa, O.A., Developing scaling and order of magnitude analyses in coarse to fine-scale reactor thermal-hydraulics, Ph.D. Thesis, University of Idaho, March 2014.

Seaver, N., Initial experiments in thermal jet mixing of water, MS Technical Report, May 2014.

APPENDIX A: Experimental Apparatus Design and Operation

ACTIVITY PRINCIPAL INVESTIGATOR, LAB LEAD, and SPONSORING ASSOCIATE DIRECTOR

PI(s): Akira Tokuhiro
LL: Travis McLing
AD: Bob Smith

ACTIVITY LOCATION BY LAB ROOM NUMBER
Deflagration room Lab 114

Principal Investigator, Laboratory Lead, and CAES Safety Officer Approvals

	Print	Sign	
Principal Investigator:	Akira Tokuhiro		Date:
	Print	Sign	
Laboratory Lead:	Travis McLing		Date:
	Print	Sign	
CAES Safety Officer:	Kristi Moser-Mcintire		Date:

RESEARCH STAFF
Nathan Seaver, M.S. Student of Mechanical Engineering, University of Idaho
Other graduate students working for PI: Akira Tokuhiro

MAJOR EQUIPMENT USED IN ACTIVITY

Labconco Protector Glove box
Cabinet with Sodium Loop inside

1. PURPOSE/SCOPE/APPLICABILITY (include activity abstract and objectives)

Under NEUP-321, we propose a research project to address some of the principal technology issues related to sodium-cooled fast reactors (SFR); primarily concurrent development and demonstration of ultrasonic measurement diagnostics linked to effective thermal convective sensing under anticipated normal and off-normal operations and maintenance.

Sodium, although well suited as the heat transfer medium for the SFR, is chemically reactive and (optically) opaque. As such, sodium presents engineering accessibility constraints relative to light water reactors (LWR) operations and maintenance (O&M) and in-service inspection (ISI) technologies. Thus in terms of thermo-hydraulic measurements under normal conditions, and before/after off-normal events (maintenance, unanticipated events), there are limited sensing options. Acoustic methods, primarily ultrasonic, are a key measurement technology with applications in non-destructive testing, under-sodium (components) imaging, thermometry and velocimetry. Here, the co-PIs aim to demonstrate ultrasonic technology in a small sodium-based heat transfer experiment.

Research Activity Description (include activity approach)

1.1.1 Introduction

The international sodium fast reactor R&D effort, most recently summarized in the R&D Program Plan for the Sodium Fast Reactor (SFR), rests on relatively well-established technologies and reactor engineering knowledge and experience base. Thus, within the context of renewed interest in the SFR and the closed fuel cycle, the majority of the R&D issues that remain are technology performance and demonstration related issues, rather than feasibility of concepts. Both under the Generation IV and GNEP objectives, there is a need to re-address the probability of SFR realization in terms of design concept economics, in-service inspection and repair, verification of inherent safety and updated analyses (i.e. advanced simulations).

Sodium, although well suited as the heat transfer medium for the SFR, is chemically reactive and (optically) opaque. As such, sodium presents engineering accessibility constraints relative to LWR operations and maintenance (O&M) and in-service inspection (ISI) technologies. Thus in terms of thermo-hydraulic measurements under normal conditions, and before/after off-normal (maintenance, unanticipated events) events, there are limited sensing options. Acoustic methods, primarily ultrasonic, are a key measurement technology with applications in non-destructive testing, under-sodium (components) imaging, thermometry and velocimetry. Here, the University of Idaho co-PIs aim to demonstrate ultrasonic technology by addressing remaining issues as follows:

1) Design, construct and operate a university-based, small, simple but purposeful sodium flow loop with inventory of approximately 9 liters.
2) Develop and demonstrate ultrasonic velocimetry and thermometry, with focus toward improved SFR O&M. That is, velocimetry and thermometry as diagnostic tools during normal and off-normal operations.
3) Using the ANL sodium loop, the following may be accomplished: test a compact sodium-to-supercritical CO_2 heat exchanger and generate convective heat transfer

data, correlations and operational experience under normal and off-normal operations.

As further described, the project will yield a better qualitative understanding and quantitative means to sense the thermo-hydraulic condition of sodium under varied flow conditions. This project supports the R&D Program Plan for the SFR, within the current Gen' IV roadmap and emerging GNEP missions. The scope of work will demonstrate and evaluate ultrasonic technologies and define instrumentation options for the SFR. This will maintain and extend the U.S. nuclear SFR knowledge base, as well as educate the next generation of professionals familiar with the SFR.

1.1.2 Equipment Description

Enclosure

The enclosure was previously constructed and is currently located in the Deflagration room of the CAES fluids lab. Currently, it houses the natural convection cell as described and approved in a prior, separate project plan (CAES-P-024). It is a framework that can contain accidental sodium release by providing a heat sink floor. Acrylic sheets are available to be installed on the enclosure frame to prevent liquid sodium from spraying/splashing outside the enclosure in the direction of the experimenters.

Sodium Loop

The system consists of a number of key components connected via stainless steel tubing. The capability to fill an upper chamber and then conduct gravity induced flow measurement tests is necessary to the function of the loop. Figure 1 below shows these key elements.

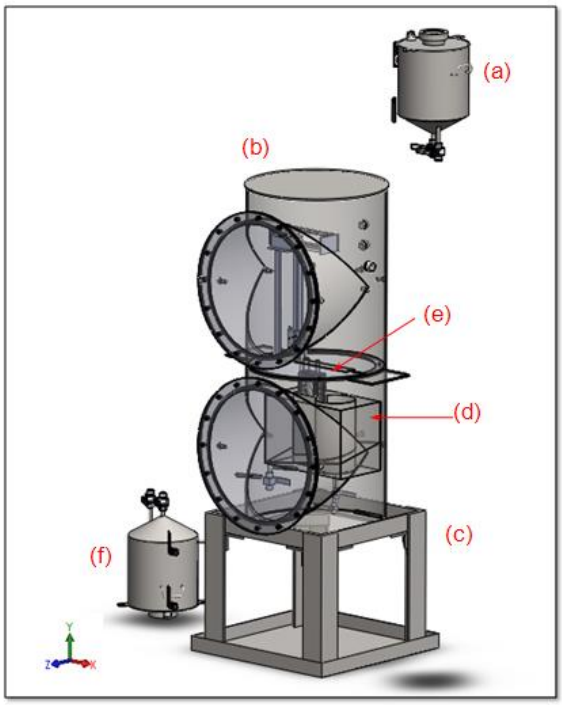

Figure 4. Basic elements of Sodium Loop; (a) Upper Transfer Tank (expansion tank), (b) Instrumentation Tank, (c) Support Base, (d) Test Section (Weir Assembly), (e) Multiple Transducer Cooling Jacket, (f) Lower Transfer Tank (Dump Tank).

The various components that enable function of the sodium loop and facilitate experiments are described below in conjunction with the diagram shown in Figure 1:
(a & f in diagram above) Transfer tanks- These tanks facilitate the movement of solid sodium ingots to the apparatus where sodium can be melted and then used for experiments. They are the primary storage container for the sodium inventory. The tanks are designed such that they can be taken in and out of the system under continuously inert atmosphere as necessary, and can be inserted into a glovebox for handling of solidified sodium under inert cover gas. Note that although these systems are air-tight, they should not exceed more than 15 psig; as such, there is no ASME pressure vessel stamp required.

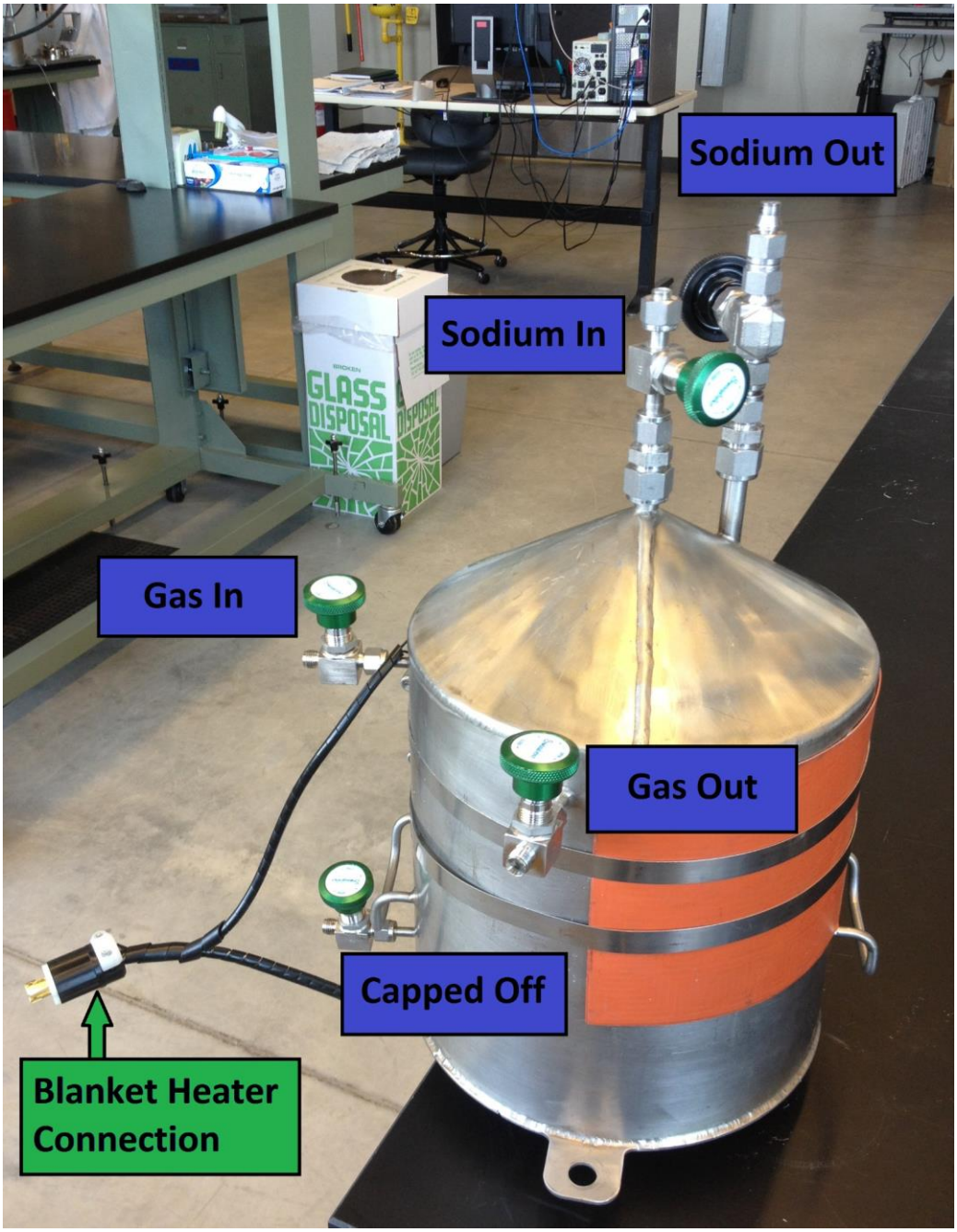

Picture 1. Transfer Tank Connections

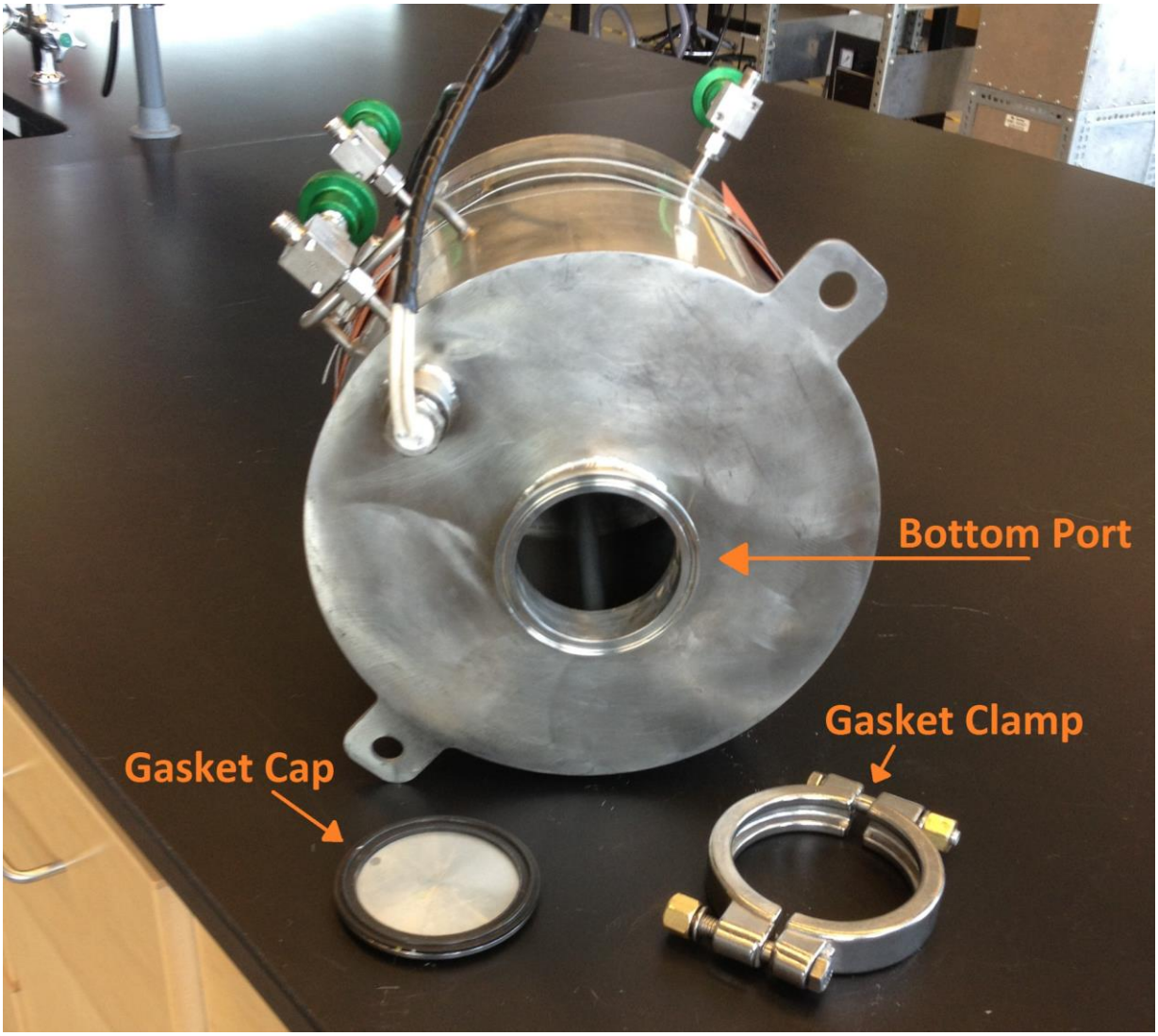

Picture 2. Transfer Tank

(b) Instrumentation tank- This large vessel houses the test section instrumentation movement and other sodium testing components such as probes, heaters and support systems for the tests. It is designed to maintain an air-tight seal and is continuously maintained having inert argon atmosphere to prevent the sodium from reacting with oxygen. Note that although the system is air-tight, it should not exceed more than 15 psig; as such, there is no ASME pressure vessel stamp required. There are two large gasket equipped ports to allow access to the interior of the container and which can be bolted securely with standard hardware. This section must be purged prior to the introduction of sodium into the system; therefore all instruments will be positioned and installed by hand prior to installation of transfer tanks (containing sodium inventory). During experiments and at other times, instruments may be adjusted via remote control using devices housed within the Instrumentation Tank. For this purpose, this vessel is equipped with transducer glands providing power and electrical control of items within the vessel.

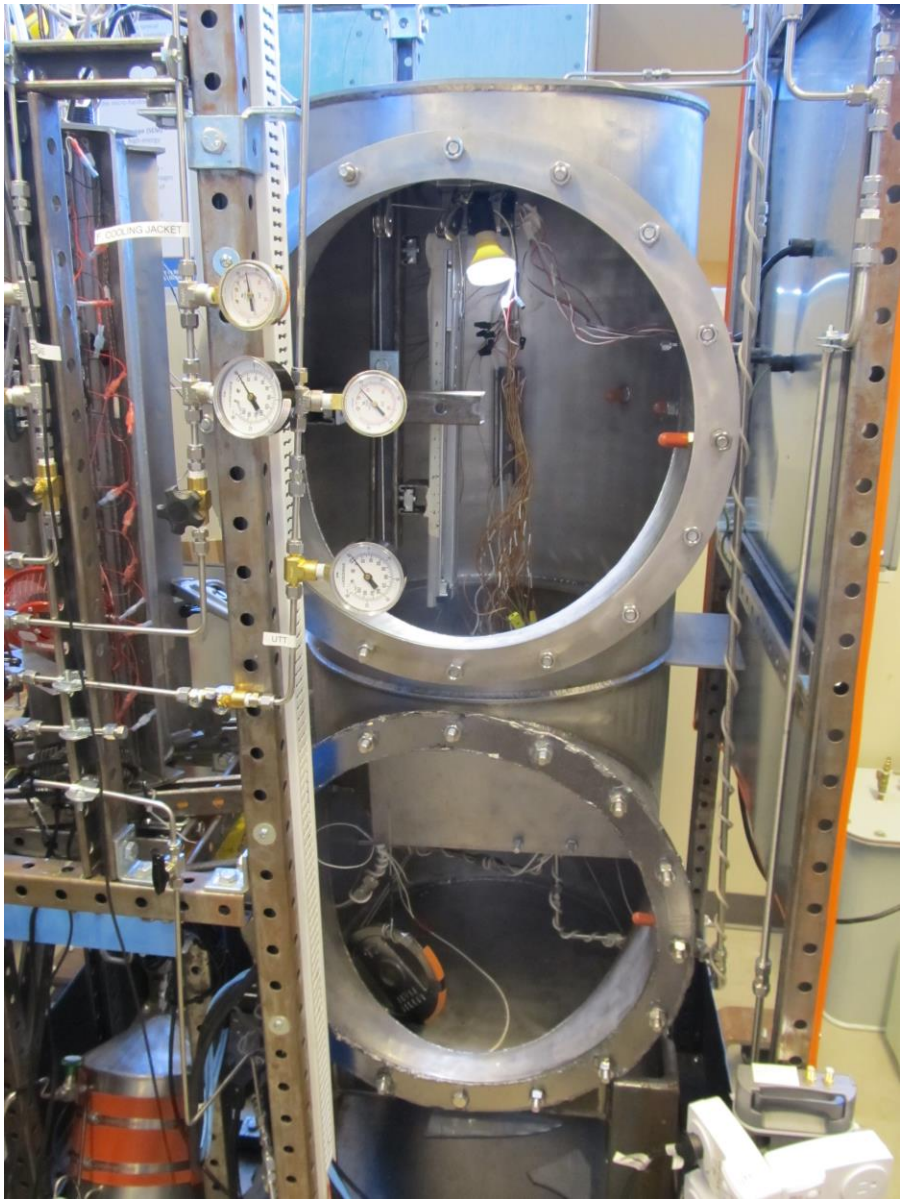

Picture 3. Instrumentation Tank

(b)

(a)

Picture 4a and 4b. Instrumentation Tank Electrical and Instrument Penetrations

(c) Support base- The support base's primary function is to elevate the Instrumentation Tank. The Instrumentation Tank must be high enough to allow natural draining of the sodium to the dump tank. Draining occurs after each test and must be available for emergency drainage under loss of power conditions.

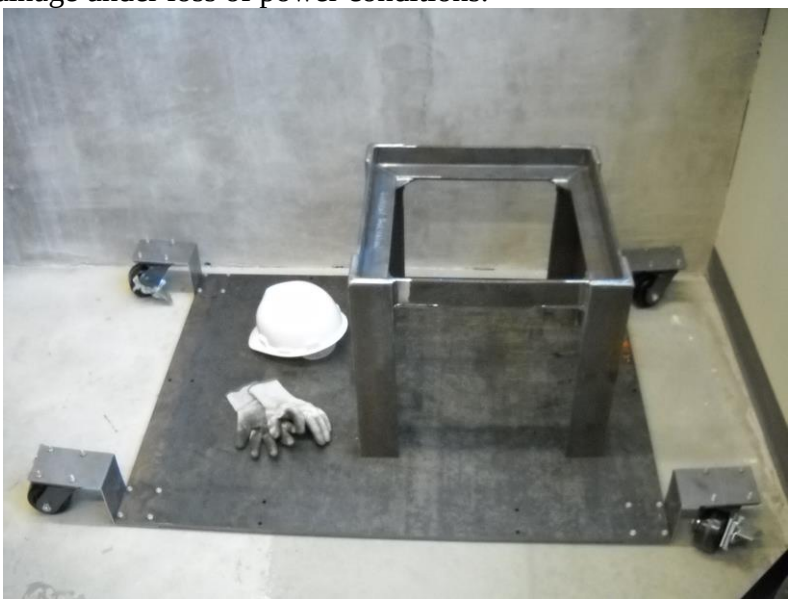

Picture 5. Support Base and Enclosure Floor

(d) Forced convection test section- The test section for the project is constructed in such a way that two liquid sodium streams fill a portion (weir) continuously. As excess sodium enters the volume, it spills from the weir into a collection pool referred to as the weir catch box. These volumes together are larger than necessary to collect the entire inventory of sodium released during a test. After each test this inventory is all drained to the dump tank (LTT) for storage or a subsequent test. Test durations may last more than a minute. The weir location is where actual data acquisition takes place using specially developed sensors. These sensors take measurements of temperature and velocity of the fluid streams as they interact with the sodium volume within the weir. A picture of this general concept is shown in figure 2.

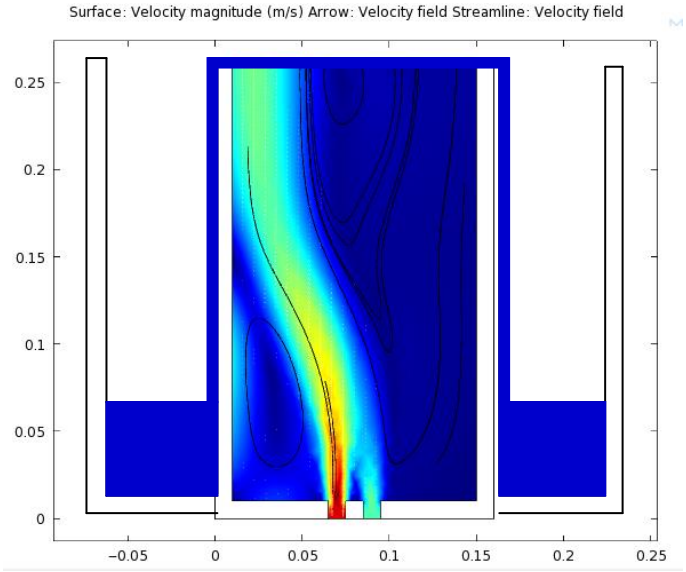

Figure 2 Schematic of weir, weir catch box, and fluid jets. Sensors are not shown, but would enter from the top, being inserted into the weir full of liquid sodium. Sodium is apparent colored portion shown spilling over the weir into the weir catch box. (Units in meters)

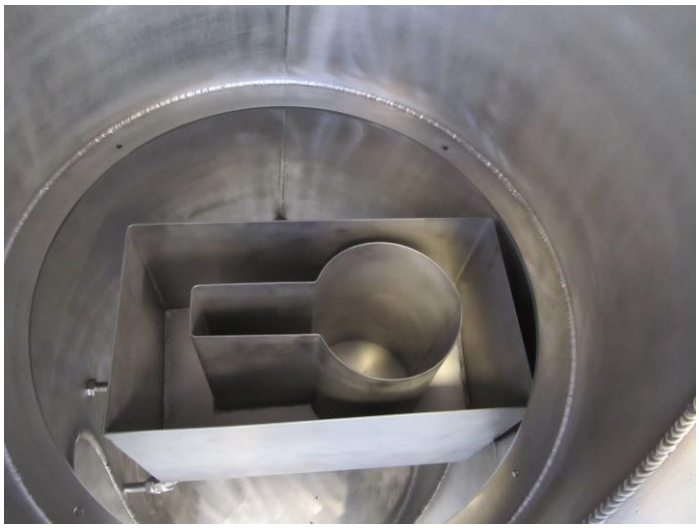

Picture 6. Weir

(e) Transducer cooling jacket- The transducers used (described below) are limited to use below the temperature limit at which sodium melts. An array of transducers, as implemented in the project, must be cooled by inert gas flow within a protective housing.

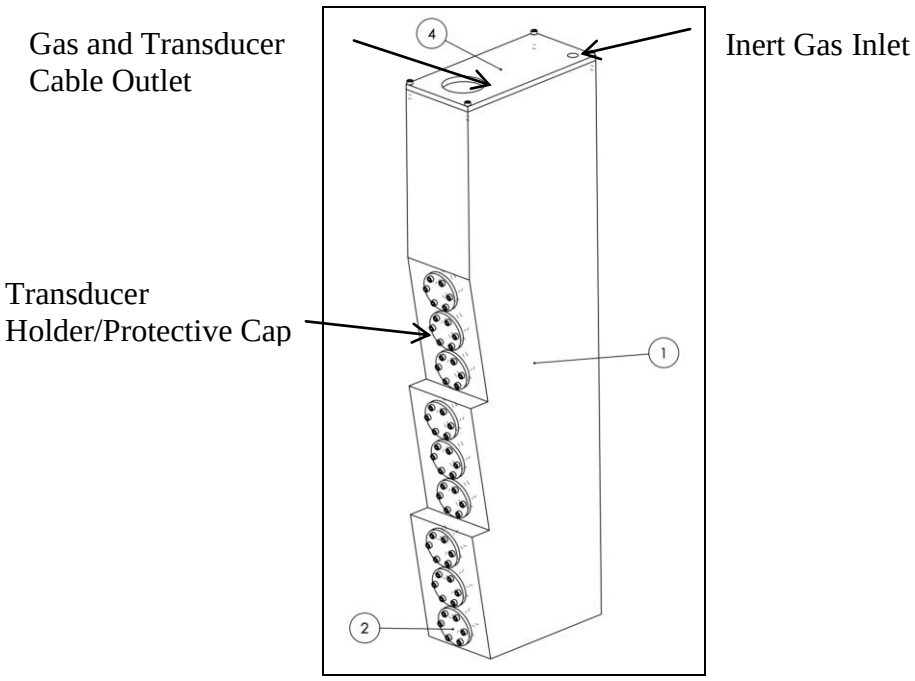

Figure 3. Multiple Transducer Cooling Jacket.

Cooling is to occur over the duration of a test and provide sufficient protection to maintain transducers under the allowable temperature. Figure 3 shows the cooling jacket that will be used to protect the transducers from the sodium environment. Argon will be fed through a pipe on the top of the cooling jacket at a pressure higher than atmosphere to exploit the Joule-Thompson cooling effect. The gas inlet has internal piping that extends to the bottom of the cooling jacket housing. Expanded gases will evacuate through an open port at the top of cooling jacket and into the instrumentation tank.

Note: The following are either not shown or labeled in the diagram shown above and may be somewhat difficult to find therein.

Ultrasonic transducers (UTS)- The transducers will use ultrasonic Doppler velocimetry (UDV) as the primary method to obtain velocity and temperature data during testing. 4 MHz transducers from Met-Flow with a maximum operating temperature of 60°C are used, see Picture 7. Due to the temperature limit these transducers will be mounted inside of the cooling jacket during testing. Velocity data is recorded using the Met-Flow Duo Multiplexer, and software installed on a computer.

Picture 7. Met-Flow Ultrasonic Transducer

Actuator- The actuator is used to relocate the cooling jacket in and out of the sodium volume. Following each test run, the cooling jacket will be withdrawn from the sodium volume to allow cooling. The cooling jacket may be removed from the heat of the liquid sodium during testing if the UTS approach a critical temperature. The vertical translation also allows the UTS to be repositioned in the volume of sodium to take readings of different profiles of the jets' flow.

Picture 8. Actuator

Data Acquisition System (DAQ)- Instruments composed of a computer, National Instruments (NI) chassis, switch, nano-volt resolution multi-meter and associated hardware and software. This must be in close proximity to the Instrumentation Tank because of length restrictions on thermocouple sensor wires. The electronic components and hardware reside outside of the Instrumentation Tank, and collect data via a "wire gland" which is a hermitically (impervious to air) sealed wire feed-through.

Temperature and Valve Controllers- Temperature controllers are used to control the heaters in the system to maintain the valves and sodium lines at the desired temperature such that sodium in its liquid state. K Type thermocouples are placed on sodium lines and all remote valves to monitor the temperatures in the system. Thermocouples placed on the UTT, LTT, Weir, gravity jet line, pressure jet line, and sodium transfer line provides temperature feedback to the temperature controllers. Electrical switches also remotely actuate several sodium flow valves to control the flow of sodium throughout the system.

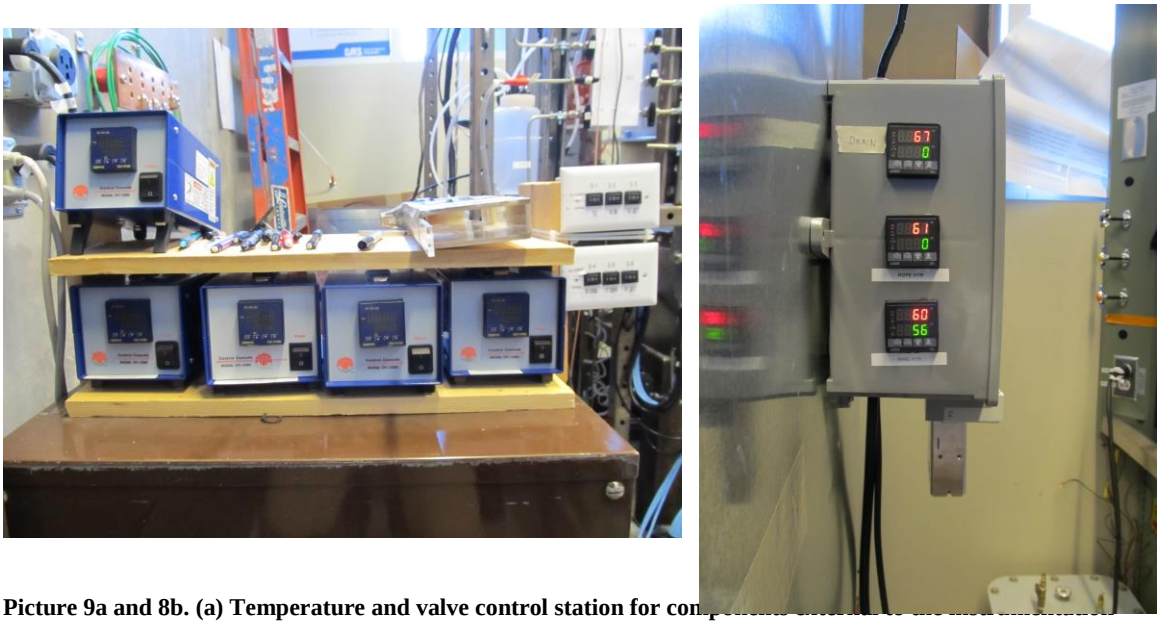

Picture 9a and 8b. (a) Temperature and valve control station for components external to the instrumentation tank. (b) Temperature control station for components internal to the instrumentation tank

NI based user interface- Labview software control panel through which several system parameters may be monitored. Labview is used to monitor the temperatures from k-type thermocouples throughout the system that are not connected to the controllers and record the temperature profile within the weir during experimentation. Monitored process control thermocouples were installed on all six remote valves and one on the vertical run of the gravity jet near the penetration into the instrumentation tank. Thirty experimental data collection thermocouples penetrate into the instrumentation tank and are monitored through the Labview program. The thermocouples are connected to the DAQ through terminal block interface modules; see Picture 9. A sample of the Labview code to collect and display temperature is shown in Appendix E.

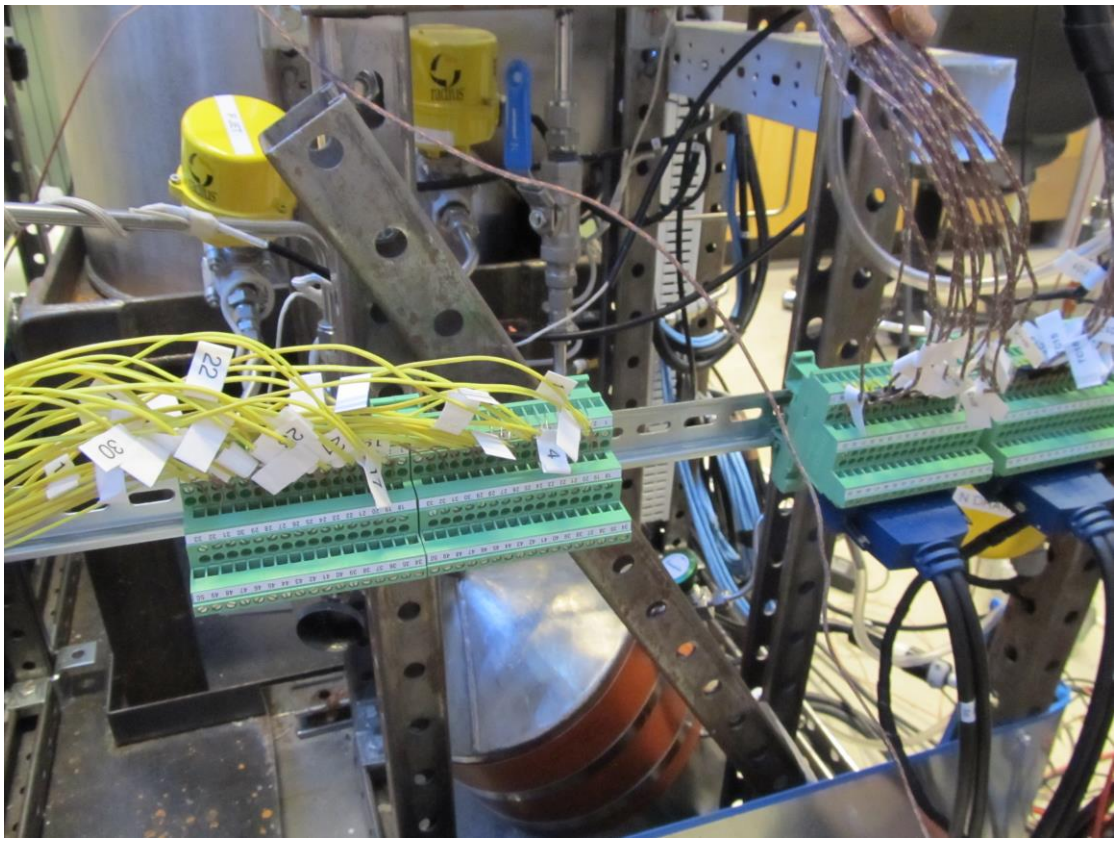

Picture 10. Terminal block interface

Loop Operations and Function- The loop will be installed next to the currently operational Natural Convection Cell, which is described in the project plan called, "SODIUM NATURAL CONVECTION NERI-037." This will require a number of important discrete benchmarks to reach operational status. How the loop is installed, tested, and operated will be described here.

Containers for transporting the sodium to and from a glove box (Transfer Tanks) will have already been incorporated into the natural convection system under the previously mentioned project plan. These are matched to compatible hardware allowing the tanks to be moved from one setup to another within the same enclosure. Transport of sodium to the loop by this means will be a last step in bringing the system into operation.

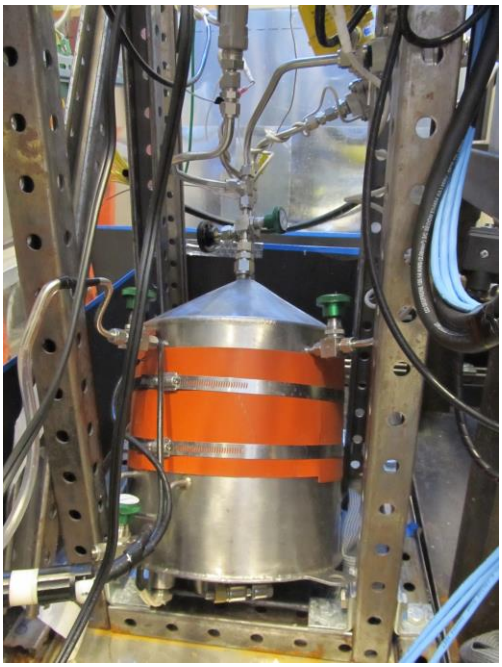

Picture 11a and 9b. (a) LTT and (b) UTT Connections to Natural Sodium Loop (a) (b) **Convection Cell and**

The basic operation of the loop begins with setting the temperature controllers to the desired temperature to melt the sodium in the LTT and heat the entire system to appropriate temperatures. Next the instrumentation and DAQ systems are powered up. Argon flow is initiated and the LTT is pressurized. Sodium is transferred from the LTT up through the transfer line and into the UTT. When the desired amount of sodium has been transferred the gravity jet and pressure jets are initiated and data is collected. When the sodium is depleted in the UTT or LTT (it is preferred to deplete the UTT before the LTT to reduce sodium splatter inside the test section) the pressure in the system is vented and all valves are closed. Once the pressure in the LTT has been reduced to near atmospheric levels the overflow drain valve is opened and the sodium is allowed to drain back into the LTT where the process may be repeated. All the sodium lines are sloped to drain into the LTT so that for any reason should the power be lost or the experiment shutdown the sodium will drain to a single location and in a place that is considered safe.

Installation of loop components into the enclosure involves the following steps and may not be an exhaustive list:

Project Steps

During the test there are 5 major steps: 1. Construction of apparatus. 2. Leak detection and verifying air-tightness. 3. Preparing the apparatus. 4. Running the test while monitoring the speed, temperatures and velocity. 5. Shutting down. These are generally going to consist of the bulleted steps. Please note these are overall steps and the final testing procedure is provided in Appendix C. Also, part of verifying the integrity of the apparatus

and test procedures steps 4 and 5 are to be conducted with water first, and part of step 3 after water testing will require a thorough cleaning and dry out. The process for cleaning and drying the apparatus as preparation to receiving sodium is provided in Appendix B.

1. Construction

- Instrumentation Tank must be set on stand within the enclosure.
- Enclosure must be completed.
- Test Section must be installed in the Instrumentation Tank.
- Sodium and Argon gas tubing must be installed and ready for Transfer Tanks.
- Electrically actuated valves must be installed as part of the sodium lines.
- Uni-strut framework must be installed to physically support Transfer Tanks.
- The actuator must be fixed within the upper section of the Instrumentation Tank.
- Class D fire extinguisher must be present and readily accessible.
- Electrical systems must be wired with heat resistant wiring.
- Heating apparatus (wires, tapes, elements) must be installed.
- Electricians must complete power upgrade to deflagration room.
- Thermal shielding and insulation (plates, foils, blankets, cements, filler, bricks etc.) put in place as needed.
- Initial instruments and probes must be placed.
- A small lamp and video camera device installed for remote visual inspection of test cavity.
- Venting system to handle off gasses (Argon, any off gasses from sodium etc.) needs to be in place. This must vent to the hood available.
- Installation of instruments.

2. Leak Detection and Verifying Air-Tightness

- The apparatus and enclosure will be completed.
- Pressure test to ensure the system will hold pressure at 14 psig overnight.
- It is intended that Helium leak testing will be performed on the system as a whole and modifications made until apparatus no longer leaks. Helium may be too difficult a test gas because of small atomic size, so this step may need to be replaced by the previous step where Helium may be used at pressure or, some other inert gas.

3. Preparing the Apparatus

- Computer and instruments will be turned on and all programmed control processes will be activated and system parameters will begin being monitored.
- Argon will be used to flush the entire loop volume including all chambers, tanks and tubing.
- Placement of Transfer Tanks with Sodium into the system and final tubing connections made.

4. Conducting a Test:

- The lower container having Sodium will be heated to above 100°C to melt contents.
- All system components heated above 100°C to maintain appropriate experimental temperatures and to prevent solidification of sodium in tubing.
- Sodium will flow to the upper Transfer Tank via low pressure difference (pressure < 15 psig).
- Sodium will be released to flow into test section and flow behavior observed via instruments.

5. Shutting Down:

- Turn off Experiment and Data Acquisition equipment.
- At the conclusion of a run, the valves to the lower dump tank will be opened remotely and all contents will drain to this chamber.
- If another run is desired, the system can be readied and pressurized again.
- Upon completion of final experimental run, the apparatus will be allowed to cool and sodium solidified in the dump tank.
- Instruments and computers may be shut down and disconnected as appropriate.
- Turn off heaters and let device cool to room temperature.
- Remotely close Sodium Valves to seal Sodium in the bottom container.
- Close gas valves.
- Nested Cylinders and Sodium containers may be removed for storage at this time or remain in the testing enclosure for further work if needed.

Analysis of Results:

Data from the ultrasonic transducer and thermocouples will be acquired using a pre-bought data acquisition device, e.g. Met-Flow Duo and NI DAQ, and stored on a PC and saved.

2. RISK AND CONTROLS

Table 2.1 Risks and controls

Task: 1 Construction of apparatus (Sodium Loop)	**Hazard(s)**	Muscle strain, twisting, falling, pinching, hand tools, inhalation of fumes or particulate related to leak-proofing of enclosure with duct sealant and application of insulating cements to tubing, valves, etc.
	Engineering Control(s)	A lifting device may be required to install large equipment. This may be an overhead crane, or other similarly capable ground based item. Max assembly weight is approx. 400 lbs. Design of assembly for limited pinch points. Fume Hood used when mixing chemical sealants or, cements.
	Administrative Control(s)	• Work limited to 50 pound lifting limit or 1/3 of body weight whichever is less.

		• When placing items or moving equipment, ensure that three point contact is constantly maintained with both feet solidly on the ground. • Use appropriate tool for job. • Keep tools in good working condition. • Use appropriate ventilation when applying sealants and mix powders/binders and or water etc., in a fume hood.
	PPE	• Leather or cut resistant gloves when working with sharp objects • Nitrile or latex gloves when using sodium. • Eye protection is worn at all times in the lab. • Hard-hat when doing work above head or, when in close proximity to beams, hanging or, protruding objects.
	Special Instruction(s)	All employees using the loop should read and understand the MSDS for sodium. This is to be included in the MSDS binder in the Fluids Lab.
	Task Specific Training	Hand and Power Tool Training

Task: 2 Sodium Transport and Charging of Loop	**Hazard(s)**	Contact with sodium, fire, caustic fumes, muscle strain
	Engineering Control(s)	Sodium is delivered in sealed bottles under Argon. All transfer of sodium from shipping containers to the upper tank is to be done in a glovebox under cover gas. Valves control the atmosphere of the transfer tank while installation is finalized. Use of Argon cover gas in sealed containers prevents air from contacting sodium. Solid phase sodium is less prone to fire than liquid phase. Melting temperature is 98 °C and gloveboxes require that objects never come close to this temperature.
	Administrative Control(s)	• A measuring device such as a thermometer or thermocouple will be used to ensure that the glovebox never reaches more than 35 °C. • One person shall lift not more than 50 lbs. at once. • Industrial valves will be closed prior to transport ensuring that air does not infiltrate container. Argon is denser than air and will prevent infiltration.
	PPE	Nitrile gloves, safety glasses
	Special Instruction(s)	• Open assemblies must not be left unattended for any reason. • Apparatus will be purged with Argon prior to heating or draining of sodium into lower cylinders.

		• Any smoke or unusual odors should be reported to the operator and preventative action should be taken to isolate and contain any sodium residue or fragments.
	Task Specific Training	Read MSDS for Sodium. Other training as specified in Appendix …Glovebox training as required.

Task: 3 Test Procedures at Operating Conditions	**Hazard(s)**	Overheating vessel, fire during operation
	Engineering Control(s)	• Containment for the apparatus will remain charged with Argon even while not in operation. It will be vented to the fume hood only. • Oxygen sensors will be incorporated into the assembly to detect concentrations of oxygen and will alarm in the event that maximum concentrations are exceeded. • Thermocouples will be used to monitor inside temperatures of devices and enclosures. • Test assembly is kept within enclosed cabinet with Argon cover gas. • The thermal mass of the outer containment is designed large enough to quickly solidify liquid sodium spills to prevent sodium from migrating outside of the container. All structural parts are rated for high operating temperature.
	Administrative Control(s)	• At least one operator shall oversee each test run. • The assembly is to be kept within the secured deflagration room of the CAES fluids lab during all procedures involving electrically generated heat. • Water access within the deflagration room is to be uninstalled or turned off at a valve outside of the deflagration room and lines drained previous to any sodium entering the deflagration room. • Sodium shall not be stored or transported in anything except a sealed container with inert gas cover. • A bucket of sand will be kept at hand to smother smoldering or burning materials should there be a vessel failure. • A Class D, recommended fire extinguisher for alkali metal fires is to be kept outside the deflagration room.
	PPE	Heat resistant gloves are required when handling items >124°F.
	Special Instruction(s)	
	Task Specific Training	

Task: 4 Shut Down	**Hazard(s)**	Freezing of sodium in tubing or valves
	Engineering Control(s)	Sodium is gravity driven to a tank where expansion of volume is safely accomplished as liquid freezes. Tubes and valves are heated to ensure there is no blockage.
	Administrative Control(s)	It is intended that any sealed fitting or will be disturbed as little as possible, therefore, if it becomes necessary to open any sealed item, a review processes will be undertaken to minimize likelihood of sodium contacting air.
	PPE	
	Special Instruction(s)	
	Task Specific Training	

3. WASTE GENERATION

No test material waste is to be expected from this project. Sodium will be reused for a separate experiment. The seal for the cap and the seals for the feed-through may need to be replaced if the lid of the experiment needs to be opened.

Type of Waste	Anticipated Volume	Container Type	Disposal Responsibility
General packaging materials, boxes, bags, cans, buckets, etc.	Large	bag	Dispose in Garbage.
Stainless steel scrap	<Liter	Box?	Dispose in Garbage or recycle
Spills of insulating cements, Spills of ducting sealant	<Liter	Bag	Scrape up and dispose of dry materials in garbage.
List any special needs/requirements for storage and handling and disposal of wastes.			
If a spill occurs, how will it be cleaned up? Use wipes and disposed of in cold waste.			

4. EMERGENCY PROCEEDURES

See Collocated Hazards Sheet

5. EXIT STRATEGY

Other graduate students will use the apparatus as a continuation of the NEUP-321 and NERI projects under Akira Tokuhiro. If funding is no longer available for the project, the apparatus will be stored outside of the CAES building by Akira Tokuhiro.

6. SUPPORTING DOCUMENTATION

Additional Documents Supporting this Project Plan

6.2 References

None

7. DRAWINGS AND DIAGRAMS

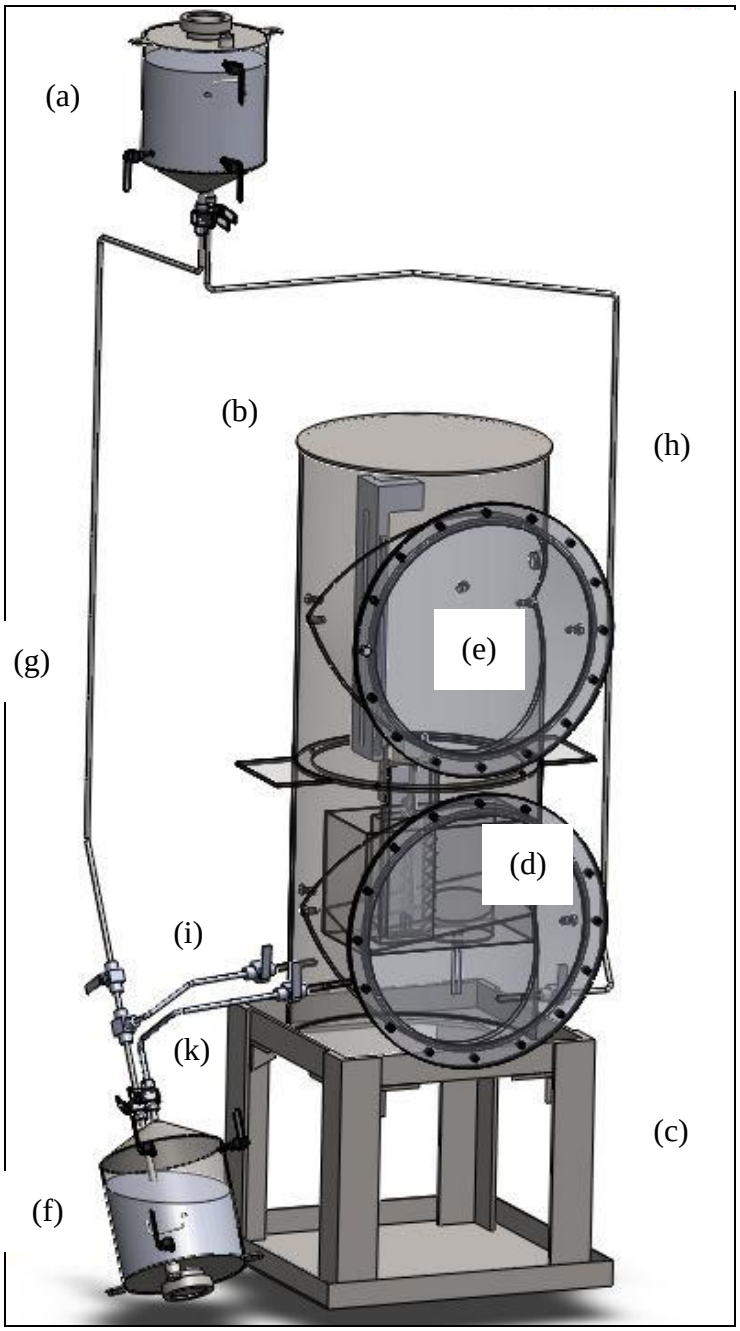

Figure 5. Basic Elements of Sodium Loop; (a) Transfer Tank (expansion tank), (b) Instrumentation Tank, (c) Support Base, (d) Test Section (Weir Assembly), (e) Instrument Area/Multiple Transducer Cooling Jacket, (f) Transfer Tank (Dump Tank), (g) Transfer Line, (h) Gravity Jet, (i) Pressure Jet, (k) Drain.

Picture 12. Fabricated Instrumentation Tank waiting for final positioning

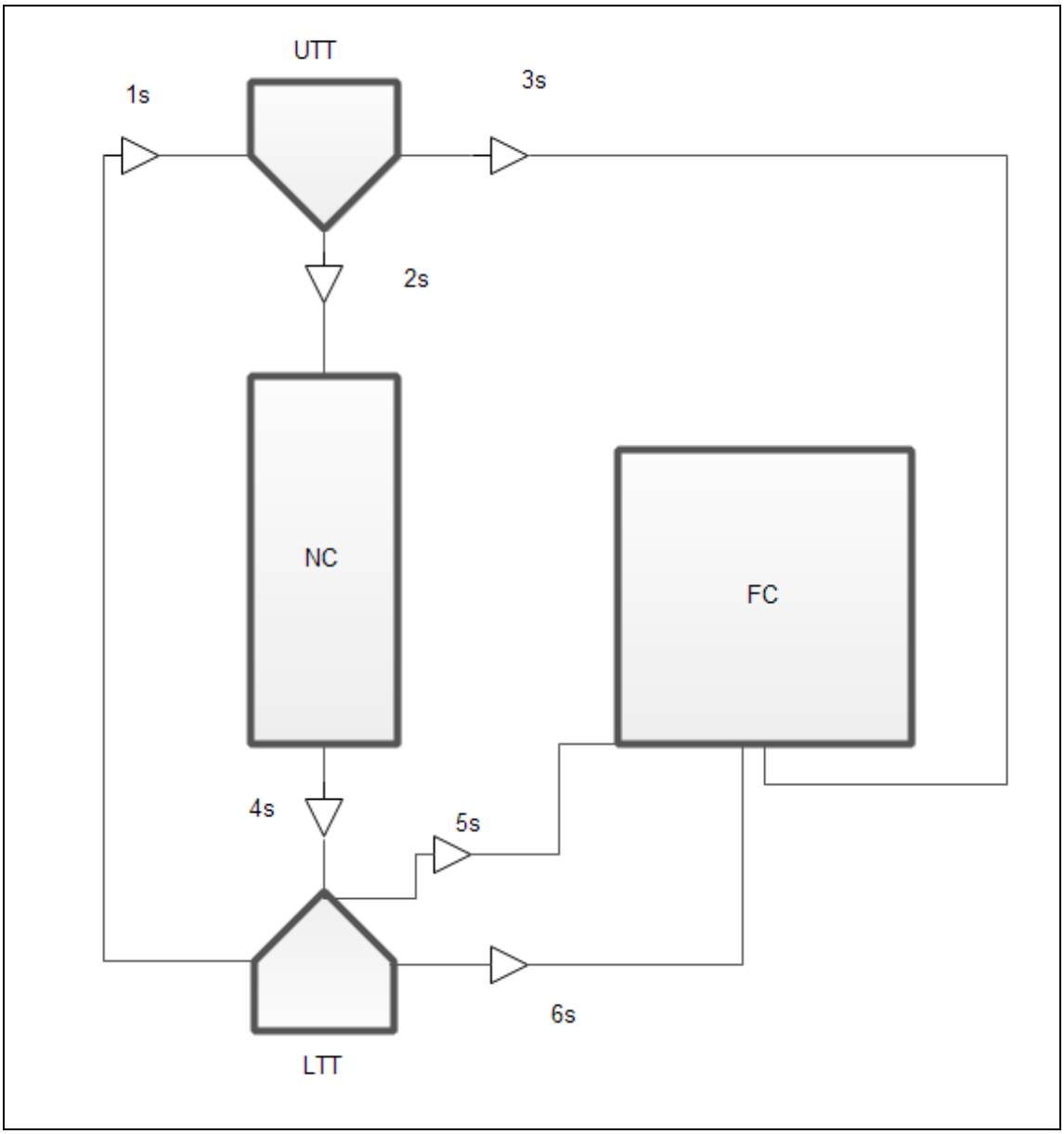

Figure 6. Sodium loop and remote actuated valve lines.

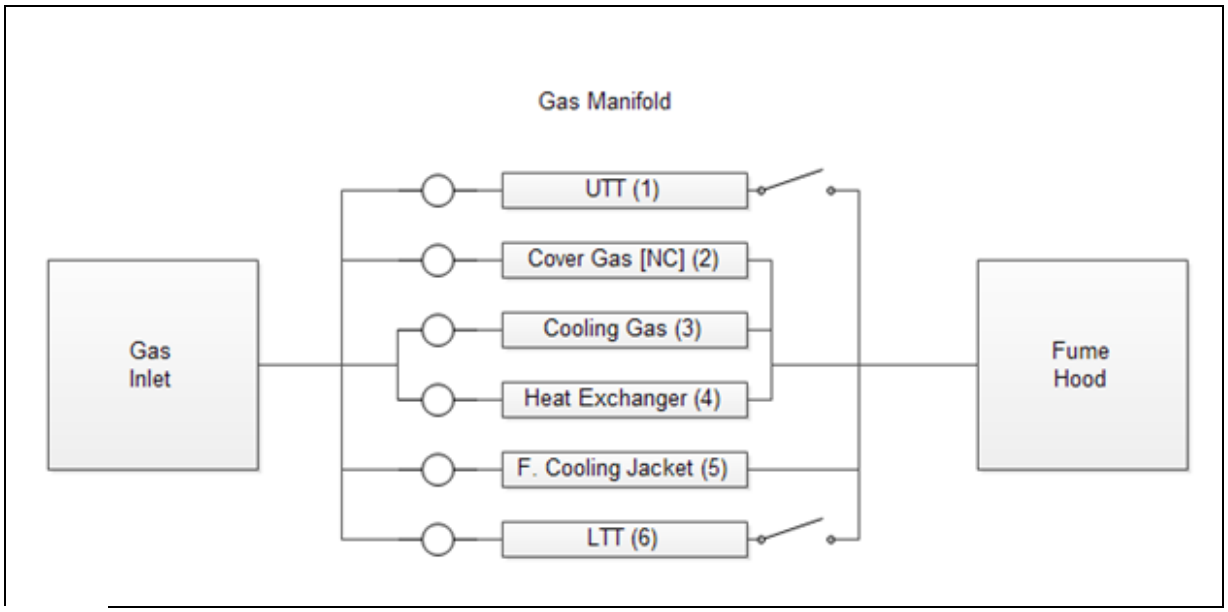

- Electronic Valve

- Pressure Gauge

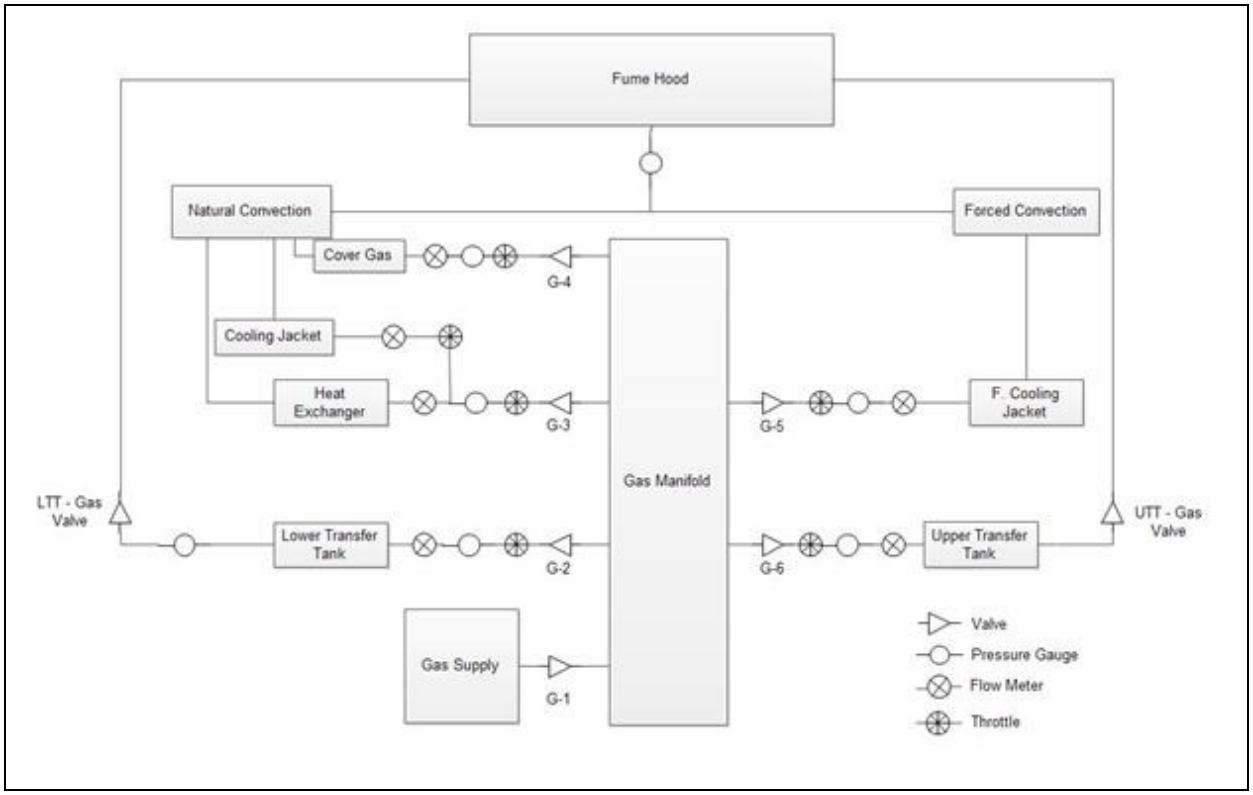

Figure 7. Gas flow diagram

8. APPENDICES

Appendix A1, Chemical Inventory

Appendix A2, Water Cleanout and Dry Out SOP
Appendix A3, Water and Sodium SOP
Appendix A4, Electrical Circuit Diagrams
Appendix A5, Sample Labview Code
Appendix A6, Test Matrix and Volume Calculations
Appendix A7, Met-Flow Duo Settings by Test Case

DOCUMENT COMMENTS

This document is a living document. Please provide recommendations below so that your inputs can be reviewed and incorporated into the next revision of this document.			
Contributor Name	Document Section	Comment	Date

Appendix A1

Chemical Inventory

Supporting Information: Chemical Inventory (Chemical hazards are captured in the body of the Project Plan - this section only provides a list of chemicals used in execution of the plan.)

Name	CAS Number	NFPA/ Known Hazards	Maximum Storage Volume	Comments
Sodium (Na)	Not yet assigned	Health 3 Fire 3 Reactivity 3	8-10 liters	
Industrial Argon	7440-37-1	Health 0 Fire 0 Reactivity 0 USDOT 2.2	~50 ft^3 per test	
Metal-Duct Sealant	100304	None	(2) 5lb	
Sauereisen Ceramic Cement	NA			
Graphite Based Thread Sealant	NA			

Appendix A2
Water Cleanout and Dry out SOP

Removal of water and air from the sodium loop prior to the introduction of sodium

A) Inspecting/preparing the system

1. Ensure that the system has undergone successful water testing (refer to the project checklist). If this has not been completed, do not proceed with this procedure. Sodium will not be introduced to the system without prior safety verification.
2. Ensure that all piping that will carry argon to the system is in place and unobstructed. This is important to do now before the system is heated and potentially dangerous to work with.
3. Remove all instrumentation that is not rated to operate in temperatures near 175 DGC (i.e. UVPs). This must be done because they will not be protected from heat during this procedure.
4. Make a visual inspection to ensure that there will be no flammable materials in contact with the system at any time during this procedure because it will get very hot.
5. Install "Experiment in Progress" and "Caution Hot Surface" signs to notify other persons as to what is being done to the system, particularly that it is hot and not safe to touch.
6.

B) Drying the system

1. Ensure that the entire system is drained of water by opening valves 1S-6S and the LTT and UTT vents (See Figure 2).
2. After draining for XXs valves 1S-6S and the LTT vent may be closed.
3. Close all of the LTT manual valves.
4. Remove the LTT from the system by undoing the piping on the outflow side of the LTT's valves, uncoiling the rope heaters from the LTT, disconnecting the blanket heaters that are mounted on the LTT, and removing the strapping that holds the LTT in place.
5. Holding the LTT upside down, remove the gasket cap and clamp. This will require more than one person so that the weight of the tank may be supported while unfastening occurs.
6. Drain the LTT into a sink in the Fluids Laboratory (CAES 113).
7. Use paper towels to dry the inside of the LTT as best as possible. This can be accomplished easiest if the person drying is able fit their hand completely inside the LTT. This should not be a forced fit due to the risk of not being able pull the hand out easily.
8. Refill the LTT with XXL isopropyl alcohol while holding it upside down.
9. Replace the gasket cap and secure the clamp. Securing the clamp is done by tightening both sides evenly until they are very snug.
10. Reinstall the LTT into the system by setting the LTT in position in the system, strapping the LTT in place, reconnecting the fittings that attached to the tank valves, reconnecting the tank's blanket heaters, and coiling the rope heaters.
11. Ensure that pressurized air is tied into the system so that it will flow through the argon lines (See Figure 1 to determine the correct inlet).
12. Open the supply line of the pressurized air source so that it is available to the system.
13. Open valve 6G and maintain the pressure of the LTT at 5 psi (See Figure 1).
14. Open valve 1S and the UTT vent (See Figure 2).

15. Allow the alcohol to flow to the UTT for about XXs so that it may be assumed that the total volume has been transferred.
16. Close valve 1S then open the LTT vent and stop the airflow into the LTT (See Figure 2).
17. Open valve 2S and allow the alcohol to drain from the UTT into the natural convection test section (See Figure 2). This will take about XXs to complete.
18. Open valve 4S and allow the alcohol to drain from the natural convection test section to the LTT (See Figure 2). This will take about XXs to complete.
19. Close valves 2S, 4S, and the LTT vent (See Figure 2).
20. Repeat step 14 and close valve 1S XXs after opening it, which will leave a portion of the system's alcohol in the LTT. This will allow alcohol to flow into the FC test section through both jets.
21. While continuing to maintain pressure in the LTT, open valves 6S and 3S so that alcohol can flow into the forced convection test section (See Figure 2).
22. After the alcohol has flowed for XXs, close valve 6S, stop airflow to the LTT, and open the LTT vent (See Figure 2).
23. Alcohol will continue to flow from the UTT for about XXs, after which valve 3S may be closed.
24. Open valves 5S and 6S to allow the outer and inner weirs of the test section to drain (See Figure 2). This will take about XXs.
25. Drain the entire system to the LTT by opening the LTT and UTT vent, valves 1S, 2S, 3S, 4S, 5S, and 6S (See Figure 2). Allow the system to drain for at least XXs to ensure complete draining.
26. Seal off the LTT completely by closing all of its manual valves (See Figure 3).
27. Disconnect the LTT from the system by undoing the piping on the outflow side of the LTT's valves, uncoiling the rope heaters from the LTT, disconnecting the blanket heaters that are mounted on the LTT, and removing the strapping that holds the LTT in place.
28. Holding the LTT upside down, remove the gasket cap and clamp. This will require more than one person so that the weight of the tank may be supported while unfastening occurs.
29. Dilute the alcohol in the LTT to XX%. This will make it safe to pour down a drain in the Fluids Laboratory (CAES 113).
30. Pour out the alcohol through a coffee filter into a sink in the Fluids Laboratory (CAES 113).
31. Use paper towels to dry the inside of the LTT as best as possible. This can be accomplished easiest if the person drying is able fit their hand completely inside the LTT. This should not be a forced fit due to the risk of not being able pull the hand out easily.
32. Reinstall the LTT into the system by setting the LTT in position in the system, strapping the LTT in place, reconnecting the fittings that attached to the tank valves, reconnecting the tank's blanket heaters, and coiling the rope heaters.
33. Plug in heater controllers, laptops, electronic valves, and DAQ.
34. Open all of manual and electronic valves found in the system and both transfer tank valves (See Figure X). This will maximize the evaporation of the fluid in the system.
35. Activate all of the heaters installed in the system to increase the rate of evaporation.
36. Use installed TCs to monitor the temperature of the system (this will require opening the Labview program or using separate readout units). The infrared heat gun may be used as well to spot check other areas of the system where TCs do not measure.
37. The temperature of the system should be maintained near 175 DGC per Pat Kern's recommendation.
38. The system should remain near 175 DGC for at least 2hrs to ensure complete dryness in the system.
39. Prepare to immediately begin Process C once the required time at full temperature expires.

40. Deactivate the heating units once the required time at full temperature has expired.
41.

C) Implementing cover gas and sealing the system

1. Ensure that pressurized argon is tied into the system so that it will flow through the argon lines (See Figure 1 to determine the correct inlet).
2. Turn on the argon gas flow at the storage cylinder so that the gas will be available to the system.
3. Ensure that the gas outflow piping is going from the system to the fume hood (See Figure 1)
4. Open 1G-6G and allow argon to flow through the system for XXs to ensure complete flooding.
5. Close the UTT vent and then the LTT vent.
6. Monitor the pressure in the system so that it does not go above 10 psi as the valves/vents are closed in this order: 5S, 6S, 3S, vents, all manual valves, 4S, 2S, 1S (See Figure 2). Reduce the gas flow as needed and turn off the gas completely once the manual valves of the LTT are closed. The trapped gas will remain in the system for when the sodium is introduced.
7. **If** removing the LTT for moving the sodium, follow step 4 of Process B and cap the lines that are disconnected from LTT as quickly as possible.

Appendix A3

Water and Sodium SOP

Aspects of this document can be distinguished as either process control or experimental procedures. Parts of this document that are process control related refer to the procedures that are critical to the safety of those operating the experiment. These will be highlighted in red to make them readily apparent. Parts of this document that are related to the steps that will be taken to obtain measurements while operations are within the bounds of process control are experimental procedures.

Water testing for leak detection and test process refinement

A) Leak and Residue Detection

1. Remove the LTT from the system by undoing the piping on the outflow side of the LTT's valves, uncoiling the rope heaters from the LTT, disconnecting the blanket heaters that are mounted on the LTT, and removing the strapping that holds the LTT in place.
2. Measure the weight of the empty tank using the scale in the Fluids Laboratory (CAES 113). The scale was moved to the Fluids Laboratory from the Analytical Chemistry Laboratory (CAES 210) and will need to be returned upon project completion.
3. Ensure all of the tank's manual valves are closed (turn directions are labeled) and remove the gasket clamp and cap found on the bottom of the tank (See Figures 3, 4).
4. Fill the LTT with 9 L of water by measuring with a large open beaker found in the Fluids Laboratory (CAES 113) and pouring it in through the port opened in the bottom of the LTT (See Figure 4). This will require two people because one person will need to hold and secure the tank upside down while the other fills it with water.
5. Replace the gasket cap and secure the clamp. Securing the clamp is done by tightening both sides evenly until they are very snug.
6. Measure the weight of the full tank using the scale in the Fluids Laboratory (CAES 113).
7. Reinstall the LTT into the system by setting the LTT in position in the system, strapping the LTT in place, reconnecting the fittings that attached to the tank valves, reconnecting the tank's blanket heaters, and coiling the rope heaters.
8. Wrap each joint with a colored paper towel using tape to secure it. In the event that any water leaks from a joint, the darkened spots on the colored towels will make noting them easier. Note: while paper towels are in contact with the system, the heaters will NOT be activated to avoid fire hazard.
9. Open the LTT manual valves labeled sodium out, sodium in, gas out, and gas in completely and ensure that the LTT vent is closed (See Figure 3). Opening these valves will allow water to be sent into the entire system.
10. Ensure that pressurized air is tied into the system so that it will flow through the argon lines (See Figure 1 to determine the correct inlet). The fume hood may provide the pressurized air supply.
11. Open the supply line of the pressurized air source so that it is available to the system.
12. Open valve G-6 and maintain the pressure of the LTT at (TBD) psi by using the G-6 line's throttle (See Figure 1).
13. Open valve S-1 and the UTT vent to begin water flow (See Figure 2).
14. Allow the water to flow to the UTT for about XXs so that it may be assumed that the total volume has been transferred.
15. Close valve S-1 then open the LTT vent and stop the airflow into the LTT (See Figure 2).

16. Take time to inspect the LTT, UTT, and transfer line that is regulated by valve S-1 for leaks. Make appropriate adjustments if leaks found (i.e. tightening fittings using Swagelok spacer tool, replace defective fittings, re-apply Rectorseal).
17. Open valve S-2 and allow the water to drain from the UTT into the natural convection test section (See Figure 2). This will take about XXs to complete.
18. Take time to inspect the transfer line regulated by valve S-2 for leaks. Make appropriate adjustments if leaks found (i.e. tightening fittings using Swagelok spacer tool, replace defective fittings, re-apply Rectorseal).
19. Open valve S-4 and allow the water to drain from the natural convection test section to the LTT (See Figure 2). This will take about XXs to complete.
20. Close valves S-2, S-4, and the LTT vent (See Figure 2).
21. Take time to inspect the transfer line regulated by valve S-4 for leaks. Make appropriate adjustments if leaks found (i.e. tightening fittings using Swagelok spacer tool, replace defective fittings, re-apply Rectorseal).
22. Open valve S-1 and the UTT vent to begin water flow (See Figure 2). Close valve S-1 XXs after opening it, which will leave a portion of the system's water in the LTT. This will allow water to flow into the forced convection (FC) test section through both jets.
23. While continuing to maintain pressure in the LTT, open valves S-6 and S-3 so that water can flow into the forced convection test section (See Figure 2).
24. After the water has flowed for XXs, close valve S-6, close G-6, and open the LTT vent (See Figure 2).
25. Water will continue to flow from the UTT for about XXs, after which valve S-3 may be closed.
26. Take time to inspect the transfer lines regulated by valves S-6 and S-3 for leaks. Make appropriate adjustments if leaks found (i.e. tightening fittings using Swagelok spacer tool, replace defective fittings, re-apply Rectorseal).
27. Open valves S-5 and S-6 to allow the outer and inner weirs of the test section to drain to the LTT (See Figure 2). This will take about XXs.
28. Take time to inspect the transfer line regulated by valve S-5 for leaks. Make appropriate adjustments if leaks found (i.e. tightening fittings using Swagelok spacer tool, replace defective fittings, re-apply Rectorseal).
29. Take time to inspect the entire system for leaks. Make appropriate adjustments if leaks found (i.e. tightening fittings using Swagelok spacer tool, replace defective fittings, re-apply Rectorseal).
30. Repeat parts of the process where leaks occurred until there are no detectable leaks.
31. Drain the entire system to the LTT by opening the LTT and UTT vents, valves S-1 through S-6 (See Figure 2). Allow the system to drain for at least XXs to ensure complete draining.
32. Seal off the LTT completely by closing all of its manual valves (See Figure 3).
33. Disconnect the LTT from the system by undoing the piping on the outflow side of the LTT's valves, uncoiling the rope heaters from the LTT, disconnecting the blanket heaters that are mounted on the LTT, and removing the strapping that holds the LTT in place.
34. Remove the LTT and record its weight.
    - NOTE: If the second recorded water weight is less than the first by more than one percent; the system will need to be dried following steps XXX of *Drying SOP*. Upon drying the system, refill the LTT, record its full weight, and run the water through the entire system using the aforementioned processes (excluding the paper towels). This is crucial because a difference between the first and second weights shows that a residue of fluid is being left behind in the system. A residue of sodium greater than one percent the original amount left in the system is unacceptable on safety terms.

- Some of the loss during the first water testing may be due to drips or leaks. After the second water test, if the second recorded water weight is more than one percent different there may be another fault in the system. Inspect the FC test section and the UTT to see if there is water remaining in them.

Natural convection process

1. Ensure that the LTT has been installed in the system filled with 9L of water by having set the LTT in position in the system, strapped the LTT in place, reconnect the fittings that attached to the tank valves, reconnected the tank's blanket heaters, and coiled the rope heaters.

- If the aforementioned step has not been completed, follow steps 1-7 of the *Leak and Residue Detection Process*.

2. Open the LTT manual valves labeled sodium out, sodium in, gas out, and gas in completely and ensure that the LTT vent is closed (See Figure 3). This will allow water to be sent into the system.
3. Ensure that pressurized air is tied into the system so that it will flow through the argon lines (See Figure 1 to determine the correct inlet).
4. Open the supply line of the pressurized air source so that it is available to the system.
5. Open valve G-6 and maintain the pressure of the LTT at (TBD) psi (See Figure 1).
6. Open valves S-1 and S-2 and the UTT vent (See Figure 2).
7. Allow the water to flow to the UTT for about XXs so that it may be assumed that the total volume has been transferred to the natural convection test section.
8. Close valve G-6 to stop the airflow to the LTT and open the LTT vent (See Figure 1).
    - Close valve S-2.
9. Initialize all associated instrumentation: laptops, DAQ, Labview, Duo,
10. Take initial temperature readings of the NC test section and record them in the designated lab notebook.
11. Activate the heaters and coolers of the NC test section to induce natural convection.
12. Allow the heaters and coolers to operate until steady state conditions are obtained. Steady state is considered obtained when the hot side of the test section is at XXDGC while the cold side is at XXDGC for XXs
13. Make desired measurements (outlined measurements can be found in *Natural Convection Measurement Procedures*).

- Keep an eye out for off normal events (i.e. leaks, over/under heating). If an off normal event occurs make note of the occurrence and resolve it if possible. Continue taking measurements once the event has been resolved.

15. Deactivate heater and coolers.
16. Open valves S-2 and S-4 to allow the water to drain completely into the LTT (See Figure 2). Draining time will be about XXs.
17. Power down instrumentation and unplug all system components (i.e. heaters, computers, DAQ, Duos) from their wall outlet power sources.
18. Close all of the manual valves of the LTT

- If desired, disconnect the LTT from the system by undoing the piping on the outflow side of the LTT's valves, uncoiling the rope heaters from the LTT, disconnecting the blanket heaters that are mounted on the LTT, and removing the strapping that holds the LTT in place. Record the tanks weight. Note whether or not the second measured fluid weight is within one percent of the first recorded weight.

C) Forced convection process

1. Ensure that the LTT has been installed in the system filled with 9L of water by having set the LTT in position in the system, strapped the LTT in place, reconnect the fittings that attached to the tank valves, reconnected the tank's blanket heaters, and coiled the rope heaters.

- If the aforementioned step has not been completed, follow steps 1-7 of the *Leak and Residue Detection Process*.

2. Open the LTT manual valves labeled sodium out, sodium in, and gas in (See Figure 3). This will allow water to be sent into the system.
3. Ensure that pressurized air is tied into the system so that it will flow through the argon lines (See Figure 1 to determine the correct inlet).
4. Open the supply line of the pressurized air source so that it is available to the system.
5. Open valve G-6 and maintain the pressure of the LTT at 5 psi (See Figure 1).
6.
7. Activate all associated instrumentation: laptops, Labview, DUOs, DAQ,
8. Open valves S-1 and the UTT vent (See Figure 2).
9. Allow water to flow to the UTT for XXs then close valve S-1.
10. Open valve S-6 to fill the forced convection test section with water for XXs then open valve S-3.
11. Take desired measurements for up to XXs and then close valve S-6, open the LTT vent, and close valve G-6 (See Figures 1, 2).
12. Open valve S-5 to drain the outer weir of the test section (See Figure 2). This will take XXs.
13. Open valves S-2 and S-4 to drain the UTT (See Figure 2). This will take XXs.
14. Close valves S-5, S-2, and S-4.
15. Repeat steps 5-12 as desired.

Appendix A4

Electrical Circuit Diagrams

There are five outlets in the deflagration room. Below is a table listing the maximum electrical rating of all the electrical equipment and how they are to be organized so as to not overload any one circuit. After the table are simple wiring diagrams for some of the components.

Outlets 1-5	Circuit	Component	Watts	A/Component
1	**Rope Heaters**		1250	**14.6**
		3-ft	125	1.04
		3-ft	125	1.04
		10-ft	500	4.16
		10-ft	500	4.16
		10-ft	500	4.16
2	**LLT**		1920	**16**
		SRFG-624/5	720	6
		SRFG-508/5	200	1.66
		Cartridge heater	1000	8.33
3a	**Upper strip heater**		500	**4.2**
3a	**Lower strip heater**		500	**4.2**
3b	**Ring heater**		500	**4.2**
3b	**Laptops**			**3**
4a	**UTT**		920	**7.66**
		SRFG-624/5	720	6
		SRFG-508/5	200	1.66
4a	**Solenoid Gas Valves**		8	**0.07**
4a	**Solenoid Gas Valves**		8	**0.07**
4a	**Peltier Coolers**			**1.5**
4b	**Actuated Valves (1)**		96	**0.81**
			32	0.27
			32	0.27
			32	0.27
4b	**Actuated Valves (2)**		96	**0.81**
			32	0.27
			32	0.27
			32	0.27
4b	**DAQ**			**4**
4b	**UVP**			**0.5**
5a	**2-Jet Circuit**		1000	**8.4**
		6-ft	250	2.1
		Ring heater	750	6.3
5b	**Actuator**			**3.2**

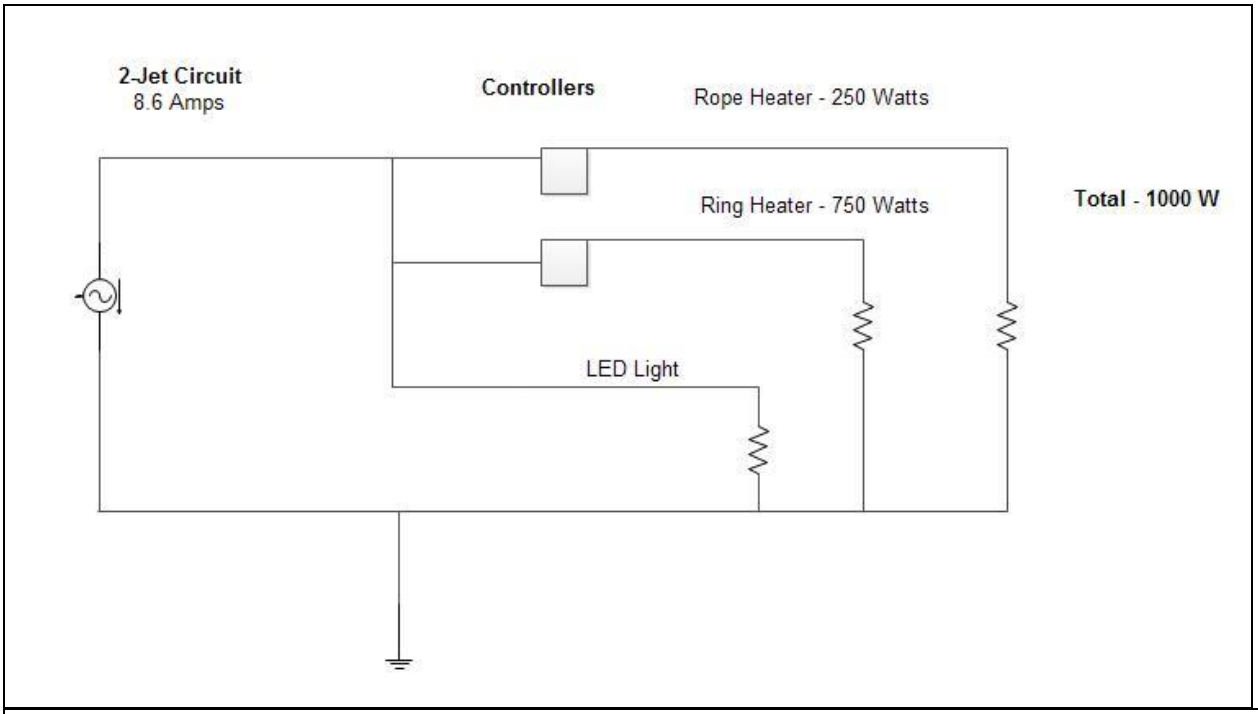
2-Jet Circuit
8.6 Amps
Controllers
Rope Heater - 250 Watts
Ring Heater - 750 Watts
Total - 1000 W
LED Light

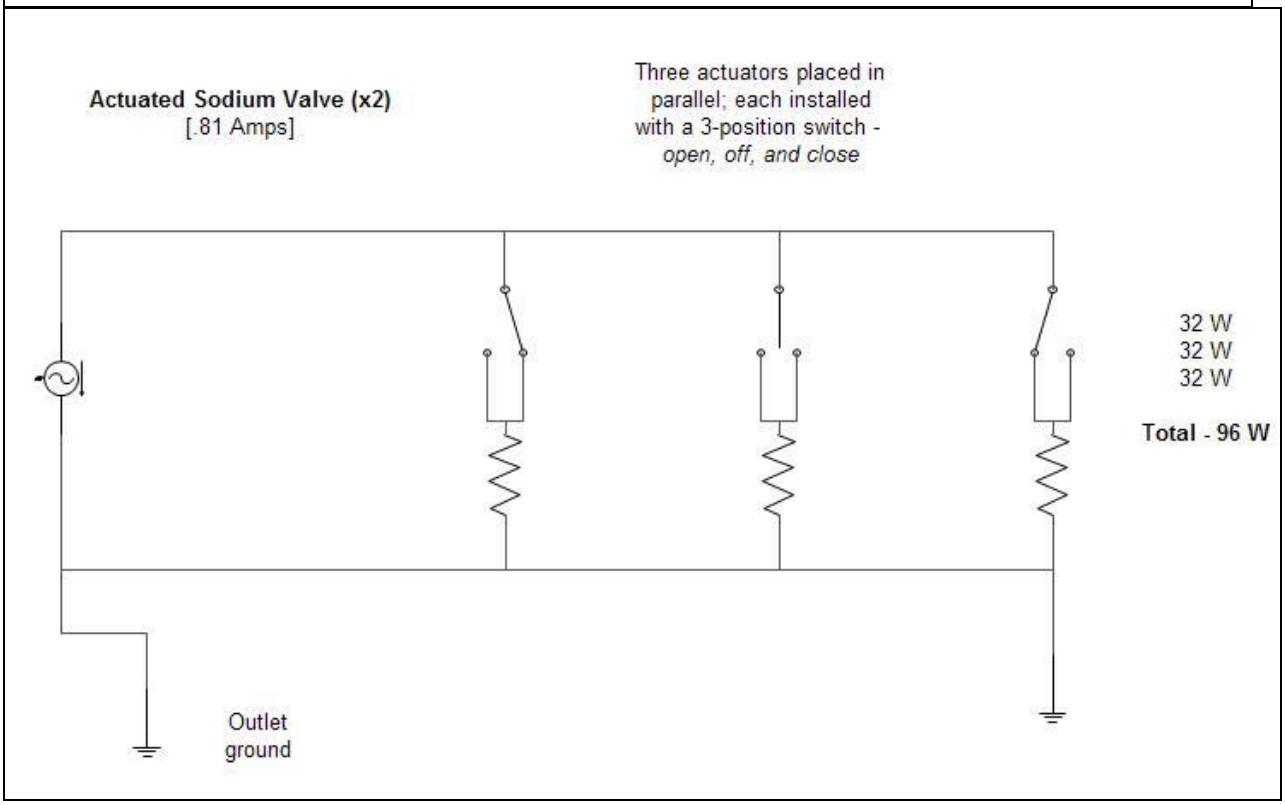
Actuated Sodium Valve (x2)
[.81 Amps]
Three actuators placed in parallel; each installed with a 3-position switch - open, off, and close
32 W
32 W
32 W
Total - 96 W
Outlet ground

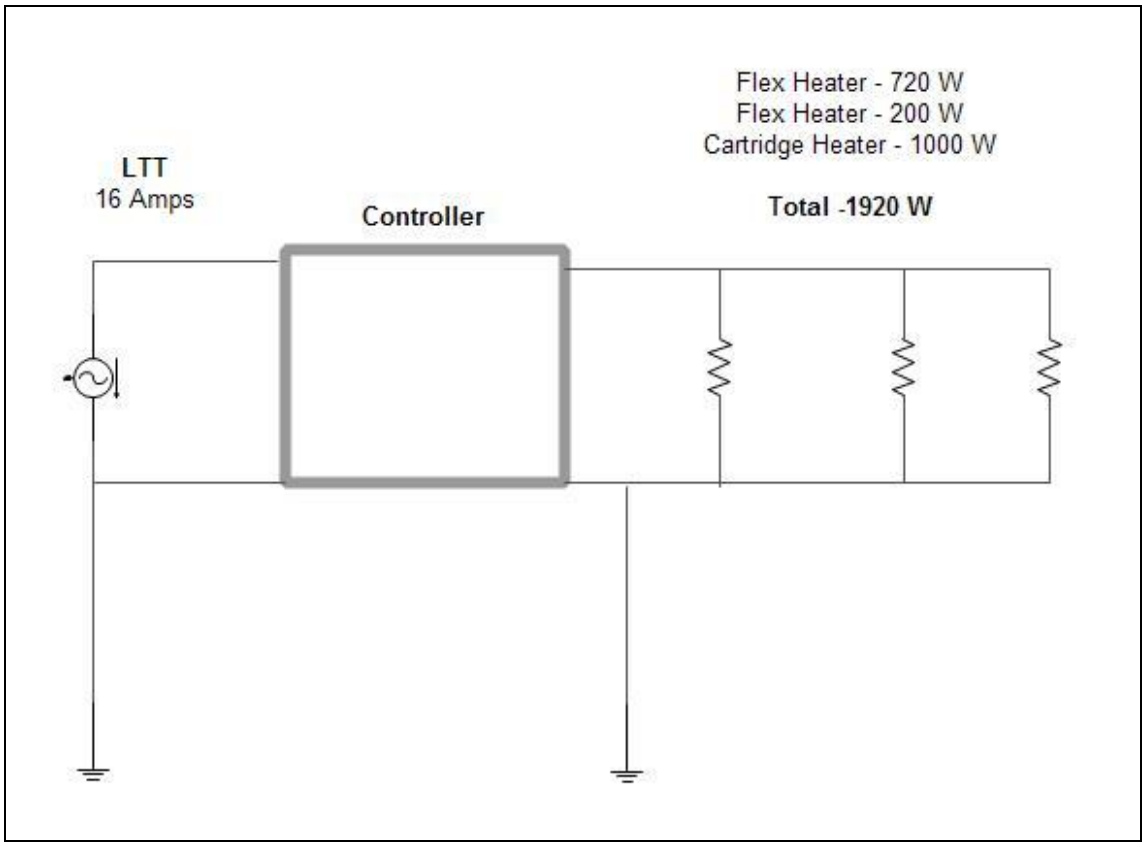
Flex Heater - 720 W
Flex Heater - 200 W
Cartridge Heater - 1000 W
LTT
16 Amps
Controller
Total -1920 W

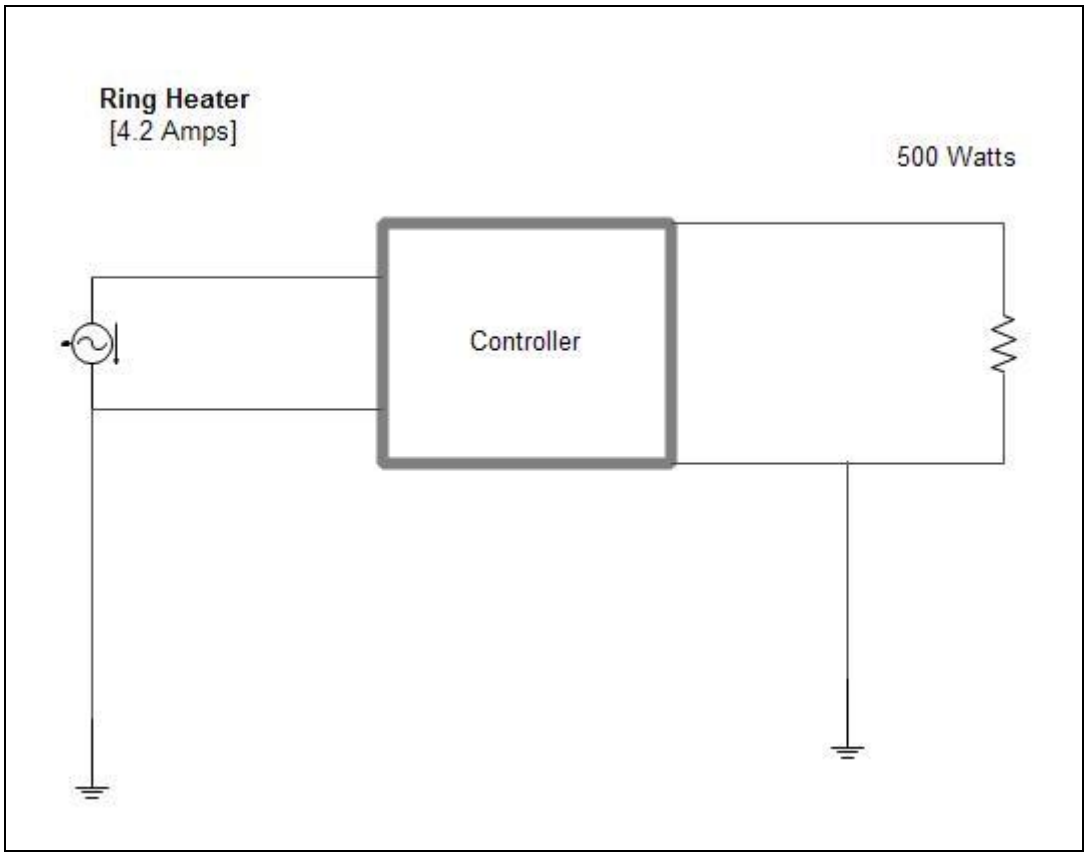
Ring Heater
[4.2 Amps]
500 Watts
Controller

Appendix A5

Sample Labview Code

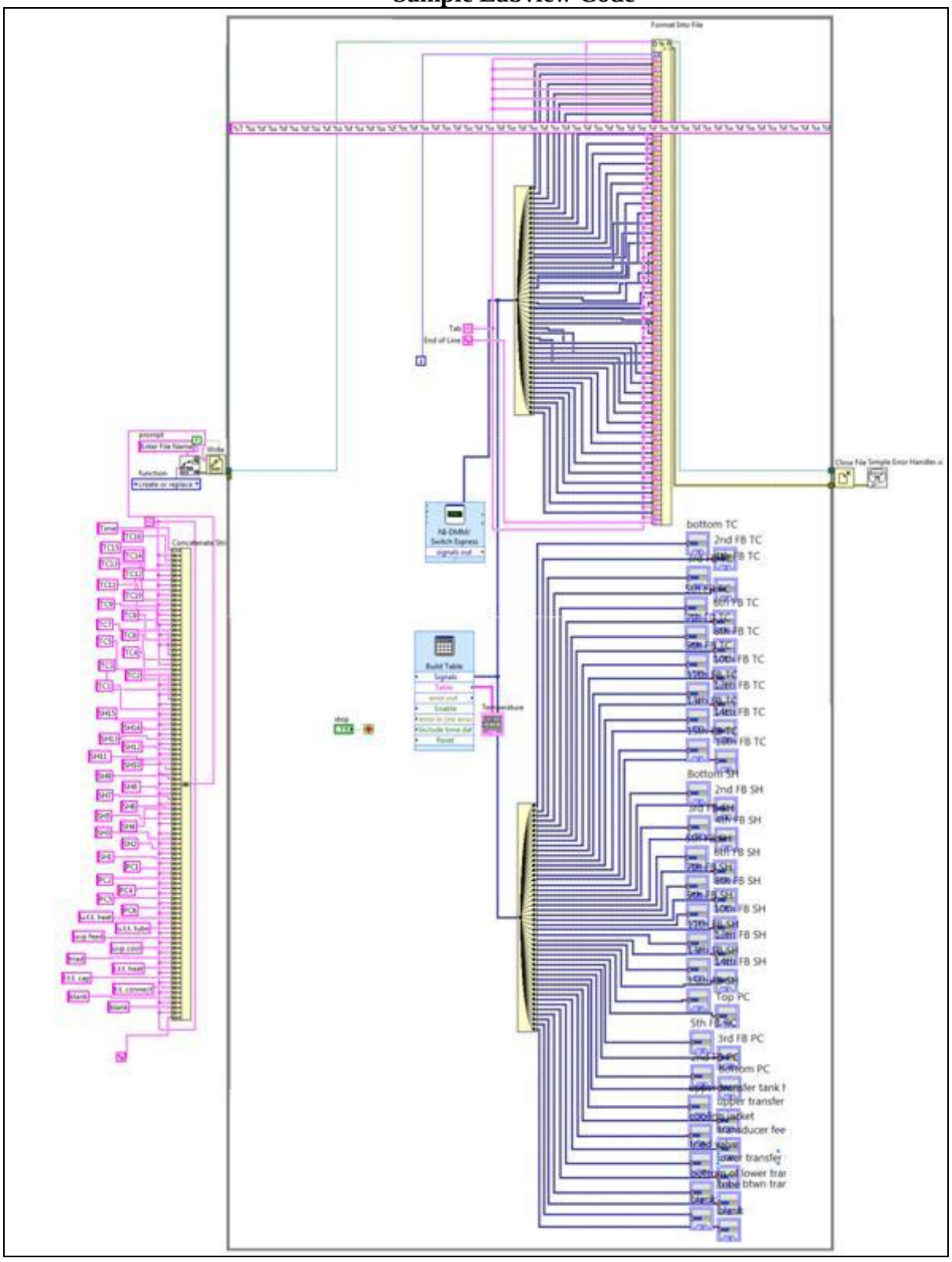

Appendix A6
Test Matrix and Volume Calculations

The following is a table, Table A6.1 of the complete test matrix. Presently, only seven cases have been run using water. Those cases are also identified below.

Table A6. 1. Test Matrix

Velocity Ratio Between Jets	Temperature Difference Between Jets (ΔT, °C) 0	10	20	30
0.0	Momentum Mixing Case 1	Thermal Mixing		
0.3	Case 2	Case 5		
0.5	Case 3	Combined Momentum and Thermal Mixing Case 6		
0.7	Case 4			Case 7

To determine the volumetric flow rate it was timed how long it took the jet to fill a specific volume under certain conditions, see Table A6.2. That flow rate was used to determine the average exit velocity and the total volumes required for each test case. Using the calculated velocity and known test pressure, the LTT pressure to cause a specific velocity ratio was determined, see Table A6.3. In Table A6.3 the green cells indicate the LTT pressure and gravity jet manual valve position used to achieve the desired velocity ratio.

Table A6. 2. Time Trials and Velocity Calculations

Gravity Jet	Fill Weir Minute	Second	Total (sec)	Velocity (cm/s)
3s	5	3.3	303.3	
	5	3.7	303.7	
		Average	303.5	**58.00**
Full Open	3	40.78	220.78	
	3	43.81	223.81	
		Average	222.295	**79.19**

Pressure Jet	Minute	Second	Total (sec)	Velocity (cm/s)

3 psi	3	12.48	192.48	
	3	17.1	197.1	
		Average	194.79	**90.37**
4 psi	2	20.69	140.69	
	2	36.93	156.93	
	2	30.74	150.74	
		Average	153.835	**114.43**
5 psi	2	11.08	131.08	
	2	10.73	130.73	
		Average	130.905	**134.47**
6 psi	1	48.31	108.31	
	1	48.45	108.45	
		Average	108.38	**162.42**
7 psi	1	39.61	99.61	
	1	35.63	95.63	
		Average	97.62	**180.32**

Table A6. 3. Velocity Ratio to Corresponding LTT Pressure

	Gravity Jet 3/4	**Gravity Jet Full**
Ratio	**LTT Pressure (psi)**	**LTT Pressure (psi)**
1.0	1.6	**2.5**
0.7	2.7	**4.0**
0.5	**4.1**	6.0
0.3	**7.5**	10.6

Appendix A7
Met-Flow Duo Settings by Test Case

Case 1:

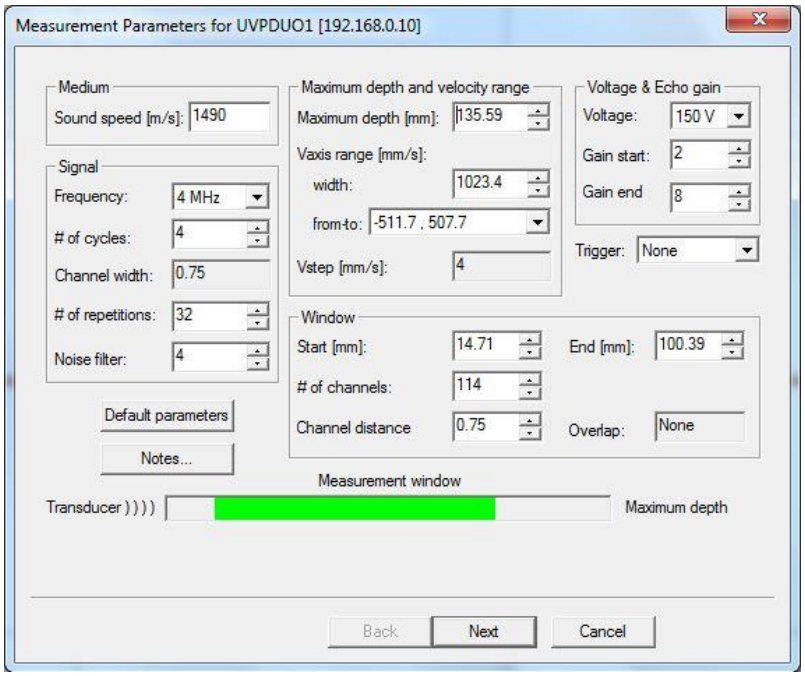

Case 2 and Case 5:

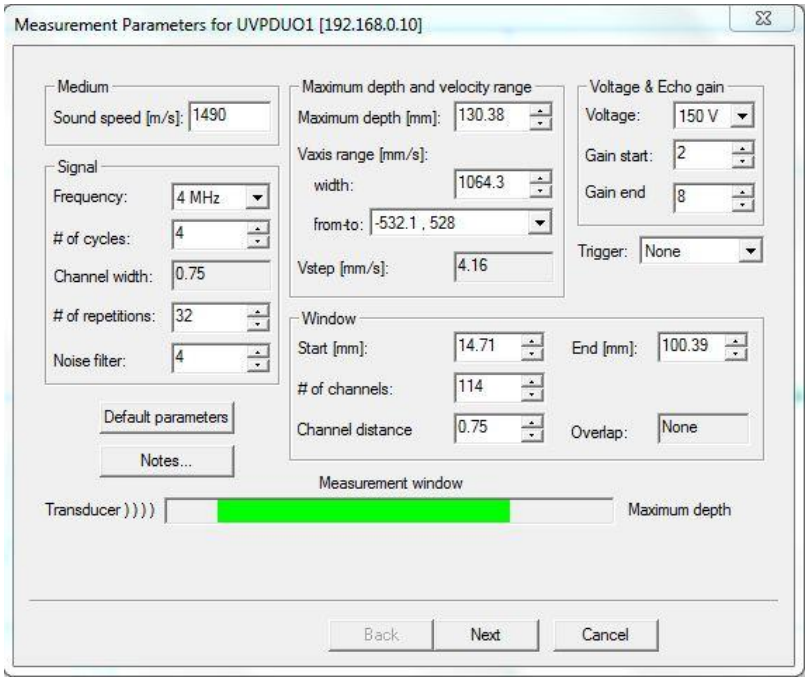

Case 3 and Case 6:

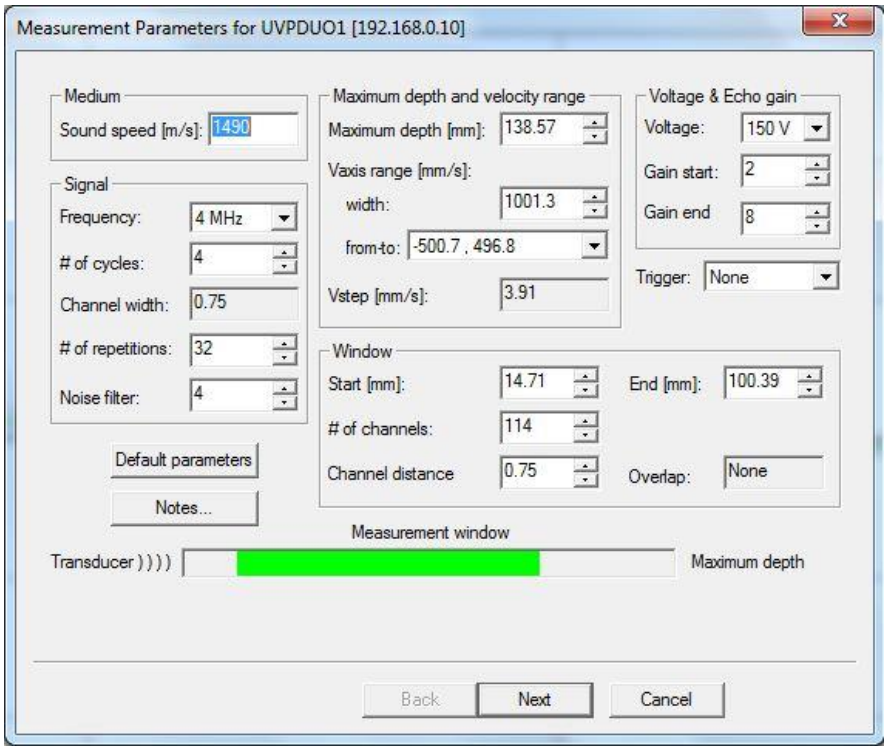

Case 4 and Case 7:

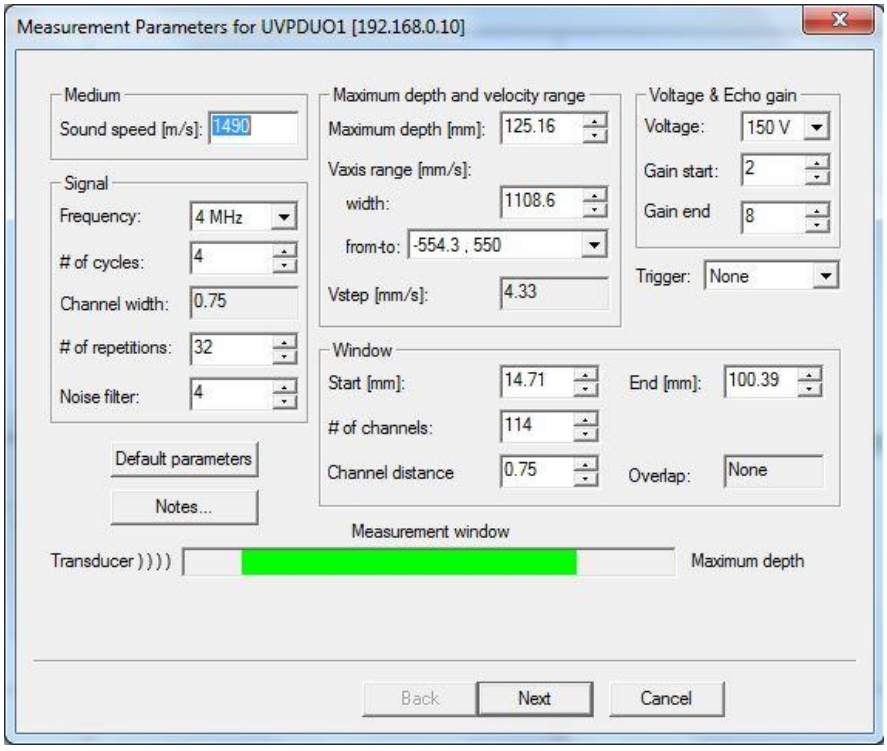

APPENDIX B: Brief Note on Ultrasonic Doppler Velocimetry

(Aug. 5, 2014. Should this be included?)

Ultrasonic Doppler Velocimetry

The principle of ultrasound Doppler velocimetry (UDV) is described the aid of Figure 3. In brief, an ultrasound (US) transducer (tdx) positioned in- or ex-situ emits a cylindrically shaped burst of US-waves into the flow field of interest (measuring line). The ex-situ configuration shows use of an US-gel to acoustically "couple" the tdx to the pipe wall. The characteristic acoustic velocity in the medium defines the medium itself (i.e. fluid/liquid). A fraction of the emitted waves are reflected from reflectants (tracer particles) moving with the flow. Single (or multiple transducers with a multiplexer), is then switched to the receive mode and measures both the time-of-flight and the Doppler shift, including the sign of the shift, at the instant of echo reception. The Doppler shift is related to velocity. By closely matching the density of the reflectant with that of the test media, one can assume 'no-slip' between particle and carrier liquid. Particles, 10-100 m, are well suited for use as reflectants. UDV thus generates a velocity profile of the component *along* the US beam in time; a time-averaged profile can be determined over 128 points (channels) over 1024 profiles in time (per probe). As the channels are over-sampled, we gain spatial-temporal information of the flow. The UDV was co-developed by Takeda and co-workers; a representative reference is given. PI1, 2 and 3 have experience with UDV.

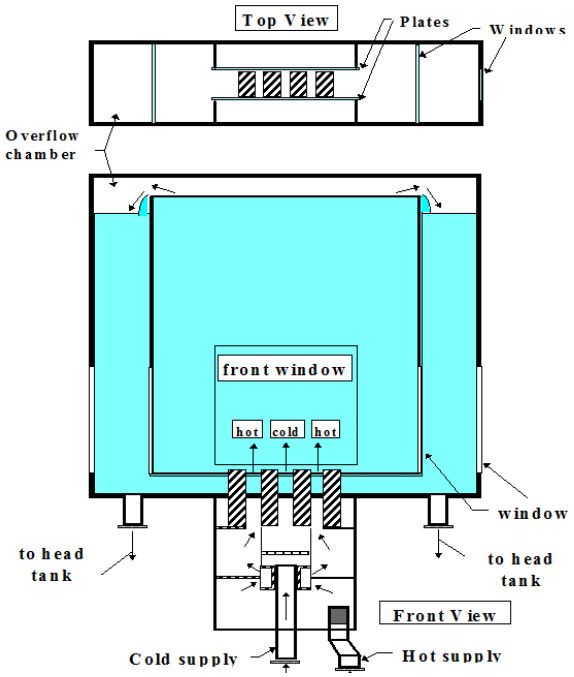

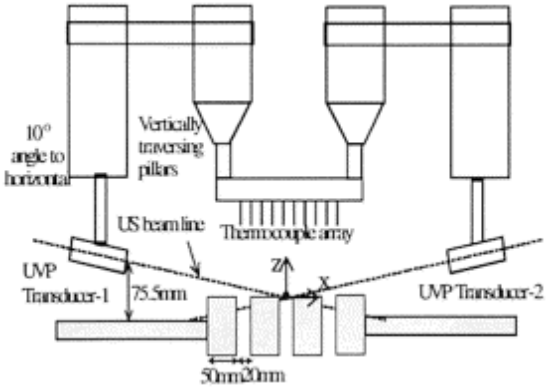

Figure 1. a. Schematic of the triple-jet test section with inner and outer enclosures. A similar configuration for dual-jet is proposed. b. Schematic of ultrasound velocimetry and temperature measurement set-up and simulation results for a triple-jet

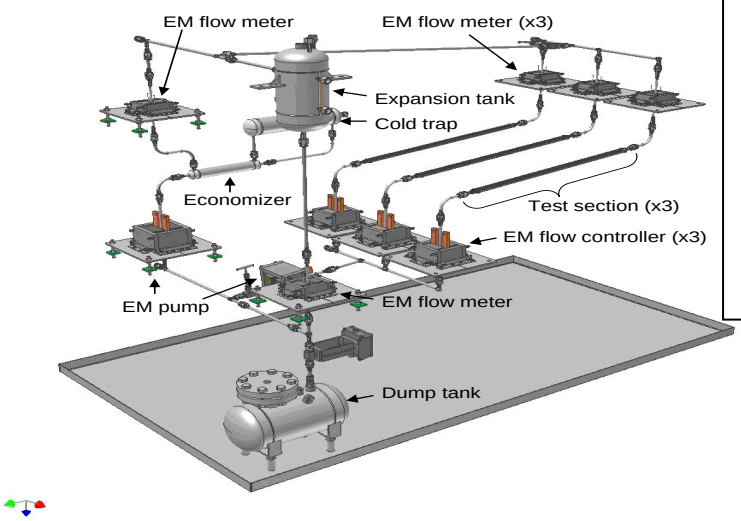

Figure 2. Schematic of a small sodium loop facility at DOE laboratory. Proposed separate effects facilities will have many of the same features and specifications for components exchange options. Initial test section will be to study thermal mixing of two parallel jets.

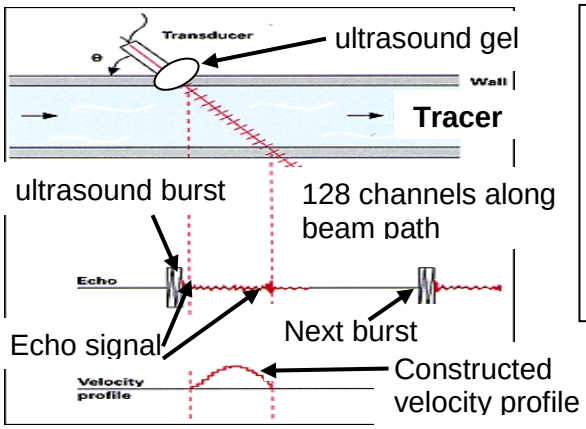

Figure 3. Principle of ultrasound Doppler velocimetry (udv) as applied to pipe-flow as an example. Transducer can be in- or ex-situ and has to be acoustically coupled to medium (solid & liquid). US burst is emitted, then echo from reflections oversampled to construct velocity profile along beamline; thus spatio-temporal.

APPENDIX C: Uncertainty for Two Jet Measurements

For velocity measurements with the UVP device both systematic (also called bias) and random (precision) uncertainty are accounted for in this appendix.

Systematic

Systematic uncertainty (B) refers to those errors that remain constant during repeated measurements under fixed operating conditions (Figliola and Beasley, 2006). The design stage uncertainty method is applied to the velocity resolution of the UVP to determine systematic contributions to the overall uncertainty in velocity measurements. This term is simply half the resolution of the measuring instrument. From Equation 8 in Chapter 3, the velocity range of the UVP instrument is given as,

$$V_{range} = \frac{c^2}{4 f_0 P_{max}} \quad \text{(C1)}$$

Where, c speed of sound in the medium [m/s]
f_0 emitted frequency [Hz]
P_{max} maximum measurable depth [m]

while the velocity resolution from Equation 9 is,

$$\Delta V = \frac{V_{range}}{N_{DU}} = \frac{V_{range}}{256} \quad \text{(C2)}$$

Where, N_{DU} number of 'Doppler units' [-]

Then, the systematic uncertainty (95% probability) associated with UVP measurements is given as (Figliola and Beasley, 2006; Equation 5.1)

$$B = \pm\frac{1}{2}\text{resolution} = \pm\frac{\Delta V}{2} \quad \text{(C3)}$$

Using Equations C1-C3, the systematic uncertainty associated with UVP measurements (B_1) was calculated in Table C.1, assuming constant sound speed (c).

Table C.1 Systematic Uncertainty for UVP by Test Case

	c	P_{max}	P_{max}	V_{range}	ΔV	**B_1**
	[m/s]	[mm]	[m]	[mm/s]	[mm/s]	**[mm/s]**
Test Case 1	1490	135.59	0.13559	1023.4	3.998	**1.999**
Test Case 2	1490	130.38	0.13038	1064.3	4.157	**2.079**
Test Case 3	1490	138.57	0.13857	1001.3	3.911	**1.956**
Test Case 4	1490	125.16	0.12516	1108.6	4.330	**2.165**
Test Case 5	1490	130.38	0.13038	1064.3	4.157	**2.079**
Test Case 6	1490	138.57	0.13857	1001.3	3.911	**1.956**
Test Case 7	1490	125.16	0.12516	1108.6	4.330	**2.165**

Using the test-averaged velocity resolution, the design-stage uncertainty associated with UVP velocity measurements is approximated to be,

$$(\pm 1.956 \leq B_1 \leq \pm 2.165)\ \frac{mm}{s}$$

Random

Random error (P) is simply the scatter of measured data from repeated measurements under fixed operating conditions (Figliola and Beasley, 2006). According to Met-Flow, UVP measurement precision is 0.5% of the measured value. The random uncertainty associated with the two jet UVP measurements (P_1) was calculated in Table C.2, assuming constant sound speed (c). The geometric centerline profile maximum (V_{max}) method was used to represent the random uncertainty.

Table C.2 Random Uncertainty for UVP by Test Case

	V_{max}	**P_1**
	[mm/s]	**[mm/s]**
Test Case 1	412	**2.060**
Test Case 2	508	**2.540**
Test Case 3	613	**3.065**
Test Case 4	638	**3.190**
Test Case 5	539	**2.695**
Test Case 6	437	**2.185**
Test Case 7	519	**2.595**

The random uncertainty for UVP measurements (P_1) was calculated to range from $(\pm 2.060 \leq P_1 \leq \pm 3.190)\ \frac{mm}{s}$

Combined UVP Uncertainty

To determine the overall uncertainty associated with UVP measurements, the systematic (B) and random uncertainties (P) must be combined (Figliola and Beasley, 2006). This is accomplished by the root-sum-squares method (RSS) defined by,

$$u_{UVP} = (B^2 + P^2)^{1/2} \quad \text{(C4)}$$

Using Equation C4, overall measurement uncertainties by test case were calculated in Table C.3.

Table C.3 Overall Uncertainty of UVP Data from Single-Phase Tests

	B_1	P_1	**Combined**
	± [mm/s]	± [mm/s]	**± [mm/s]**
Test Case 1	1.999	2.060	**2.870**
Test Case 2	2.079	2.540	**3.282**
Test Case 3	1.956	3.065	**3.636**
Test Case 4	2.165	3.190	**3.855**
Test Case 5	2.079	2.695	**3.404**
Test Case 6	1.956	2.185	**2.932**

Test Case 7	2.165	2.595	**3.380**

Temperature Measurements

To analyze the uncertainty in temperature measurements, the entire data acquisition system (DAS) must be analyzed. This includes the thermocouple, thermocouple connectors and cable extensions, as well as the data acquisition device. As stated in Appendix C, there are both systematic (also called bias) and random (precision) uncertainties that must be accounted for. Though typical uncertainty analysis involves determining both types of uncertainties to a specific confidence interval (i.e., 95%, 99%), this is not always possible. Most manufacturers actually report associated "accuracy" or "error" associated with measurements as either a maximum value or percentage of the reading. Thus, according to Nakos (2004), the uncertainty is given below by Equation C5,

$$U_{MAX} = \pm [B_T + R_T] \quad \text{(C5)}$$

Where, B_T maximum total systematic uncertainty

R_T maximum total random uncertainty

These uncertainties can be determined by Equations C6 and 1C as follows

$$B_T = (B_1^2 + B_2^2 + B_3^2 + \cdots)^{1/2} \quad \text{(C6)}$$

and

$$R_T = (R_1^2 + R_2^2 + R_3^2 + \cdots)^{1/2} \quad \text{(C7)}$$

where B_1, B_2, B_3 and R_1, R_2, R_3 are the individual systematic and random uncertainty terms, respectively. Thus, both systematic and random uncertainties must be determined for all the components in the data acquisition system.

Thermocouple

As stated in Appendix B.1, type K thermocouple tolerance is 2.2°C or 0.75% of the measured value, whichever is greater, for a temperature range from 0 to 1250°C. This is generally considered a systematic uncertainty, thus the overall uncertainty associated with the thermocouple would be

$\mathbf{B_1} = \pm \mathbf{2.2}$°C

$R = 0$

Thermocouple Extension Wire

Because the thermocouples are located inside the experiment apparatus, extension wire is needed to connect them to the data acquisition device. According to ASTM specifications [ASTM, 1993], extension wire tolerance is the same as the thermocouple itself, thus

$\mathbf{B_2} = \pm \mathbf{2.2}$°C

$R = 0$

Thermocouple Connector

Additional uncertainty is introduced with the connectors used to attach the thermocouple to the extension wire. Previous thermocouple connector uncertainty analysis [ASTM, 1993] has assumed a ΔT of 2°C across the thermocouple connector pins. However, a ΔT of only 0.5°C was assigned for a similar configuration with conditions approaching

1010°C (Nakos, 2004). Therefore, with the temperatures common with this experiment (~20-60°C), a ΔT of 0.5°C is acceptable, thus

$\mathbf{B_3 = \pm 0.5°C}$

$R = 0$

Thermocouple Installation Method and Environment

Another potentially significant systematic error can occur from the chosen thermocouple installation method. This error, while important for high-temperature environments, can be neglected for the relatively low-temperature environment (~100°C) present with the two jet experiment (Nakos, 2004). Therefore,

$\boldsymbol{B = 0}$

$R = 0$

Data Acquisition Unit – National Instruments NI 4070

Aside from the thermocouple and accompanying equipment, errors are also present with the data acquisition unit itself, in this case, the NI 4070. These include errors associated with the voltage, temperature coefficient, and general system accuracy.

Voltage

The typical way of expressing accuracy is:

Accuracy = ±(X ppm of reading + Y ppm of range

The voltage range is within the specified 100mV range limit. If considering a maximum jet water temperature in the test section of ~60°C, then according to Omega's Type K thermocouple tables, the voltage output would be 2.436 mV. The NI 4070 specification lists a 40 ppm uncertainty in the reading and a 20 ppm uncertainty in the range. Thus, the associated error would be

$\boldsymbol{B_4 = \pm}\ 40\ ppm(2.436\ mV) + 20\ ppm(100\ mV) = \pm\ 2.10\ \mu V = \mathbf{\pm\ 0.054°C}$

$R = 0$

Temperature Coefficient

The temperature coefficient accounts for the relative change in a physical property (in this case, voltage) where the temperature is changed by 1 K. For the NI 4070, it is reported as 0.03 °C/°C. Again considering a water temperature of ~60°C, then

$(0.03)(60°C) = 1.80°C$

Therefore,

$\boldsymbol{B_5 = \pm\ 1.80°C}$

$R = 0$

General System

Accuracy and resolution is also given for the overall system, excluding thermocouple errors. These values include cold junction compensation and are based on the one-year stability specification. For a type K thermocouple, within a temperature range of -100 to 1372°C, the accuracy and resolution are ±0.5°C and 0.10°C, respectively. Therefore,

$\boldsymbol{B_6 = \pm\ 0.5 + 0.10°C = \pm\ 0.6°C}$

$R = 0$

It is noted that noise was not considered with this uncertainty analysis. Also, the user's manual assumes that the unit is operated in a 'relatively' still air environment.

Combined Temperature Measurement Uncertainty

Combining all these uncertainties into Equation D18 gives,

$$B_T = (B_1^2 + B_2^2 + B_3^2 + B_4 + B_5 + B_6)^{1/2} \quad \text{(C8)}$$

and thus, the overall uncertainty is calculated as,

$$B_T = [(2.2)^2 + (2.2)^2 + (0.5)^2 + (0.054)^2 + (1.80)^2 + (0.6)^2]^{1/2}$$

$$\boldsymbol{B_T = \pm 3.68°C}$$

Because there are no random errors, the combined temperature measurement uncertainty is,

$$\boldsymbol{U_{MAX} = B_T = 60 \pm 3.68°C}$$

References:

ASTM. "Manual on the Use of Thermocouples in Temperature Measurement." 4th ed. Manual Series: MNL 12, Revision of Special Technical Publication (STP) 470B. (1993).

Figliola, R.S., and D.E. Beasley. *Theory and Design for Mechanical Measurements*. 4th ed. Hoboken: John Wiley & Sons, Inc. (2006): 148-182. Print.

Kline, S.J., and F.A. McClintock. "Describing Uncertainties in Single Sample Experiments." *Mechanical Engineering*. 75. (1953). Print.

Nakos, J.T. "Uncertainty Analysis of Thermocouple Measurements Used in Normal and Abnormal Thermal Environment Experiments at Sandia's Radiant Heat Facility and Lurance Canyon Burn Site." *Sandia National Laboratories Report*. SAND2004-1023 (2004): 1-82. Print.

NI 4070/4072 Specifications. National Instruments Corporation (2008). Print.